

## Nanoscale Science and Technology Room 114 - Session NS1+2D+QS-MoA

### Functionality in 2D Nanostructures and Devices

Moderators: Nikolai Klimov, NIST, Andy Mannix, Stanford University

1:30pm **NS1+2D+QS-MoA-1 Low-Dimensional Neuromorphic Electronic Materials and Applications, Mark Hersam**, Northwestern University  
**INVITED**

The exponentially improving performance of digital computers has recently slowed due to the speed and power consumption issues resulting from the von Neumann bottleneck. In contrast, neuromorphic computing aims to circumvent these limitations by spatially co-locating logic and memory in a manner analogous to biological neuronal networks [1]. Beyond reducing power consumption, neuromorphic devices provide efficient architectures for image recognition, machine learning, and artificial intelligence [2]. This talk will explore how low-dimensional nanoelectronic materials enable gate-tunable neuromorphic devices [3]. For example, by utilizing self-aligned, atomically thin heterojunctions, dual-gated Gaussian transistors have been realized, which show tunable anti-ambipolarity for artificial neurons, competitive learning, spiking circuits, and mixed-kernel support vector machines [4,5]. In addition, field-driven defect motion in polycrystalline monolayer MoS<sub>2</sub> enables gate-tunable memristive phenomena that serve as the basis of hybrid memristor/transistor devices (i.e., 'memtransistors') that concurrently provide logic and data storage functions [6]. The planar geometry of memtransistors further allows multiple contacts and dual gating that mimic the behavior of biological systems such as heterosynaptic responses [7]. Moreover, control over polycrystalline grain structure enhances the tunability of potentiation and depression, which enables unsupervised continuous learning in spiking neural networks [8]. Finally, the moiré potential in asymmetric twisted bilayer graphene/hexagonal boron nitride heterostructures gives rise to robust electronic ratchet states. The resulting hysteretic, non-volatile injection of charge carriers enables room-temperature operation of moiré synaptic transistors with diverse bio-realistic neuromorphic functionalities and efficient compute-in-memory designs for low-power artificial intelligence and machine learning hardware [9].

- [1] V. K. Sangwan, *et al.*, *Matter*, **5**, 4133 (2022).
- [2] V. K. Sangwan, *et al.*, *Nature Nanotechnology*, **15**, 517 (2020).
- [3] M. E. Beck, *et al.*, *ACS Nano*, **14**, 6498 (2020).
- [4] M. E. Beck, *et al.*, *Nature Communications*, **11**, 1565 (2020).
- [5] X. Yan, *et al.*, *Nature Electronics*, **6**, 862 (2023).
- [6] X. Yan, *et al.*, *Advanced Materials*, **34**, 2108025 (2022).
- [7] H.-S. Lee, *et al.*, *Advanced Functional Materials*, **30**, 2003683 (2020).
- [8] J. Yuan, *et al.*, *Nano Letters*, **21**, 6432 (2021).
- [9] X. Yan, *et al.*, *Nature*, **624**, 551 (2023).

2:00pm **NS1+2D+QS-MoA-3 Defect Manipulation in van der Waals Heterostructures and its Applications, Son Le**, Laboratory for Physical Sciences; T. Mai, M. Munoz, A. Hight Walker, C. Richter, 100 Bureau Dr.; A. Hanbicki, A. Friedman, 8050 Greenmead Dr.  
**INVITED**

Reliable and accurate spatial doping of 2-dimensional (2D) materials is important for future applications using this novel class of materials. Here, we present our work on photo-doping of an h-BN/Graphene/h-BN heterostructure. Natural defect states in bulk h-BN can remotely dope graphene and can be optically activated or deactivated. In this way, we can modify both the carrier density and type in graphene accurately and reversibly by several orders of magnitude. Using a spatially-resolved light source, we can activate photo-dopants in selected areas of the sample, and by laterally modulating the doping, we have created PNP junction (PNPJ) devices. *In-situ* quantum Hall measurements were used to demonstrate the effectiveness of this doping technique and characterize the electrostatic profile of the PNPJ. Doping and undoping the heterostructure in a specific sequence, we were able to introduce and destroy correlation among the dopants. Defect correlation greatly enhances carrier mobility while the destruction of this correlated state significantly degrades the carrier mobility in the graphene, effectively creating a mobility switch. An elegant demonstration of this mobility switch is the observation of spin and valley-resolved Landau levels of the graphene in the quantum Hall regime with high-mobility, dopant correlated states, and spin and valley -degenerate Landau levels in the low-mobility, dopant uncorrelated states. I will discuss

ongoing studies to better understanding the nature of these defects with photo-doping measurements of different hBN thicknesses as well as hBN from different sources. This doping technique opens up the possibility to engineer novel device and expand the applications of 2D heterostructures.

2:30pm **NS1+2D+QS-MoA-5 Extraordinary Tunnel Electroresistance in Layer-by-Layer Engineered Van Der Waals Ferroelectric Tunnel Junctions, Qinqin Wang**, Department of Electrical and Computer Engineering and Quantum Technology Center, University of Maryland, College Park

The ability to engineer potential profiles of multilayered materials is critical for designing high-performance tunneling devices such as ferroelectric tunnel junctions (FTJs). FTJs comprise asymmetric electrodes and a ferroelectric spacer, promising semiconductor platform-compatible logic and memory devices. However, the traditional FTJs consisting of metal/oxide/metal multilayer heterostructures can only exhibit modest tunneling electroresistance (TER, usually  $<10^6$ ), which is fundamentally undermined by the unavoidable defect states and interfacial trap states. Here, we constructed van der Waals (vdW) FTJs by a layered ferroelectric CuInP<sub>2</sub>S<sub>6</sub> (CIPS) and graphene. Owing to the gigantic ferroelectric modulation of the chemical potentials in graphene by as large as  $\sim 1$  eV, we demonstrated a giant TER of  $10^9$ . While inserting just a monolayer MoS<sub>2</sub> between CIPS/graphene, the off state is further suppressed, leading to  $>10^{10}$  TER. Our discovery opens a new solid-state paradigm where potential profiles can be unprecedentedly engineered in a layer-by-layer fashion, fundamentally strengthening the ability to manipulate electrons' tunneling behaviors and design advanced tunneling devices.

Keywords: 2d materials, ferroelectric tunnel junctions, tunneling electroresistance

2:45pm **NS1+2D+QS-MoA-6 Scanning Tunneling Microscopy Studies of Twisted Transition Metal Dichalcogenides, Adina Luican-Mayer**, STEM 150 Louis Pasteur Private, Canada

Material systems, devices, and circuits, based on the manipulation of individual charges, spins, and photons in solid-state platforms are key for quantum technologies. Two-dimensional (2D) materials present an emerging opportunity for the development of novel quantum technologies, while also pushing the boundaries of fundamental understanding of materials. Our laboratory aims to create quantum functionality in 2D systems by combining fabrication and assembly techniques of 2D layers with atomically precise microscopy.

In this talk, I will focus on experimental observations of novel phenomena in moiré structures created by twisting 2D layers using scanning tunnelling microscopy and spectroscopy. I will discuss the demonstration of reversible local response of domain wall networks using scanning tunneling microscopy in ferroelectric interfaces of marginally twisted WS<sub>2</sub> bilayers. Moreover, in the case of twisted WS<sub>2</sub> bilayers close to 60°, we observe signatures of flat bands and study the influence of atomic relaxation on their band structure.

## 2D Materials

Room 122 - Session 2D+AP+EM+QS+SS+TF-TuM

### 2D Materials: Synthesis and Processing

Moderators: **Jyoti Katoch**, Carnegie Mellon University, **Huamin Li**, University at Buffalo-SUNY

8:00am **2D+AP+EM+QS+SS+TF-TuM-1 Tailored Growth of Transition Metal Dichalcogenides Monolayers and Their Heterostructures, *Andrey Turchanin***, Friedrich Schiller University Jena, Germany **INVITED**

Two-dimensional materials (2D), their van der Waals and lateral heterostructures possess a manifold of unique electronic, optoelectronic and photonic properties which make them highly interesting for fundamental studies and technological applications. To realize this potential, their tailored growth as well as understanding of the role of their intrinsic defects and 2D-material/substrate interactions are decisive. In this talk, I will present an overview of our recent progress on the synthesis by chemical vapor deposition (CVD), material characterization and studying of fundamental electronic and photonic properties of 2D transition metal dichalcogenide (TMDs) including some applications in electronic and optoelectronic device as well as observing of new excitonic phenomena. A particular focus will be on the lateral heterostructures of TMD monolayers with atomically sharp boundaries and Janus TMDs.

#### References

- [1] A. George et al. *J. Phys. Mater.* **2**, 016001, 2019.
- [2] S. Shree et al. *2D Mater.* **7**, 015011, 2020.
- [3] I. Paradeisanos et al. *Nat. Commun.* **11**, 2391 (2020).
- [4] G. Q. Ngo et al., *Adv. Mater.* **32**, 2003826 (2020).
- [5] A. George et al. *npj 2D Mater. Appl.* **5**, 15 (2021).
- [6] S. B. Kalkan et al., *npj 2D Mater. Appl.* **5**, 92 (2021).
- [7] E. Najafidehaghani et al. *Adv. Funct. Mater.* **31**, 2101086 (2021).
- [8] Z. Gan et al. *Adv. Mater.* **34**, 2205226 (2022).
- [9] Z. Gan et al. *Small Methods* **6**, 2200300 (2022).
- [10] D. Beret et al., *npj 2D Mater. Appl.* **6**, 84 (2022).
- [11] G. Q. Ngo et al. *Nat. Photonics* **16** 769-776 (2022)
- [12] S.B. Kalkan, *Adv. Opt. Mater.* **11**, 2201653 (2023).
- [13] R. Rosati et al., *Nat. Commun.* **14**, 2438 (2023).
- [14] H. Lamsaadi et al., *Nat. Commun.* **14**, 5881 (2023).
- [15] J. Picker et al., *Nanoscale Adv.* **6**, 92-101 (2024).

8:30am **2D+AP+EM+QS+SS+TF-TuM-3 High-Coverage MoS<sub>2</sub> Growth by Two-Step Annealing Process, *Shinichi Tanabe*, *H. Miura***, Tokyo Electron Ltd., Japan; *N. Okada*, *T. Irisawa*, AIST, Japan; *Y. Huang*, *H. Warashina*, *A. Fukazawa*, *H. Maehara*, Tokyo Electron Ltd., Japan

Continuation of Moore's Law scaling requires thin channels in nanosheet field-effect transistor architecture. In this respect, transition-metal dichalcogenides (TMDs) are candidates for the channel material because TMDs are expected to show higher mobility than Si when thickness of the channel is extremely thin. Compatibility to Si nanosheet field-effect transistor fabrication process requires TMD/buffer multilayer film. To obtain such film, alternative preparation of TMD and buffer layers is necessary. Although high-quality TMD can be obtained on a buffer layer by transferring TMD from other substrates, development of a reliable transferring method is challenging. Thus, direct growth of a TMD on a buffer layer is preferable.

We report on a successful growth of high-coverage MoS<sub>2</sub> on SiO<sub>2</sub>/Si substrate. The process starts with growing an initial film on SiO<sub>2</sub>/Si substrate. Here, a continuous initial film can be easily grown by this process with high growth rate. Next, the initial film is sulfurized by a first annealing step followed by crystallization of the film by a second annealing step. The obtained film is a continuous layered film which was confirmed by cross-sectional TEM images. In addition, typical Raman spectra consisted of E<sub>2g</sub> and A<sub>1g</sub> peaks are observed in entire substrate which shows that MoS<sub>2</sub> is grown with high coverage. The difference of E<sub>2g</sub> and A<sub>1g</sub> peaks is about 21 cm<sup>-1</sup>. These results indicate that the two-step annealing process is suitable for obtaining MoS<sub>2</sub> in large area.

8:45am **2D+AP+EM+QS+SS+TF-TuM-4 Anomalous Isotope Effect on the Optical Bandgap in a Monolayer Transition Metal Dichalcogenide Semiconductor, *Kai Xiao***, Center for Nanophase and Materials Sciences Oak Ridge National Laboratory; *Y. Yu*, School of Physics and Technology, Wuhan University, China; *V. Turkowski*, Department of Physics, University of Central Florida; *J. Hachtel*, Center for nanophase and Materials Sciences Oak Ridge National Laboratory; *A. Puzetzyk*, *A. Ievlev*, *C. Rouleau*, *D. Geohegan*, Center for Nanophase and Materials Sciences Oak Ridge National Laboratory

Isotope effects on optical properties of atomically thin 2D materials have rarely been studied to date due to significant challenges posed by sample-to-sample variations resulting from defects, strain, and substrate interactions, complicating the interpretation of optical spectroscopic results. Here, we report a novel two-step chemical vapor deposition method to synthesize isotopic lateral junctions of MoS<sub>2</sub>, comprising monolayer single crystals with distinct isotopic regions. This method allowed the minimization of shifts in photoluminescence due to synthetic heterogeneities necessary to confirm the intrinsic isotope effect on the optical band gap of 2D materials. Raman measurements and temperature-dependent photoluminescence spectra revealed an unusual 13 (± 7) meV redshift as the Mo isotope mass increased in monolayer MoS<sub>2</sub>. This shift is distinct from the trend observed in conventional semiconductors and quantum wells (Si, GaAs, diamond, hBN, etc.). Our experimental characterization, along with time-dependent density-functional theory (TDDFT) and many-body second-order perturbation theory, disclosed that this anomalous shift in the optical band gap in 2D MoS<sub>2</sub> resulted from significant changes in the exciton binding energy induced by strong exciton-phonon scattering. This study provides fundamental insights into understanding the effect of exciton-phonon scattering on the optoelectronic properties of atomically thin 2D materials.

Synthesis science was supported by the U.S. Dept. of Energy, Office of Science, Materials Science and Engineering Division. This work was performed at the Center for Nanophase Materials Sciences, which is a DOE Office of Science User Facility.

9:00am **2D+AP+EM+QS+SS+TF-TuM-5 CVD Growth and Characterization of High-Quality Janus SeMoS and SeWS Monolayers, *Julian Picker***, Friedrich Schiller University Jena, Germany; *M. Ghorbani-Asl*, Helmholtz Zentrum Dresden-Rossendorf, Germany; *M. Schaal*, *O. Meißner*, *F. Otto*, *M. Gruenewald*, *C. Neumann*, *A. George*, Friedrich Schiller University Jena, Germany; *S. Kretschmer*, Helmholtz Zentrum Dresden-Rossendorf, Germany; *T. Fritz*, Friedrich Schiller University Jena, Germany; *A. Krashennnikov*, Helmholtz Zentrum Dresden-Rossendorf, Germany; *A. Turchanin*, Friedrich Schiller University Jena, Germany

Structural symmetry breaking of two dimensional (2D) materials leads to novel physical phenomena. For 2D transition metal dichalcogenides (TMDs) such symmetry breaking can be achieved by exchange of one chalcogen layer with another one. The resulting, so-called Janus TMD structure exhibits an intrinsic dipole moment due to the different electronegativity values of the top and bottom chalcogen layers. Since Janus TMDs do not exist as bulk crystals, they cannot be obtained by exfoliation and need to be synthesized. Recently, we developed a route to grow Janus SeMoS monolayers (MLs) by chemical vapor deposition (CVD). [1] In this approach MoSe<sub>2</sub> monolayers are firstly grown on Au foils and then sulfurized to exchange the bottom selenium layer with sulfur atoms. The formation of high-quality Janus SeMoS MLs and the growth mechanism are proven by Raman and X-ray photoelectron spectroscopy (XPS), photoluminescence measurements, transmission electron microscopy and density functional theory (DFT). Here we present an investigation down to the atomic scale of Janus SeMoS MLs grown on Au(111). From low-energy electron diffraction (LEED) and scanning tunneling microscopy (STM) measurements we determine experimentally the lattice parameters of Janus SeMoS for the first time. The obtained results are in good agreement with the respective DFT calculation. Based on the angle-resolved ultraviolet photoelectron spectroscopy (ARUPS) study, we also obtain the spin-orbit splitting value of the valence band at the K point. Moreover, applying the same approach, we grow and characterize Janus SeWS MLs and provide a comparative analysis with the Janus SeMoS system.

- [1] Z. Gan, I. Paradeisanos, A. Estrada-Real, J. Picker, C. Neumann, A. Turchanin et al., *Chemical Vapor Deposition of High-Optical-Quality Large-Area Monolayer Janus Transition Metal Dichalcogenides*, *Adv. Mater.* **34**, 2205226 (2022).

# Tuesday Morning, November 5, 2024

9:15am **2D+AP+EM+QS+SS+TF-TuM-6 Location-Selective CVD Synthesis of Circular MoS<sub>2</sub> Flakes with Ultrahigh Field-Effect Mobility**, *Chu-Te Chen, A. Cabanillas, A. Ahmed, A. Butler, Y. Fu, H. Hui, A. Chakravarty, H. Zeng*, University at Buffalo-SUNY; *A. Yadav*, Applied Materials, Inc.; *H. Li*, University at Buffalo-SUNY; *K. Wong*, Applied Materials, Inc.; *F. Yao*, University at Buffalo-SUNY

Two-dimensional (2D) semiconducting transition metal dichalcogenides (TMDs) have been considered as promising channel material candidates for future nanoelectronics. The device performance has been significantly improved over the years due to the advancements in understanding of TMD materials, device design, and fabrication process. Despite the early success in demonstrating proof-of-concept devices, scalable and single-crystal growth of TMD films on suitable substrates remains a formidable roadblock to the development of commercially viable TMD-based nanoelectronics. To mitigate this problem, we exploit a controlled growth of high-quality TMD layers at desired locations and demonstrate excellent and consistent electronic properties in transistor device architectures. Taking MoS<sub>2</sub> as an example, we develop a precursor-seeded growth strategy for the direct and site-specific synthesis on SiO<sub>2</sub> substrates using chemical vapor deposition (CVD). By employing electron-beam lithography to pattern seed layers, precise nucleation and growth at designated positions are achieved. Through systematic exploration of CVD synthesis parameters, ordered arrays of circular MoS<sub>2</sub> flakes are successfully grown with the MoO<sub>3</sub> seeds serving as the nucleation sites. A comprehensive suite of microscopic/spectroscopic characterizations along with electrical measurements is utilized to analyze the microstructural and transport properties of the as-grown MoS<sub>2</sub> flakes. The tri-layer circular MoS<sub>2</sub> arrays possess an adjustable and uniform size and exhibit a consistent field-effect mobility up to ~20 cm<sup>2</sup>/V·s with Bi/Au electrode contacts. These findings showcase a technological breakthrough to 2D material synthesis and hold great promise for future integration of 2D materials in the next generation nanoelectronics.

9:30am **2D+AP+EM+QS+SS+TF-TuM-7 Optoelectronic Properties of Exfoliated and CVD Grown TMD Heterostructures**, *Elycia Wright, K. Johnson, S. Coye, M. Senevirathna, M. Williams*, Clark Atlanta University

Transition metal dichalcogenides (TMDs) have attracted significant attention due to their distinctive electronic band structures, which result in intriguing optoelectronic and magnetic properties such as direct bandgap in the visible-infrared range, large exciton binding energies and the presence of two intrinsic valley-contrasting quantities—the Berry curvature and the orbital magnetic moment. Researchers have recently shown interest in studying heterostructures made from different TMD materials. The idea is to combine these materials to create synergistic effects, which can result in even more exciting properties than those found in individual TMDs. For instance, MoS<sub>2</sub>/WS<sub>2</sub> heterostructure can exhibit novel and enhanced optoelectronic performances, including bipolar doping and photovoltaic properties. TMD-based heterostructures may open many possibilities for discovering new physics and developing novel applications. While the science of TMDs and TMD-based heterostructures has made significant strides over the past decade, the field has not yet matured. Numerous challenges, particularly in realizing TMD-based practical applications, remain unresolved. This underscores the importance of our collective efforts in pushing the boundaries of this field.

Exfoliation is a common method for assembling TMD heterostructures, but it has limitations in producing TMD heterostructures on a large scale. The chemical vapor deposition (CVD) method can be used to grow TMD heterostructures on a large scale, which is required in massive device production. However, there are numerous challenges in growing high-quality TMD heterostructures with large areas by CVD, which need to be solved before TMD-based practical applications can be achieved. Our research will focus on the growth of heterostructures (MoS<sub>2</sub>/WS<sub>2</sub>) on various substrates (such as sapphire and SiO<sub>2</sub>/Si) using chemical vapor deposition (CVD). We will explore different mechanisms to achieve large area heterostructures and compare the resulting optoelectronic properties with exfoliated heterostructures. The properties will be characterized using Raman and Fourier Transform infra-red (FTIR) spectroscopy and confocal laser optical microscopy.

9:45am **2D+AP+EM+QS+SS+TF-TuM-8 Pulsed Laser Deposited Amorphous Boron Nitride for 2D Materials Encapsulation**, *Daniel T. Yimam, S. Harris, A. Puzetky, I. Vlasiouk, G. Eres, K. Xiao, D. Geohegan*, Oak Ridge National Laboratory, USA

Recent advancements in 2D materials have opened new avenues in optoelectronics and microelectronics. However, their integration is

hindered by challenges related to materials stability and degradation. Realizing the full potential of 2D materials requires synthesizing and functionalizing an encapsulation layer with desired properties. Recently amorphous boron nitride (aBN) has attracted attention as an ideal low-k material suitable for 2D electronics due to its effectiveness as a protective encapsulation layer. Unlike hexagonal boron nitride (h-BN), which requires high temperatures for deposition and poses challenges for large-area synthesis and integration, aBN can be deposited at significantly lower temperatures. This property makes aBN highly attractive and compatible for back-end-of-line (BEOL) processes in the semiconductor industry.

In this work, we demonstrate that pulsed laser deposition (PLD) enables the deposition of aBN with precise kinetic energy control of precursors, facilitating direct deposition onto 2D materials without significant defect formation. Various in situ plume diagnostics and monitoring tools during deposition were utilized to identify optimal deposition conditions, ensuring ideal kinetic energy ranges and accurate thickness control. This enhances the aBN as an effective encapsulation and barrier against 2D materials thermal degradation, while improving photoluminescence of encapsulated 2D materials. We believe our work significantly impacts future microelectronics by providing low thermal budget method for encapsulating 2D materials and understanding strain and defect evolution. Our work not only advances the practical applications of 2D materials but also paves the way for in situ experimental analysis and diagnostics in the field of material science.

This work was supported by the U.S. DOE, Office of Science, Materials Sciences and Engineering Division and the Center for Nanophase Materials Sciences, which is a DOE Office of Science User Facility.

**Keywords:** Pulsed Laser Deposition, Amorphous Boron Nitride, 2D Materials, Encapsulation, In Situ Diagnostics.

11:00am **2D+AP+EM+QS+SS+TF-TuM-13 Topotaxy for Compositional Variations of Transition Metal Dichalcogenides**, *Matthias Batzill*, University of South Florida

Topotaxy is a kind of solid-state reaction in which the product crystal is crystallographically related to the initial crystal. In 2D materials the initial crystal could be a single sheet or a few layers that are being reacted with same or dissimilar elements to produce novel 2D materials that may not exist in the bulk. Here we investigate such topotactical reactions for transition metal dichalcogenides (TMDs) by reacting them with vapor deposited transition metals. This can result in phase transformations of known layered materials, such as PtTe<sub>2</sub> + Pt => Pt<sub>2</sub>Te<sub>2</sub> [1], new phases such as mirror twin grain boundary networks in MoSe<sub>2</sub> or MoTe<sub>2</sub> [2], or covalently linking bi-layer TMDs by intercalants of the same or different TMs [3]. The studies are performed on MBE grown TMDs and are further modified by post-growth reaction with TM. The resulting structures are characterized by surface probes, such as STM, photoemission, and LEED. In general, the open structure of many 2D materials make them ideal for topotaxy and provide an approach for modifying their composition and induce new properties. Moreover, it allows to locally modify an extended 2D sheet and thus produce in-plane heterojunctions between 'original' and modified 2D domains in a first step to create in-plane device structures.

[1] P.M. Coelho, H.P. Komsa, H. Coy Diaz, Y. Ma, A.V. Krasheninnikov, M. Batzill.

Post-Synthesis Modifications of Two-Dimensional MoSe<sub>2</sub> or MoTe<sub>2</sub> by Incorporation of Excess Metal Atoms into the Crystal Structure.

ACS Nano 12, 3975-3984 (2018)

[2] K. Lasek, J. Li, M. Ghorbani-Asl, S. Khatun, O. Alanwoko, V. Pathirage, A.V. Krasheninnikov, M. Batzill.

Formation of In-Plane Semiconductor–Metal Contacts in 2D Platinum Telluride by Converting PtTe<sub>2</sub> to Pt<sub>2</sub>Te<sub>2</sub>.

Nano Letters 22, 9571-9577 (2022)

[3] V. Pathirage, S. Khatun, S. Lisenkov, K. Lasek, J. Li, S. Kolekar, M. Valvidares, P. Gargiani, Y. Xin, I. Ponomareva, M. Batzill.

2D Materials by Design: Intercalation of Cr or Mn between two VSe<sub>2</sub> van der Waals Layers.

Nano Letters 23, 9579-9586 (2023)

11:15am **2D+AP+EM+QS+SS+TF-TuM-14 Solid State Reaction Epitaxy to Create van der Waals Heterostructures between Topological Insulators and Transition Metal Chalcogenides**, *Salma Khatun, O. Alanwoko, V. Pathirage, M. Batzill*, University of South Florida

Van der Waals (vdW) heterostructures have emerged as a promising avenue for exploring various quantum phenomena. However, the formation of these heterostructures directly is complicated, as individual materials could have different growth temperatures, and alloying can occur at the interface. We present an alternative process akin to a solid-state reaction to modify the surface layer of quantum materials and introduce new properties. Specifically, we used vapor-deposited transition metals (TMs), Cr and Mn, with the goal to react with  $\text{Bi}_2\text{Se}_3$  and transform the surface layer into  $\text{XBi}_2\text{Se}_4$  ( $X = \text{Cr, Mn}$ ). Our results demonstrate that the TMs have a high selenium affinity that drives Se diffusion toward the TM. We found that when a monolayer of Cr is evaporated, the surface  $\text{Bi}_2\text{Se}_3$  is reduced to  $\text{Bi}_2$ -layer, and a stable (pseudo) 2D  $\text{Cr}_{1+x}\text{Se}_2$  layer is formed, whereas  $\text{MnBi}_2\text{Se}_4$  phase is formed with a mild annealing for monolayer amount of Mn deposition.<sup>[1]</sup> However, this phase only occurs for a precise amount of initial Mn deposition. Sub-monolayer amounts dissolve into the bulk, and multilayers form stable MnSe adlayers. Our study highlights the delicate energy balance between adlayers and desired surface-modified layers that govern the interface reactions.<sup>[1]</sup> The success of obtaining the  $\text{MnBi}_2\text{Se}_4$  septuple layer manifests a promising approach for engineering other multicomponent vdW materials by surface reactions.

## REFERENCE

[1] S. Khatun, O. Alanwoko, V. Pathirage, C. C. de Oliveira, R. M. Tromer, P. A. S. Autreto, D. S. Galvao, and M. Batzill, *Adv. Funct. Mater.* **2024**, 2315112

11:30am **2D+AP+EM+QS+SS+TF-TuM-15 AVS National Student Awardee Talk: Quasi-Van Der Waals Epitaxial Growth of Thin  $\gamma'$ -GaSe Films**, *Mingyu Yu*<sup>1</sup>, University of Delaware; *S. Law*, Pennsylvania State University

As an advanced two-dimensional (2D) layered semiconductor, GaSe has various appealing properties, such as rare intrinsic p-type conductivity, nonlinear optical behavior, high transparency in 650-1800nm, and a shift from an indirect-bandgap single-layer film to a direct-bandgap bulk material. These features make GaSe rich in potential in quantum photonic devices, field-effect transistors, photodetectors, etc. GaSe has a hexagonal crystal structure composed of Se-Ga-Ga-Se quadruple layers (QLs). Each QL is bonded by weak van der Waals (vdW) forces, enabling multiple polymorphs:  $\epsilon$ -(2H),  $\beta$ -(2R),  $\delta$ -(4H), and  $\gamma$ -(3R). They have identical non-centrosymmetric QL with a  $D_{3h}$  space group. Besides the four extensively explored polymorphs, a new polymorph,  $\gamma'$ -(3-R) GaSe, was proposed for the first time in 2018.  $\gamma'$ -GaSe is unique for its centrosymmetric  $D_{3d}$  QL (Fig. S1), for which  $\gamma'$ -GaSe is predicted to show intriguing properties compared to other polymorphs. However, there are few existing reports on the observation of  $\gamma'$ -GaSe due to its less-favorable formation energy. Moreover, the wafer-scale production of pure GaSe single crystal thin films remains challenging because of the coexistence of stable multiphases and polymorphs.

We developed a quasi-vdW epitaxial growth method to obtain high-quality pure  $\gamma'$ -GaSe nanometer-thick films on GaAs(111)B at a wafer scale. It results in GaSe thin films exhibiting a smooth surface with a root-mean-square roughness as low as 7.2 Å (Fig. S2a) and a strong epitaxial relationship with the substrate (Fig. S2b). More interestingly, we observed a pure  $\gamma'$ -polymorph using scanning transmission electron microscopy (Fig. S2c,d). Through density-functional theory analysis (Fig. S3),  $\gamma'$ -GaSe can be stabilized by Ga vacancies since its formation enthalpy tends to become lower than that of other polymorphs when Ga vacancies increase. We also observed that, unlike other GaSe polymorphs,  $\gamma'$ -GaSe is inactive in room-temperature photoluminescence tests. This may be related to its centrosymmetric QL structure, which we are exploring further. Meanwhile, we systematically studied the growth window for GaSe with high structural quality and identified that GaAs(111)B is more suitable than c-sapphire as a substrate for GaSe growth. Overall, this study advances the wafer-scale production of  $\gamma'$ -GaSe films, and elucidates a method for direct epitaxial growth of hybrid 2D/3D heterostructures with atomically sharp interfaces, facilitating the development of heterogeneous integration. In the future, we will focus on developing the properties and applications of  $\gamma'$ -GaSe, and delving into the understanding of the epitaxial growth mechanism.

11:45am **2D+AP+EM+QS+SS+TF-TuM-16 Investigation of Dry Transfer of Epitaxial Graphene from SiC(0001)**, *Jenifer Hajjuz, D. Pennachio, S. Mack, R. Myers-Ward*, U.S. Naval Research Laboratory

Transfer of high-quality graphene from its growth substrate to substrates of technological interest can be necessary to enable its use in certain applications, however it remains challenging to achieve large-area transfer of graphene that is clean and intact. This work utilizes a dry transfer technique in which an adhesive metal stressor film is used to exfoliate epitaxial graphene (EG) from SiC(0001) [1]. In this method, the strain energy in the metal film must be high enough to allow for uniform exfoliation, but low enough such that self-exfoliation of graphene does not occur.

We investigate the dry transfer of monolayer EG (MEG) and hydrogen-intercalated, quasi-freestanding bilayer graphene (QFBEG) grown by sublimation of Si from nominally on-axis 6H-SiC(0001) in a CVD reactor in Ar ambient. A magnetron sputtered Ni stressor layer is used to exfoliate EG and transfer to GaAs, glass, and  $\text{SiO}_2/\text{Si}$  substrates. The Ar pressure during sputtering is found to impact the stress, film density, and roughness of the Ni film, as determined from wafer curvature and X-ray reflectivity (XRR) measurements. By using appropriate sputtering conditions, the Ni/graphene film exfoliates from the entire area of the SiC substrate with use of thermal release tape. Atomic force microscopy (AFM), scanning electron microscopy, Raman spectroscopy, x-ray photoelectron spectroscopy (XPS), and Nomarski microscopy are used to characterize the graphene. The Ni 2p peak was not detected in XPS of the transferred graphene after removal of the Ni film by etching in acid. Additionally, XPS revealed minimal oxide present at the graphene-GaAs interface, consistent with previous reports for this dry transfer method [2].

Raman spectroscopy mapping showed that predominately monolayer graphene is transferred from MEG, while predominately bilayer graphene is transferred from QFBEG. Raman spectroscopy of the SiC substrate after MEG exfoliation shows the  $6\sqrt{3}$  buffer layer that forms during growth on SiC(0001) remains on the SiC substrate. Consequently, if there are regions of exposed  $6\sqrt{3}$  buffer layer in the as-grown MEG on SiC, AFM shows that there are corresponding gaps in the transferred graphene film where the areas of exposed buffer layer do not transfer. The  $6\sqrt{3}$  buffer layer is not present in QFBEG due to the hydrogen-intercalation process. It is found that the same Ni sputtering conditions that led to uniform exfoliation and transfer of MEG result in micron-scale tears in the Ni/QFBEG film. By lowering the strain energy in the sputtered Ni film, these tears can be reduced or eliminated.

[1] Kim, J., *et al.*, *Science*, **342**, 833 (2013).

[2] Kim, H., *et al.*, *ACS Nano*, **15**, 10587 (2021).

12:00pm **2D+AP+EM+QS+SS+TF-TuM-17 Nickel Foams Enable Space-Confined Chemical Vapor Deposition (CVD) Synthesis of High-Quality MoS<sub>2</sub> Films**, *Taylor Currie, L. Tetard, T. Jurca*, University of Central Florida

Space-confined chemical vapor deposition (CVD) is a variation on traditional CVD syntheses in which the space between the substrate and precursor is restricted, which can lead to more consistent growth of high-quality two-dimensional (2D) materials. Space-confinement can be achieved by, for example, (1) using a shorter tube of smaller diameter inside the reactor tube, or (2) placing the substrate and precursor very close to each other. In both cases the concentration of reactants reaching the substrate is limited, which prevents excessive and rapid (lateral) growth and instead favors 2D film growth. In our approach, a growth substrate (c-plane sapphire wafer) was placed directly on top of nickel foam (NF) pre-loaded with molybdenum oxide ( $\text{MoO}_x/\text{NF}$ ). A quartz boat containing sulfur powder was placed upstream in a 275 °C temperature zone, and a second boat containing the substrate and  $\text{MoO}_x/\text{NF}$  was placed in a separately controlled temperature zone at 850, 900, or 950 °C. Using this approach, high-quality  $\text{MoS}_2$  monolayers were grown at 1, 5, or 15 min, as confirmed by optical microscopy, Raman and photoluminescence spectroscopies, energy-dispersive x-ray spectroscopy, and atomic force microscopy. We determined that the quality and thickness (i.e. monolayer, few layer, multilayer, bulk) of the  $\text{MoS}_2$  films were dependent on temperature and hold time used for the growth, with trials at 850 °C for 15 min, 900 °C for 15 min, and 950 °C for 5 min resulting in the best films. The use of a readily available metal foam with inherent porosity enhances the ease and accessibility of this space-confined CVD approach. This provides many more opportunities for modifications (e.g. varying the metal precursor used to decorate NF, surface coverage of precursor on NF, porosity of NF, and/or distance between substrate and NF).

<sup>1</sup> AVS National Student Awardee

# Tuesday Afternoon, November 5, 2024

## 2D Materials

### Room 122 - Session 2D+LS+NS+SS-TuA

#### Electronics Properties

**Moderators:** Masa Ishigami, University of Central Florida, Slavomir Nemsak, Advanced Light Source, Lawrence Berkeley National Laboratory

2:15pm **2D+LS+NS+SS-TuA-1 NanoARPES for the Study of 2D Materials, Aaron Bostwick**, Advanced Light Source, Lawrence Berkeley National Laboratory **INVITED**

Angle-resolved photoemission spectroscopy (ARPES) is the premier technique for the determination of the electronic bandstructure of solids, and has found wide application for many classes of materials, such as oxides, semiconductors, metals, and low-dimensional materials and surfaces. Among the important topics it addresses are the underlying many-body interactions that determine the ground and excited state functionalities of all materials. Recently the development of nanoARPES using microfocused x-ray beams has opened ARPES to a wider class of samples and enabled the measurement of 2D devices *in-situ* with applied electric fields, currents, strain and femtosecond laser pulses to the samples. In this talk I will give an introduction to the ARPES technique, the MAESTRO facility and share some of our recent work on the bandstructure and many-body interactions in 2D heterostructures of chalcogenides, graphene, and boron nitride and light induced metastable phases in 1T-TaS<sub>2</sub>.

2:45pm **2D+LS+NS+SS-TuA-3 Observation of Interlayer Plasmon Polaron in Graphene/WS<sub>2</sub> Heterostructures**, S. Ulstrup, Aarhus University, Denmark; Y. Veld, Radboud University, Netherlands; J. Miwa, A. ones, Aarhus University, Denmark; K. McCreary, J. Robinson, B. Jonker, Naval Research Laboratory; S. Singh, Carnegie Mellon University, USA; R. Koch, E. Rotenberg, A. Bostwick, C. Jozwiak, Advanced Light Source, Lawrence Berkeley National Laboratory; M. Rosner, Radboud University, Netherlands; **Jyoti Katoch**, Carnegie Mellon University, USA

Van der Waals heterostructures offer us exciting opportunity to create materials with novel properties and exotic phenomena such as superconductivity, bound quasiparticles, topological states as well as magnetic phases. In this talk, I will present our work on directly visualizing the electronic structure of graphene/WS<sub>2</sub>/hBN heterostructure using micro-focused angle-resolved photoemission spectroscopy (microARPES). Upon electron doping via potassium deposition, we observe the formation of quasiparticle interlayer plasmon polarons in graphene/WS<sub>2</sub> heterostructure due to many-body interactions. I will discuss that such low-energy quasiparticle excitation is important to consider as they can have huge implications on the electronic and optical properties of heterostructures based on 2D transition metal dichalcogenides.

3:00pm **2D+LS+NS+SS-TuA-4 Harnessing the Synergy of X-ray Photoelectron Spectroscopy (XPS) and Argon Cluster Etching for Profound Analysis of MoS<sub>2</sub> and Graphene**, Jonathan Counsell, Kratos Analytical Limited, UK; C. Maffitt, D. Surman, Kratos Analytical Inc.; L. Soomary, K. Zahra, Kratos Analytical Limited, UK

Understanding the intricate properties of two-dimensional (2D) materials such as MoS<sub>2</sub> and graphene is pivotal for advancing their applications across diverse fields. However, achieving comprehensive characterization at the nanoscale requires advanced analytical techniques. This study explores the synergistic potential of X-ray Photoelectron Spectroscopy (XPS) coupled with Gas Cluster Ion Source (GCIS) etching and depth profiling to delve deeper into the structural and electronic intricacies of MoS<sub>2</sub> and graphene.

By integrating XPS with GCIS etching, we not only discern the elemental composition, chemical bonding, and electronic states of these materials with exceptional precision but also unravel their depth-dependent characteristics. The incorporation of GCIS etching facilitates controlled removal of surface layers, enabling depth profiling to uncover buried interfaces, defects, and contamination effects that influence spectral results.

The combined approach allows for the characterization of MoS<sub>2</sub>-graphene heterostructures, providing insights into interfacial interactions and electronic coupling mechanisms. Through systematic analysis, we demonstrate the complementary advantages of XPS and GCIS etching in elucidating the structural and electronic complexities of 2D materials.

The integration of GCIS etching with XPS not only enhances the depth resolution and sensitivity of the analysis but also offers a deeper understanding of the nanoscale landscape of MoS<sub>2</sub>, graphene, and their heterostructures. This multidimensional approach accelerates the

development of tailored devices and applications based on 2D materials, propelling advancements in nanotechnology and beyond.

3:15pm **2D+LS+NS+SS-TuA-5 Monark Quantum Foundry: Advancing 2d Quantum Materials Through Automated Pipelines**, Amirhossein Hasani, N. Borys, Montana State University, USA; H. Churchill, University of Arkansas

At the MonArk Quantum Foundry, located at Montana State University and the University of Arkansas, we are advancing the field of 2D quantum materials through the development of 2D Quantum Materials Pipelines (2D-QMaPs). These pipelines automate and streamline the critical stages of 2D quantum material sample preparation and device fabrication.

**Robotic Exfoliation and Flake Hunting:** Our process begins with an automated robotic exfoliator designed to produce up to 50 chips per hour, each measuring 1 cm by 1 cm. This machine carefully peels off thin layers from bulk materials, allowing precise control over factors such as temperature, pressure, and applied force, which is crucial for producing high-quality thin flakes, including single-layered crystals. After exfoliation, an automated optical cataloger identifies and catalogs the thin flakes. This system scans the entire chip, locates these flakes, and stores their information in a database. The cataloger uses advanced machine learning and AI algorithms for quick and accurate detection and features a motorized stage with photoluminescence and Raman spectroscopy capabilities, completing a full scan at 20x magnification in approximately 5 minutes.

**Device Fabrication and Packaging:** The identified flakes are then transferred to a specialized environment for device fabrication and packaging. This stage employs high-resolution thermal scanning probe lithography, laser writing systems, and electron beam evaporators to create devices. The entire process is conducted in an inert atmosphere (glove box), preserving the material's integrity by preventing exposure to air and moisture.

**Characterization:** The final stage integrates quantum device characterization tools, including photoluminescence (PL), Raman spectroscopy, magneto-optical probes, nano-optical spectroscopy, bulk and nanoscale cryogenic magnetometry, and magneto-transport measurements. These tools provide a comprehensive analysis of material and device properties, including mobilities, transition temperatures, photon autocorrelations, coherence times, and more.

Through the development of the 2D-QMaPs, the MonArk Quantum Foundry is revolutionizing the study of 2D quantum materials, paving the way for significant advancements in quantum computing, sensing, and other technologies.

4:00pm **2D+LS+NS+SS-TuA-8 Manipulation of Chiral Interface States in a Moiré Quantum Anomalous Hall Insulator**, Tiancong Zhu, Purdue University **INVITED**

Quantum anomalous Hall (QAH) effect reflects the interplay between magnetism and non-trivial topology characterized by integer Chern numbers, which is expressed by chiral edge states that carry dissipationless current along sample boundaries. The recent discovery of QAH effect in van der Waals moiré heterostructures provides new opportunities in studying this exotic two-dimensional state of matter. Specifically, magnetism in these moiré QAH systems is induced by orbital motion of electrons, which allows full electrical control of the magnetic and the corresponding topological state. In this talk, I will discuss our recent scanning tunneling microscopy and spectroscopy (STM/STS) measurements on twisted monolayer-bilayer graphene (tMBLG), where QAH effect with gate-switchable Chern numbers have been observed previously in transport measurement. First I will discuss local scanning tunneling spectroscopy measurements on the correlated insulating states at  $\nu = 2$  and  $\nu = 3$  electrons per moiré unit cell, where the  $\nu = 3$  state shows a total Chern number of  $\pm 2$ . Under a small magnetic field, the sign of Chern number at the  $\nu = 3$  states can be switched by changing the local carrier concentration with gating, which is a result of competition between bulk and edge orbital magnetization of the QAH state.<sup>1</sup> The observation of a gate-switchable Chern number provides us an opportunity to directly visualize the chiral edge state in a moiré QAH insulator for the first time, which I will show through gate-dependent STS measurement and  $dI/dV$  mappings.<sup>2</sup> I will also demonstrate the capability to manipulate the spatial location and chirality of the QAH edge state through controlling the local carrier concentration with the STM tip.

<sup>1</sup> C. Zhang, T. Zhu et al., Nature Communications, 14, 3595 (2023)

<sup>2</sup> C. Zhang, T. Zhu et al., Nature Physics (2024)

# Tuesday Afternoon, November 5, 2024

4:30pm **2D+LS+NS+SS-TuA-10 Scanning Tunneling Microscopy and Spectroscopy of Single Layer NiTe<sub>2</sub> on Au**, *Stephanie Lough*, University of Central Florida; *M. Ishigami*, University of Central Florida

Previous angle-resolved photoemission studies [1, 2] have shown that NiTe<sub>2</sub> is a type II Dirac material that possesses a Dirac point very close to the Fermi level. In addition, the material has a topological surface state which can be valley spin-polarized. A recent study [3] has shown that this state can be exploited to develop Josephson diodes with potential applications as memory devices which can be coupled to qubits. There has been a significant interest [3-5] in studying properties of single layer NiTe<sub>2</sub> due to its strong interlayer coupling in bulk via Te Pz orbitals.

In this talk, we will discuss the properties of single layer NiTe<sub>2</sub> on Au generated by gold-assisted exfoliation measured using low temperature scanning tunneling microscopy and spectroscopy. We find that this interface possesses rectangular lattice with periodicities that are different from bulk NiTe<sub>2</sub> or Au (111) by over 30%. Tunneling spectra reveals strong coupling between NiTe<sub>2</sub> and Au (111). We compare these results recent theoretical calculations [6] on strained NiTe<sub>2</sub> and its impact on topological surface states.

1. Ghosh, S., et al., *Observation of bulk states and spin-polarized topological surface states in transition metal dichalcogenide Dirac semimetal candidate NiTe<sub>2</sub>*. Physical Review B, 2019. **100**.

2. Mukherjee, S., et al., *Fermi-crossing Type-II Dirac fermions and topological surface states in NiTe*. Scientific Reports, 2020. **10**(1).

3. Pal, B., et al., *Josephson diode effect from Cooper pair momentum in a topological semimetal*. Nature Physics, 2022. **18**(10): p. 1228-+.

4. Zhao, B., et al., *Synthetic Control of Two-Dimensional NiTe Single Crystals with Highly Uniform Thickness Distributions*. Journal of the American Chemical Society, 2018. **140**(43): p. 14217-14223.

5. Zheng, F.P., et al., *Emergent superconductivity in two-dimensional NiTe crystals*. Physical Review B, 2020. **101**(10).

6. Ferreira, P.P., et al., *Strain engineering the topological type-II Dirac semimetal NiTe*. Physical Review B, 2021. **103**(12).

4:45pm **2D+LS+NS+SS-TuA-11 Nanoscale heterogeneities at Transition Metal Dichalcogenide-Au Interfaces**, *Taisuke Ohta*, *A. Boehm*, *A. Kim*, *C. Spataru*, *K. Thuermer*, *J. Sugar*, Sandia National Laboratories; *J. Fonseca Vega*, *J. Robinson*, Naval Research Laboratory

Two-dimensional geometry renders unique screening properties in transition metal dichalcogenides (TMDs). Consequently, the electronic properties of TMDs are susceptible to extrinsic factors (*e.g.*, substrate, strains, and charge transfer), and display spatial nonuniformities. Thus, material combinations (*i.e.*, TMD, dielectrics, and metals) and their nuanced interactions need to be considered when designing TMD-based devices. Of particular importance are the interfaces with metallic contacts. Uncovering the origin of heterogeneities at TMD-metal interfaces and establishing strategies to control TMD-metal interfaces could enable engineering pathways for future applications. We show that the electronic structures of exfoliated WS<sub>2</sub>-Au interfaces exhibit pronounced heterogeneity arising from the microstructure of the supporting metal. These electronic structure variations indicate spatially nonuniform doping levels and Schottky barrier height across the junction. Through examination using photoelectron emission microscopy, we reveal key differences in the work function and occupied states. With *ab initio* calculation, electron backscatter diffraction, and scanning tunneling microscopy, our measurements show distinct variations in excess of 100meV due to the crystal facets of Au. Additionally, when multilayer WS<sub>2</sub> and Au(111) facets are azimuthally aligned, strong interactions induce mechanical slippage of the interfacing WS<sub>2</sub> layer, with respect to the rest of the WS<sub>2</sub> layers, resulting in local stacking variations with an occupied state energy shift of 20-50meV. Finally, we employed oxygen plasma treatment of Au to fabricate homogenous TMD-Au interfaces while also tuning the electronic properties of the TMDs. Our findings illustrate that the electronic properties of TMDs are greatly impacted by the interface interactions at energy and length scales pertinent to electronics and optoelectronics.

The work at Sandia National Laboratories (SNL) was supported by LDRD program and the US Department of Energy (DOE), Office of Basic Energy Sciences, Division of Materials Sciences and Engineering (BES 20-017574). The work at the US Naval Research Laboratory was funded by the Office of Naval Research. SNL is a multi-mission laboratory managed and operated by National Technology and Engineering Solutions of Sandia, LLC., a wholly-owned subsidiary of Honeywell International, Inc., for the US DOE's National Nuclear Security Administration under contract DE-NA0003525.

Tuesday Afternoon, November 5, 2024

This paper describes objective technical results and analysis. Any subjective views or opinions that might be expressed in the paper do not necessarily represent the views of the US DOE or the US Government.

5:00pm **2D+LS+NS+SS-TuA-12 Xenon Trapping in Silica Nanocages Supported on Metal Powder**, *Laiba Bilal*, SBU; *A. Boscoboinik*, Brookhaven National Laboratory

Trapping of Xenon gas atoms in silica nanocages supported on metal powders (Ru and Co) is investigated by lab-based ambient pressure X-ray photoelectron spectroscopy (AP-XPS). Xenon, being a noble gas, has very low reactivity<sup>1</sup>. This makes it useful for applications where chemical reactions are unwanted. The first use for Xenon was in flash lamps used in photography<sup>2</sup>, and it is still used for this purpose today. It has wide applications, from its use in the cells of plasma television as a propellant in spacecraft that use ion propulsion<sup>3</sup> to its various applications in the medical industry<sup>4</sup>.

Xenon occurs in slight traces within Earth, 1 part in 10 million by volume of dry air<sup>2</sup>. Like several other noble gases, xenon is present in meteorites and manufactured on a small scale by the fractional distillation of liquid air. However, Xe's concentration in the earth's crust and the atmosphere are much lower than predicted, which is also known as the "missing Xenon paradox"<sup>5</sup>.

The Discovery of an effective way to trap and separate Xenon from other gases can have significant advantages. The presence of Xenon in nuclear fuel rods was partially responsible for the Chernobyl accident<sup>6</sup>. Consequently, the nuclear energy industry is also trying to imprint a way to control the release of Xe, produced during the nuclear fission of uranium. Characteristics of chemical interactions between Xe and metal surfaces have been observed and explained, also several low-energy electron diffraction studies at cryogenic temperatures have experimentally demonstrated an on-top site adsorption preference for Xe adatoms on metal surfaces<sup>7</sup>.

Prior studies on 2D silicate bilayers grown on metal supports at Brookhaven National Lab showed that these structures could irreversibly trap all noble gases larger than Ne<sup>8</sup> at room temperature. The noble gas atoms were trapped within hexagonal prism-shaped silicate nanocages-like structures and could then be released by heating the materials to different temperatures, *i.e.*, Ar: 348 K, Kr: 498 K, Xe: 673 K, Rn: 775 K<sup>8,9</sup>. Figure 1A illustrates the potential energy diagram for a noble gas atom getting trapped in a silica nanocage. It can be seen that the activated physisorption mechanism that traps noble gas atoms has a high desorption energy barrier (*E<sub>des</sub>*).

Figure 1B shows a silicate bilayer structure (side and top views), while Figure 1C shows a hexagonal prism nanocage, the building block of the bilayer structure.<sup>8</sup> Since synthesizing such silicate bilayers is very expensive and time-consuming<sup>10</sup> for practical purposes, my project focuses on developing and testing scalable silicate nanocage<sup>9</sup> materials to trap noble gases, with especial focus on Xenon.

## Electronic Materials and Photonics

### Room 114 - Session EM+2D+BI+QS+TF-TuA

#### Advances in Photonic Materials and Devices

**Moderators:** Leland Nordin, University of Central Florida, Philip Lee, University of Kentucky

2:15pm **EM+2D+BI+QS+TF-TuA-1 New Materials for Metamaterials: Electrochemical Materials and Switchable Chiral Nanostructures**, *Vivian Ferry*, University of Minnesota **INVITED**

Alternative materials for metasurfaces enable new properties and lay the foundation for advantage applications. This talk will discuss two strategies for new, tunable metasurfaces. The first part of the talk will discuss the use of electrolyte gating to control the optical properties of materials, focusing on La<sub>1-x</sub>Sr<sub>x</sub>CoO<sub>3-d</sub> (LSCO) as an exemplary case. We fabricate electric double layer transistors using LSCO and an ion gel, and under application of positive gate voltage gating facilitates the formation and migration of oxygen vacancies, and a transition from a perovskite phase to an oxygen-vacancy-ordered brownmillerite phase. This is accompanied by substantial change in optical properties, as measured with spectroscopic ellipsometry. The talk will discuss how LSCO can be incorporated with metasurfaces to produce tunable optical response. The second part of the talk will discuss chiral metamaterials, and particularly novel materials comprised of

# Tuesday Afternoon, November 5, 2024

nanopatterned, light emitting nanocrystals with simultaneous control over both directionality and polarization state.

**2:45pm EM+2D+BI+QS+TF-TuA-3 Optoelectronic Nanowire Neuron, Thomas Kjellberg Jensen**, Lund University, Sweden; *J. E. Sestoft*, Niels Bohr Institute, Denmark; *D. Aicer*, *N. Löfström*, *V. Flodgren*, *A. Das*, Lund University, Sweden; *R. D. Schlosser*, *T. Kanne Nordqvist*, Niels Bohr Institute, Denmark; *M. Borgström*, Lund University, Sweden; *J. Nygård*, Niels Bohr Institute, Denmark; *A. Mikkelsen*, Lund University, Sweden

Three different semiconductor nanowires are combined into a single optoelectronic artificial neuron. In general, artificial neurons sum and weight input signals, and output a signal according to a non-linear function which may be sigmoid-shaped (a generalized artificial neuron is shown in Fig. 1a). Figure 1b schematically shows the artificial neuron realized using nanowires. Here, neural excitation/inhibition is achieved by balancing inputted light across two pin-diode nanowires outputting a summed voltage measured by a nanowire-based field-effect transistor (FET).

The false-colored electron microscope image shown in Figure 1c depicts the fabricated nanowire neuron. In Figure 1d we show the current measured across the FET nanowire as a function of laser beam position, demonstrating the excitatory and inhibitory behavior. Selectively illuminating the excitatory nanowire diode, the change in conductance follows a sigmoidal curve as a function of linearly increasing light intensity (Figure 1e) – the necessary non-linear part of a neural network. Taken together, these properties provide the device with the basic functionalities needed for a neuromorphic computing node [1,2]. Future measurements will explore the time-domain effects.

Our artificial neuron provides a promising future platform for combining diverse materials with low power consumption and significantly reduced circuit footprint, this way addressing critical limitations for future-proofing photonics-based applications in neuromorphic computing.

## REFERENCES:

- [1] D. O. Winge, S. Limpert, H. Linke, M. T. Borgström, B. Webb, S. Heinze, and A. Mikkelsen, "Implementing an insect brain computational circuit using III-V nanowire components in a single shared waveguide optical network", *ACS Photonics*, vol. 10, pp. 2787-2798, 2020.
- [2] D. Winge, M. Borgström, E. Lind, and A. Mikkelsen, "Artificial nanophotonic neuron with internal memory for biologically inspired and reservoir network computing", *Neuromorph. Comput. Eng.*, vol. 3, no. 034011, 2023.

**3:00pm EM+2D+BI+QS+TF-TuA-4 Modulation of Optical and Plasmonic Properties of Epitaxial and Precision Titanium Nitride Thin Films**, *I. Chris-Okoro*, North Carolina A&T State University; *S. Cheron*, North Carolina A & T State Uni; *C. Martin*, Ramapo College of New Jersey; *V. Craciun*, National Institute for Laser, Plasma, and Radiation Physics, Romania; *S. Kim*, *J. Mahl*, *J. Yano*, Lawrence Berkeley National Laboratory; *E. Crumlin*, Lawrence Berkeley Lab; *D. Kumar*, North Carolina A & T State Uni; **Wisdom Akande**, North Carolina A&T State University

The present study arises from the need for developing negative-permittivity materials beyond commonly employed plasmonic metals (e.g., Au, Ag), which are often incompatible (i.e., low melting point, mechanically soft, chemically unstable) with real operating environments. This work reports a pulsed laser-assisted synthesis, detailed structural characterization using x-ray diffraction (XRD), x-ray photoelectron spectroscopy (XPS), x-ray absorption spectroscopy (XAS), Rutherford Backscattering spectroscopy (RBS), and plasmonic properties of three sets of TiN/TiON thin films. The first two sets of TiN films were grown at 600 and 700 °C under a high vacuum condition ( $\leq 2 \times 10^{-7}$  Torr). The third set of TiN film was grown in the presence of 5 mTorr of molecular oxygen at 700 °C. The purpose of making these three sets of TiN/TiON films was to understand the role of film crystallinity and the role of the oxygen content of TiN films on their optical and plasmonic properties. The results have shown that TiN films deposited in a high vacuum are metallic, have large reflectance, and high optical conductivity. The TiN films, grown in 5 mTorr, were found to be partially oxidized with room temperature resistivity nearly three times larger than those of the TiN films grown under high vacuum conditions.

The optical conductivity of these films was analyzed using a Kramers-Kronig transformation of reflectance and a Lorentz-Drude model; the optical conductivity determined by two different methods agrees very well. The good agreement between the two methods is indicative of a reliable estimate of the absolute value of reflectance in the first place. The existence of significant spectral weight below the interband absorptions is shared between two Lorentzians, one around 250  $\text{cm}^{-1}$  and one around

2,500  $\text{cm}^{-1}$ . We discuss here the dependence of the two bands on the deposition conditions and their effect on the plasmonic performances of TiN/TiON thin films, in particular on the surface plasmon polariton (SPP) and localized surface plasmon resonance (LSPR) quality factors.

This work was supported by the NSF PREM on the Collaborative Research and Education in Energy Materials (CREEM) via grant # DMR-2122067 and the DOE EFRC on the Center for Electrochemical Dynamics And Reactions on Surfaces (CEDARS) via grant # DE-SC0023415.

**3:15pm EM+2D+BI+QS+TF-TuA-5 Nano-Focusing and Characterization of the OAM Beam Through an Optical Fiber Using Plasmonic Nanostructure**, **Rohil Kayastha**, *W. Zhang*, *B. Birmingham*, Baylor University; *Z. Gao*, Texas A&M University; *J. Hu*, Baylor University; *R. Quintero-Torres*, UNAM, Mexico; *A. V. Sokolov*, Texas A&M University; *Z. Zhang*, Baylor University  
Optical vortex beam has been used in many applications such as nanoscale imaging, telecommunication, sensing, and so on due to its unique azimuthal phase distribution. Many of these applications utilize optical fibers as a sensor or to propagate the beam to transmit data and information. The vortex beam carrying an orbital angular momentum (OAM) has a phase singularity giving the beam a doughnut intensity profile. Due to its helical wavefront nature, the vortex beam carrying OAM has also been used to distinguish the enantiomers of the chiral molecule. However, coupling efficiency remains a problem due to the size mismatch of the beam and the molecule. Our work uses vortex fibers with plasmonic nanostructures to nano-focus the vortex beam to enhance the coupling between light and chiral matter. To achieve this goal, characterization of vortex beam in free space and through vortex fiber (a polarization-maintaining ring core optical fiber), and fabrication of nanostructure on fiber facet were performed.

Generation and propagation of OAM beams were characterized in free space and through a vortex fiber. The free-space OAM beam was coupled and transmitted successfully through the vortex fiber with a pure and stable output beam. The helicity characterization and polarization analysis of the free-space and fiber-coupled output vortex beams showed consistent polarization and OAM. The direction of the phase front was maintained after propagation of the OAM through the vortex fiber, as observed from the spiral interference pattern. Nano-focusing of the OAM beam using nanostructure on the fiber facet was observed from the simulation. The circular array of plasmonic nanobars was fabricated on the fiber facet core, and the far-field image of the output OAM beam was observed after transmission through the fiber with the nanostructure. The near-field image of the nano-focused OAM beam on the fiber will be investigated using a near-field scanning optical microscope (NSOM). The focusing of the OAM beam on a fiber facet with the nanostructure could enhance the coupling efficiency of the beam with chiral molecules. The nano-focused OAM on the fiber could be used as a scanning and sensing probe for single-molecule chirality detection.

**4:00pm EM+2D+BI+QS+TF-TuA-8 Templated Block Copolymer Network Thin Films as 3D Chiral Optical Metamaterials: Connecting Finite-Difference Time-Domain and Self-Consistent Field Theory Simulations**, *E. McGuinness*, *B. Magruder*, *P. Chen*, *K. Dorfman*, *C. Ellison*, **Vivian Ferry**, University of Minnesota

Optical metamaterials, whose properties depend not only on material selection but also the spatial arrangement of the material, provide access to interactions with light that are not present in bulk materials alone. Block copolymer self-assembly is a scalable method for creating 3D spatially periodic nanoscale structures to act as metamaterial templates. The gyroid morphology, whose curved, percolating structure is composed of triply connected struts, possesses chiral elements such as helices in bulk and chiral structures at certain surface terminations. As a result of their chirality, when templated with a plasmonic material, gyroids exhibit circular dichroism (CD) with applications in anti-counterfeit as well as molecular and protein sensing. While many optical simulations of gyroids assume a perfect cubic structure, most applications utilize thin films whose processing results in distortions such as compression normal to the substrate or surface rearrangements due to interactions with interfaces. Distorted gyroids, as well as the growing library of additional network structures possible from block copolymer self-assembly, are increasingly challenging to model from a purely mathematical basis and require better basis in physical reality. Combining the output of polymer self-consistent field theory (SCFT) with finite-difference time-domain (FDTD) optical simulations enables the exploration of thermodynamically equilibrated structures for both distorted gyroids and expanded network geometries. This presentation will investigate the CD response of compressed double

# Tuesday Afternoon, November 5, 2024

gyroid thin films as well as that of newly hypothesized network structures such as  $H^{181}$ . In the first example, compression of (110) oriented silver double gyroid thin films yields a switching phenomenon from left to right circularly polarized light preferential absorption, offering the potential for dynamic systems (**Figure 1a**). Mechanistically, this behavior depends both on the surface and sub-surface structures of the compressed double gyroids. In the second example, (001) oriented silver templated thin films of the newly computationally uncovered  $H^{181}$  structure are shown to support a broadband visible light CD response (spanning 200 nm) with a g-factor (CD normalized to average absorption) of at least 0.14 across that entire wavelength range (**Figure 1b**). Overall, this work moves the optical simulations of metamaterials from block copolymers closer those physically realized, introducing additional opportunities for engineering their optical response.

4:15pm **EM+2D+BI+QS+TF-TuA-9 Solution Processing of Optical Phase Change Materials**, *Brian Mills*, Massachusetts Institute of Technology; *R. Sharma, D. Wiedeman*, University of Central Florida; *C. Schwarz*, Ursinus College; *N. Li*, Massachusetts Institute of Technology; *E. Bissell*, University of Central Florida; *C. Constantin Popescu*, Massachusetts Institute of Technology; *D. Callahan*, Charles Stark Draper Laboratory, Inc.; *P. Banerjee, K. Richardson*, University of Central Florida; *J. Hu*, Massachusetts Institute of Technology

Chalcogenide optical phase change materials (O-PCM) serve as the functional material in a variety of non-volatile photonic devices, from reconfigurable metasurface lenses to tunable integrated photonic resonators. Although a handful of high figure of merit O-PCMs have been identified and implemented in prototype devices, the space of O-PCM composition remains relatively unexplored, precluding the possibility of application specific choices in material composition that optimize device performance. This is due, in large part, to the lack of time and cost efficient methods for O-PCM thin film deposition and characterization, for which vacuum chamber deposition is the most common method. In this work, we present the first implementation of a solution processing approach for O-PCM film synthesis and deposition, providing evidence of the method's viability in creating high quality, functioning O-PCM films with close adherence to target stoichiometry. This method serves as a robust platform for materials exploration of O-PCM composition and allows for the identification of candidate O-PCM, as well as an understanding of the effect of compositional changes in O-PCM optical and cycling properties.

4:30pm **EM+2D+BI+QS+TF-TuA-10 Effects of Ce Concentration on the Microstructural, Optical, and Luminescence Properties in Ce:GAGG Ceramic Phosphors**, *William Bowman*, *S. Lass*, University of Central Florida; *F. Moretti, W. Wolszczak*, Lawrence Berkeley National Laboratory; *R. Gaume*, University of Central Florida

Efficient luminescence and optical quality are necessary phosphor attributes for applications such as down-conversion layers in photovoltaics and computed tomography. Cerium-doped gadolinium aluminum gallium garnet (Ce:GAGG) is highly applicable for these purposes. It has been shown in other garnet hosts such as Ce:YAG and Ce:LuAG that Ce concentration alters both the luminescence and optical properties of the materials. In the case of Ce:GAGG single crystals and Ce concentrations lower than 1 at%, radioluminescence decay constants decrease by increasing the Ce concentration while light yield reaches a maximum at 0.3 at%. For Ce:GAGG ceramics, the effect of Ce concentration on these properties has not been systematically investigated. There is at current no work on determining the solid solubility limit of Ce in GAGG, which is critical in controlling the development of secondary phases and subsequent optical quality.

This study aims to investigate the effects of Ce concentration on the microstructural, optical, and luminescence properties of GAGG optical ceramics with dopant concentrations in the 0.1at% to 10at% range. Transmission of the material increases with increasing Ce concentration up to 5.0at%. At the same time, the optical and luminescence properties of these samples show a complex evolution upon Ce concentration, highlighting the complex interplay among optical characteristics of the samples, concentration-related luminescence quenching phenomena, and charge carrier trapping defects.

This material is based upon work supported by the U.S. Department of Homeland Security under Grant Award Number 20CWDARI00038-01-00. The views and conclusions contained in this document are those of the authors and should not be interpreted as necessarily representing the

official policies, either expressed or implied, of the U.S. Department of Homeland Security.

4:45pm **EM+2D+BI+QS+TF-TuA-11 Solution Based Processing of Ge<sub>2</sub>Sb<sub>2</sub>Se<sub>4</sub>Te<sub>1</sub> Phase Change Material for Optical Applications**, *Daniel Wiedeman, R. Sharma, E. Bissel, P. Banerjee*, University of Central Florida; *B. Mills, J. Hu*, Massachusetts Institute of Technology; *M. Sykes, J. Stackawitz, J. Lucinec, C. Schwarz*, Ursinus College; *K. Richardson*, University of Central Florida

Chalcogenide based phase change materials are important for creating novel optical and photonic devices, improving on current devices for future applications. Solution processing, via dip coating, spin coating, or drop-casting, is a low-cost, high-throughput alternative method of depositing thin films, which allows for greater composition diversity. In this work, we performed a detailed systematic study of the solution derived drop-casted film of Ge<sub>2</sub>Sb<sub>2</sub>Se<sub>4</sub>Te<sub>1</sub> alloy in an ethylenediamine and ethanedithiol mixture. The composition, morphology and structural properties of the films were analyzed by employing scanning electron microscopy, energy dispersive X-ray spectroscopy, Raman spectroscopy, and X-ray diffraction. Our findings provide insight into a potential route for scalable Ge<sub>2</sub>Sb<sub>2</sub>Se<sub>4</sub>Te<sub>1</sub> films.

5:00pm **EM+2D+BI+QS+TF-TuA-12 Multi-Dimensional p-WSe<sub>2</sub>/n-Ga<sub>2</sub>O<sub>3</sub> Enhancement-Mode Phototransistors for Stand-Alone Deep-Ultraviolet Sensing**, *J. Kim, Soobeen Lee*, Seoul National University, South Korea

$\beta$ -Ga<sub>2</sub>O<sub>3</sub> is an ultra-wide bandgap (UWBG) semiconductor with a bandgap of 4.9 eV, resulting in a high breakdown field of approximately 8 MV/cm and a high Baliga's figure-of-merit.  $\beta$ -Ga<sub>2</sub>O<sub>3</sub> is a promising material for deep-ultraviolet (DUV) photodetector (PD) applications due to its direct bandgap of 4.9 eV, excellent thermal stability, and high absorption coefficient. Self-powered  $\beta$ -Ga<sub>2</sub>O<sub>3</sub> PDs can be realized through p-n heterojunction (HJ) field-effect transistor architectures, exhibiting normally-off operation owing to the depletion region in the  $\beta$ -Ga<sub>2</sub>O<sub>3</sub> channel. With intrinsic n-type conductivity caused by unintentional doping and challenges in p-type doping, fabricating self-powered  $\beta$ -Ga<sub>2</sub>O<sub>3</sub> PDs necessitates combining  $\beta$ -Ga<sub>2</sub>O<sub>3</sub> with p-type semiconductors such as transition-metal dichalcogenides (TMDs), nickel oxide, or silicon carbide. Tungsten diselenide (WSe<sub>2</sub>), one of the TMDs, stands out as a promising material with a high monolayer mobility of approximately 180 cm<sup>2</sup>V<sup>-1</sup>s<sup>-1</sup>. Their dangling-bond-free surfaces provide an advantage in forming sharp interfaces with other materials in HJs. Moreover, efficient p-type doping of WSe<sub>2</sub> is achieved via charge transfer by utilizing the high electron affinity of its self-limiting oxide, sub-stoichiometric tungsten oxide (WO<sub>3-x</sub>), which is used as a dopant.

In this work, we introduce normally-off p-WSe<sub>2</sub>/n- $\beta$ -Ga<sub>2</sub>O<sub>3</sub> phototransistors and demonstrate their self-powered operation under 254 nm light. p-Type WSe<sub>2</sub> was realized through charge transfer doping of WO<sub>3-x</sub> formed by O<sub>3</sub> treatment, and the p-type doping effect of this oxide was confirmed through electrical characteristics. The cross-sectional structure of the fabricated p-WSe<sub>2</sub>/n- $\beta$ -Ga<sub>2</sub>O<sub>3</sub> phototransistors was analyzed, and the electrical and optical properties were evaluated before and after WSe<sub>2</sub> oxidation. The device demonstrated a responsivity of 2 A/W under 254 nm light without an external bias, surpassing the performance of previously reported p-n HJ-based  $\beta$ -Ga<sub>2</sub>O<sub>3</sub> PDs. Furthermore, we investigate the enhanced optoelectronic performance of multi-dimensional  $\beta$ -Ga<sub>2</sub>O<sub>3</sub> phototransistors with plasmonic metal nanoparticles. In this presentation, we will discuss the potential of the self-powered multi-dimensional DUV  $\beta$ -Ga<sub>2</sub>O<sub>3</sub> PDs with improved performance and their prospects in practical applications.

This work was supported by Korea Institute for Advancement of Technology (KIAT) grant funded by the Korea Government (P0012451, The Competency Development Program for Industry Specialist) and the Korea Research Institute for defense Technology planning and advancement (KRIT) grant funded by Defense Acquisition Program Administration (DAPA) (KRIT-CT-21-034, and KRIT-CT-22-046).



# Wednesday Morning, November 6, 2024

## 2D Materials

### Room 122 - Session 2D+EM+MI+QS-WeM

#### 2D Materials: Heterostructures, Twistronics, and Proximity Effects

**Moderators:** Aaron Bostwick, Advanced Light Source, Lawrence Berkeley National Laboratory, Tiancong Zhu, Purdue University

8:00am **2D+EM+MI+QS-WeM-1 Van der Waals Semiconductors: From Stacking-Controlled Crystals to Unconventional Heterostructures, Peter Sutter, E. Sutter, University of Nebraska - Lincoln** **INVITED**

2D materials have attracted broad interest due to novel properties that arise in atomically thin crystals. As interesting scientifically and important technologically, but much less explored are van der Waals (vdW) crystals that, assembled from 2D building blocks, lie between a monolayer and the bulk. In this regime, phenomena such as phase separation, transformations between crystal polymorphs, and competition between different stacking registries provide unprecedented opportunities for controlling morphology, interface formation, and novel degrees of freedom such as interlayer twist. But going beyond a single layer also poses significant challenges, both due to the diversity of the possible few-layer structures and the difficulty of probing functionality such as optoelectronics and ferroics at the relevant length scales.

Here, we discuss our recent research that addresses these challenges focusing on group IVA chalcogenides, an emerging class of anisotropic layered semiconductors promising for energy conversion, optoelectronics, and information processing. Advanced *in-situ* microscopy provides insights into the growth process, interlayer twisting, and emerging functionality such as stacking-controlled ferroelectricity. Nanometer-scale electron excited spectroscopy identifies photonic light-matter hybrid states and reveals anisotropic and valley-selective charge carrier flows across interfaces in heterostructures. Our results highlight the rich sets of materials architectures and functionalities that can be realized in van der Waals crystals and heterostructures beyond the 2D limit.

8:30am **2D+EM+MI+QS-WeM-3 Deterministic Assembly, Transfer, and Flipping of 2D Materials Using Tunable Polymer Films, Jeffrey J. Schwartz, S. Le, University of Maryland, College Park; K. Grutter, A. Hanbicki, A. Friedman, Laboratory for Physical Sciences**

Assembly of two-dimensional (2D) materials into van der Waals heterostructures is a crucial step in creating precisely engineered nanoscale and quantum devices for use in a wide variety of spintronic, electronic, and other applications. Numerous strategies exist to pick-up, stack, transfer, and even flip over these atomically thin structures. One popular strategy leverages the ability to tune the adhesion between a polymer stamp and 2D sheets to pick-up, stack, and release structures at different temperatures. Although relatively easy to implement, this technique is tedious to perform and has a low throughput. Here, we demonstrate a significant improvement to a deterministic, all-dry, polymer-assisted transfer technique using polyvinyl chloride (PVC) thin films to manipulate 2D materials and to fabricate devices. We construct stamps from pairs of commercially available PVC films that controllably pick-up and release 2D sheets within known, overlapping temperature ranges. These mechanically durable stamps can be produced quickly and without the time-consuming preparation and annealing steps required by most other commonly used polymers. Importantly, these stamps not only facilitate deterministic transfer of 2D materials, but they also enable polymer-to-polymer transfer (e.g., between separate stamps) and flipping of material stacks to create inverted heterostructures that are important for many applications, including scanning tunneling microscopy measurements. We characterize the thermal transition properties of the PVC films employed here as well as assay the cleanliness and performance of devices produced using this technique. These improvements enable rapid production of 2D devices with fewer interactions required by the operator, which is especially significant when working in controlled environments (e.g., glovebox) or in remote or autonomously controlled contexts.

8:45am **2D+EM+MI+QS-WeM-4 Cleaning of Low-Dimensionality Materials: Challenge and Solutions, Jean-Francois de Marneffe, P. Wyndaele, M. Timmermans, C. Cunha, IMEC, Belgium; B. Canto, Z. Wang, AMO GmbH, Aachen, Germany; R. Slaets, G. He, I. Asselberghs, C. J. Lockhart de la Rosa, G. Sankar Kar, C. Merckling, S. De Gendt, IMEC, Belgium**

Over the last few years, significant efforts have been made in exploring low-dimensionality materials such as single layer Graphene (SLG), transition metal dichalcogenides (TMDCs) and carbon nanotubes (CNTs), for a wide

range of applications covering beyond CMOS logic, EUV pellicles, photonics, and sensing (amongst others). Due to their intrinsic 2D or 1D nature, these materials are highly sensitive to processing damage leading to stoichiometric changes or crystalline defects. Among the many manufacturing steps required for building devices, the cleaning of these systems is an absolute requirement and a bottleneck. Typically, during processing, residual polymers or carbon of ambient origin, do contaminate the surface leading to nanometric deposits that change the intrinsic transport/optical properties of the materials, and cause parasitic dielectric drift or high contact resistance. Wet cleaning, using organic solvents, is a mainstream approach, which proves to be inefficient for irreversibly physically adsorbed polymer residues. In this paper, we explore dry cleaning approaches, based on plasma treatment and UV cure. Plasma-based cleaning proves to be very efficient but leads to material damage, which can be minimized by tuning the average ion energy, the processing temperature, the plasma chemistry or adding a post-cleaning restoration step. For TMDCs, damage consist essentially in the creation of chalcogen vacancies, which lead to metal oxidation upon ambient exposure. For Graphene and CNTs, damage consist in carbon vacancies, causing lattice distortions, oxidation and ultimately a dramatic change of the material's transport properties. Part of this presentation will explore the use of UV cure, which is a known method for cleaning polymers from semiconductor surfaces.

9:00am **2D+EM+MI+QS-WeM-5 Spin-Valley Physics in Mixed-Dimensional Van Der Waals Heterostructures, Vikram Deshpande, University of Utah** **INVITED**

Spin-valley physics has become ubiquitous in 2D materials-based van der Waals (vdW) heterostructures, particularly those hosting flat bands, wherein various ground states with spin-valley character including magnetic, insulating and superconducting states have been observed. On the other hand, mixed dimensional vdW heterostructures, such as those between 2D and 1D materials have been less explored for intricate spin-valley physics. The reduced phase space for scattering in 1D in particular might lead to qualitatively different phenomena. We are guided by our studies of ultraclean carbon nanotube quantum dots wherein we have observed subtle effects from the degeneracy lifting between the speeds of right- and left-moving electrons within a given Dirac cone or valley. Bound states can be purely fast-moving or purely slow-moving, giving rise to incommensurate energy level spacings and a vernier spectrum. Using quantum interferometry [1] and Coulomb blockade spectroscopy [2] of such ultraclean carbon nanotube quantum dots, we have found evidence for this vernier spectrum. The addition-energy spectrum of the quantum dots reveals an energy-level structure that oscillates between aligned and misaligned energy levels. Our data find that the fast- and slow-moving bound states hybridize at certain gate voltages. We extend existing theory to show that our experiment probes the degree of isospin polarization/hybridization of the various quantum states probed in our system. As a result, gate-voltage tuning can select states with varying degrees of hybridization, suggesting numerous applications based on accessing this isospin degree of freedom in conjunction with 2D materials in the form of mixed dimensional vdW heterostructures. We have fabricated prototypical mixed dimensional vdW heterostructures between carbon nanotubes and 2D materials and extended our measurements to these structures. I will discuss our recent and ongoing work studying spin-valley physics in such systems.

References:

Lotfzadeh, N.; Senger, M. J.; McCulley, D. R.; Minot, E. D.; Deshpande, V. V. Quantum Interferences in Ultraclean Carbon Nanotubes. *Phys. Rev. Lett.* 2021, 126 (21), 216802. <https://doi.org/10.1103/PhysRevLett.126.216802>.

Berg, J.; Lotfzadeh, N.; Nichols, D.; Senger, M. J.; De Gottardi, W.; Minot, E. D.; Deshpande, V. V. Vernier Spectrum and Isospin State Control in Carbon Nanotube Quantum Dots. *arXiv* November 20, 2023. <http://arxiv.org/abs/2311.12332>.

9:30am **2D+EM+MI+QS-WeM-7 Exploring Incommensurate Lattice Modulations in BSCCO van der Waals Heterostructures: Implications for Q-Bit Development, Patryk Wasik, Brookhaven National Laboratory; S. Zhao, Harvard University; R. Jangid, Brookhaven National Laboratory; A. Cui, Harvard University; J. Sinsheimer, Brookhaven National Laboratory; P. Kim, Harvard University; N. Poccia, IFW Dresden, Germany; C. Mazzoli, Brookhaven National Laboratory**

Quantum computers (QC) are poised to revolutionise computational capabilities by naturally encoding complex quantum computations, thereby

# Wednesday Morning, November 6, 2024

significantly improving computation time compared to silicon-based technologies. Currently, Q-bits, the essential components of QCs, are made from conventional superconductors that operate efficiently only near absolute zero temperatures. To address this limitation, two-dimensional van der Waals (vdW) encapsulated high-temperature superconductor (HTSC) stacks have been proposed as future Q-bit candidates, driven by recent advancements in nanofabrication techniques. However, a detailed understanding of their structural and electronic properties is crucial.

We present low-temperature resonant soft X-ray investigations on ultrathin  $\text{Bi}_2\text{Sr}_2\text{CaCu}_2\text{O}_{8-y}$  (BSCCO) vdW heterostructures, promising candidates for large-scale Q-bit applications. BSCCO crystals exhibit two incommensurate lattice modulations (ILMs), providing an excellent opportunity to explore the relationship between structure and electronic behaviour in low dimensions. We report ILMs (Cu  $L_3$ ) and structural peak (off resonance) maps obtained across the superconducting transition temperature ( $T_c \approx 60$  K). These signals, under external gating, present significant potential for further exploration offering new insights into the electronic interactions in vdW HTSC systems.

11:00am **2D+EM+MI+QS-WeM-13 Atomic Layer Deposition of Transition Metal Dichalcogenides: Precursors, Processes, and Applications Perspectives**, *Thong Ngo, A. Azcatl, N. Vu, C. Cheng, M. Miller, C. Chen, R. Kanjolia, M. Moinpour, M. Clark*, EMD Electronics, USA **INVITED**

Transition metal dichalcogenides (TMD) are three-atom-thick layer materials that possess a wide array of properties, such as insulating, semiconducting, conducting, and superconducting. While there has been a significant amount of research on TMD for various applications including energy storage, photovoltaics, biomedical, catalysis, hydrogen production processes, and healthcare, the usage of TMD for electronic applications has been researched most in the past two decades.

Each layer of TMD is a 2D sheet with the thickness of  $\sim 6\text{-}7\text{\AA}$ . These layers are bonded by Van der Waals force. The ultra-thin structure enables TMD for semiconductor industry applications, which continuously requires both size-scaling of materials layers and electrical performance improvement of devices. The semiconductor-range band gap and the high electron/hole mobility of several TMD, such as  $\text{MoS}_2$ ,  $\text{WS}_2$ ,  $\text{WSe}_2$ , and  $\text{MoSe}_2$  allow their usage for high mobility ultra-thin channel transistor. In addition, the relatively high conductivity of some other TMD, such as  $\text{TaS}_2$  and  $\text{NbS}_2$  make them promising candidates for interconnect barrier/liner as a replacement of TaN/Ta bilayer.

TMD materials need to pass certain quality requirements to provide desirable property/performance; therefore, method of synthesizing TMD plays an important role for high quality materials. Solution-based deposition, non-vacuum electrodeposition, polymer-assisted deposition, physical vapor deposition (PVD), chemical vapor deposition (CVD), and atomic layer deposition (ALD) have been used to deposit ultra-thin TMD. Among these techniques, CVD is the most popular deposition method, and to date, the highest quality of TMD for semiconductor applications is CVD-TMD. However, the need of lower thermal budget, better layer controllability, uniformity, and conformality requires the semiconductor community to explore ALD methods. In this presentation, we will review multiple ALD processes for TMD including precursors, process requirements for high mobility channel and barrier/liner applications. We will highlight challenges of TMD applications for logic, memory, and interconnects. The presentation will also feature our recent work on ALD  $\text{MoS}_2$  for high-mobility channel transistor with  $>5$  decades On/Off ratio and  $>1 \mu\text{A}/\mu\text{m}$  Ion. Our achievement of 300mm ALD  $\text{MoS}_2$  deposition brings ultra-thin TMD materials closer to a manufacturable fab process for semiconductor industry.

11:30am **2D+EM+MI+QS-WeM-15 Writing and Detecting Topological Spin Textures in Exfoliated  $\text{Fe}_3\text{-xGeTe}_2$** , *Luis Balicas*, Florida State University - National High Magnetic Field Lab - FSU Quantum Initiative

$\text{Fe}_3\text{-xGeTe}_2$  is a centrosymmetric, layered van der Waals (vdW) ferromagnet that displays Curie temperatures  $T_c$  (270-330 K) that are within the useful range for spintronic applications. Little is known about the interplay between its topological spin textures (e.g., merons, skyrmions) with technologically relevant transport properties such as the topological Hall effect (THE), or topological thermal transport. We found via high-resolution Lorentz transmission electron microscopy that merons and anti-meron pairs coexist with Néel skyrmions in  $\text{Fe}_3\text{-xGeTe}_2$  over a wide range of temperatures and probe their effects on thermal and electrical transport [1]. It turns out that we detect a THE, even at room  $T$ , that senses merons at higher  $T$ 's as well as their coexistence with skyrmions as  $T$  is lowered, indicating an on-demand thermally driven formation of either type of spin

texture. Remarkably, we also observe an unconventional THE, i.e., in absence of Lorentz force, and attribute it to the interaction between charge carriers and magnetic field-induced chiral spin textures. We find that both the anomalous Hall effect (AHE) and THE can be amplified considerably by just adjusting the thickness of exfoliated  $\text{Fe}_3\text{-xGeTe}_2$ , with the THE becoming observable even under zero magnetic field due to a field-induced unbalance in topological charges [2]. Using a complementary suite of techniques, including electronic transport, Lorentz transmission electron microscopy, and micromagnetic simulations, we reveal the emergence of substantial coercive fields upon exfoliation, which are absent in the bulk, implying thickness-dependent magnetic interactions that affect the topological spin textures (TSTs). We detected a 'magic' thickness of  $t \sim 30$  nm where the formation of TSTs is maximized, inducing large magnitudes for the topological charge density, and the concomitant AHE and THE resistivities at  $T \sim 120$  K. Their values are observed to be higher than those found in magnetic topological insulators and, so far, the largest reported for 2D magnets. The hitherto unobserved THE under zero magnetic field could provide a platform for the writing and electrical detection of TSTs aiming at energy-efficient devices based on vdW ferromagnets.

[1] B. W. Casas *et al.*, *Adv. Mater.* **35**, 202212087 (2023).

[2] A. Moon *et al.*, *ACS Nano* **18**, 4216-4228 (2024).

## Magnetic Interfaces and Nanostructures Room 121 - Session MI+2D+AC+TF-WeM

### Altermagnetism and Spin-Dependent Systems

**Moderators:** Markus Donath, Muenster University, Germany, Valeria Lauter, Oak Ridge National Laboratory

8:00am **MI+2D+AC+TF-WeM-1 Twisted Electrons in Momentum Space: A Photoemission Perspective on Spin and Orbital Angular Momentum in Quantum Materials**, *Maximilian Ünzelmann*, University of Würzburg, Germany; *B. Geldiyev*, University of Würzburg, Germany; *T. Figgemeier*, University of Würzburg, Germany; *H. Bentmann*, NTNU Trondheim, Norway; *F. Reinert*, University of Würzburg, Germany **INVITED**

Beyond the spin, electronic states in crystalline solids can exhibit finite expectation values of orbital angular momentum (OAM). This phenomenon has attracted considerable attention in recent years and can particularly be traced back to the following key applications: (i) Since OAM is formed solely by inversion symmetry breaking (ISB) – and thus can also be present without magnetism or strong spin-orbit coupling (SOC) – it appears as an interesting quantum degree of freedom raising the potential of orbital analogs to spintronic phenomena, i.e. the field of *orbitronics*. (ii) OAM has been proposed to be a useful observable to assess nontrivial topology in the band structure of topological quantum matter. Lastly, if the atomic SOC strength is sizable, OAM is coupled to the electron spin giving rise to rich spin and orbital momentum space textures.

In this talk, I will shed light on those textures from the perspective of angle-resolved photoemission spectroscopy (ARPES). Combining ARPES with light-polarization-dependent and spin-resolved measurements allows us to address the momentum-dependent properties of the spatial and spin part of the wave functions, respectively. I will present experimental results on model-like monolayer systems and topological quantum materials and show that – as well as how – the complex interplay of ISB and SOC forms striking spin-orbital textures. Based on these findings, I will discuss the potential of utilizing OAM (i) towards orbitronic transport and (ii) to detect unexpected topological features.

8:30am **MI+2D+AC+TF-WeM-3 Falicov Student Award Finalist Talk: Gap Tuning by Hole Doping in  $\text{EuZn}_2\text{As}_2$  Semimetal**, *Dejia Kong*<sup>1</sup>, University of Virginia; *S. Karbasizadeh*, University of South Carolina; *G. Narasimha*, Oak Ridge National Laboratory; *P. Regmi*, University of South Carolina; *C. Tao*, Oak Ridge National Laboratory; *S. Mu*, University of South Carolina; *R. Vasudevan*, Oak Ridge National Laboratory; *I. Harrison*, University of Virginia; *R. Jin*, University of South Carolina; *Z. Gai*, Oak Ridge National Laboratory

$\text{EuZn}_2\text{As}_2$  is an ideal candidate for topological magnetism study in comparison to other europium-based semimetals that exhibit a similar type of magnetic transition from the antiferromagnetic phase to the

<sup>1</sup> Falicov Student Award Finalist

# Wednesday Morning, November 6, 2024

ferromagnetic phase at a low temperature.<sup>1</sup> Theoretical calculations predict gapped and flatter bands in  $\text{EuZn}_2\text{As}_2$  but a gapless  $\Gamma$  point in  $\text{EuCd}_2\text{As}_2$ .<sup>2</sup> In this work, a low-temperature cleaved  $\text{EuZn}_2\text{As}_2$  crystal is studied using scanning tunneling microscopy/spectroscopy (STM/S) and density functional theory (DFT). A group of triangular-shaped defects in combining with the DFT calculations are used to identify the existence of the europium-terminated and arsenic-terminated surfaces at the cleavage. Large bandgaps are observed on the two pristine terminations. However, the bandgap width is found to be very sensitive to local heterogenous, like defects and step edges. Two defect groups that create local electron deficiency, i.e. substitutional defect of As replacing Zn, and Zn vacancy, can drastically lower the bandgap. Furthermore, the modification of the bandgap width shows a discrepancy on the two terminations, bigger on Eu termination but much smaller on As-Zn termination. So, we predict that purposely hole doping the system during the crystal growth stage may create a new topological semimetal material with a gapless europium layer sandwiched by a gapped As-Zn lattice.

Reference:

1 Blawat, J. *et al.* Unusual Electrical and Magnetic Properties in Layered  $\text{EuZn}_2\text{As}_2$ . *Adv Quantum Technol* **5** (2022).

2 Wang, Z. C. *et al.* Anisotropy of the magnetic and transport properties of  $\text{EuZn}_2\text{As}_2$ . *Phys Rev B* **105** (2022).

8:45am **MI+2D+AC+TF-WeM-4 Characterization of  $\text{LaMnO}_3/\text{SrTiO}_3$  Thin Films and Its Mn Valence State Correlated with Ferromagnetism, Ghadendra Bhandari, P. Tavazohi, V. Dewasurendra, M. Johnson, M. Holcomb, West Virginia University**

Thin films of  $\text{LaMnO}_3$  (LMO) /  $\text{SrTiO}_3$  (STO) perovskite have gained interest for their abilities to be an essential component of some heterostructures while still exhibiting an interesting magnetic phase diagram. We have grown  $\text{LaMnO}_3$  thin films on  $\text{SrTiO}_3$  using pulsed laser deposition and deposition has been monitored by reflection high energy electron diffraction (RHEED) to verify layer-by-layer growth. Structure and magnetic properties have been characterized by X-ray diffractometry (XRD), and vibration sample magnetometry (VSM).  $\text{LaMnO}_3$  thin films exhibit ferromagnetic FM phases whereas bulk  $\text{LaMnO}_3$  is antiferromagnetic A-type. All thin films are coherently strained, forcing them to have the in-plane lattice parameter of the STO substrate (3.905 Å), but the out-of-plane parameter varies (3.89-3.93 Å). The variation in the c-lattice is developed from  $\text{O}_2$  growth pressure and consequently the Mn cation is in mixed valence state  $\text{Mn}^{3+/4+}$ . The valence state of the Mn cation is realized from XPS and XAS study. The ferromagnetic magnetization is originated by the double exchange of  $\text{Mn}^{3+}$ - $\text{O}$ - $\text{Mn}^{4+}$ . The thickness averaged magnetizations from PNR measurements are comparable with magnetization obtained from VSM. The strength of magnetization correlates with content of  $\text{Mn}^{4+}$ .

9:00am **MI+2D+AC+TF-WeM-5 Altermagnetism: From Spintronics to Unconventional Magnetic Phases, Libor Šmejkal, Uni Mainz, Germany INVITED**

The search for unconventional quantum phases that break the symmetries of the crystal lattice has been a focus in physics since the early days of quantum theory, driven by both fundamental interest and potential applications. Prominent examples include cuprate superconductors, which are known for their unconventional d-wave Cooper pairing, and dissipationless transport.

In this presentation, we will discuss our recent discovery[1] of an unconventional magnetic phase motivated by our earlier predictions and observations of unconventional spintronics effects [2,3,4]. This unconventional phase, altermagnetism (see Figure), unlike common ferromagnetism and antiferromagnetism, breaks the symmetries of the crystal lattice, and features d, g, or i-partial wave characteristics simultaneously in its spin and electronic structure[1]. D-wave altermagnetism thus represents magnetic analogue of d-wave superconductivity.

We identified altermagnetism by employing and developing a symmetry framework that considers paired transformations involving electron spin and the crystal lattice. This framework is emerging as a new paradigm in the study of magnetic crystals. We will demonstrate its usefulness by discussing (i) the altermagnetic band structure of the semiconductor  $\text{MnTe}$ , which we recently experimentally observed through collaborative work using photoemission spectroscopy[5], and (ii) our identification of more than 240 realistic altermagnetic candidates.

Additionally, we will explore the rapid expansion of altermagnetic concepts to many fields with focus on ultrafast spintronics memories[6],

dissipationless transport [2-4] and two-dimensional band topology [7]. Finally, we will outline the latest developments in the field, including the theoretical identification of the magnetic analog of superfluid helium-3 and we will propose transport experiments which can be used for its detection[8].

[1] L. Šmejkal, J. Sinova, and T. Jungwirth, *Phys. Rev. X* **12**, 031042 (2022)

[2] L. Šmejkal, *et al.*, *Sci. Adv.* **6**, eaaz8809 (2020)

[3] I. Mazin, *et al.*, *PNAS* **118**, e2108924118 (2021)

[4] H. Reichlová, *et al.*, *Nature Communications* **15**, 4961 (2024)

[5] J. Krempasky\*, L. Šmejkal\*, S. Souza\*, *et al.*, *Nature*, **626**, 517 (2024)

[6] L. Šmejkal *et al.*, *Phys. Rev. X* **12**, 011028 (2022)

[7] I. Mazin, R. Gonzalez-Hernandez, and L. Šmejkal, *arXiv:2309.02355* (2023)

[8] Birk Hellenes, *et al.*, *arXiv:2309.01607v2* (2024)

9:30am **MI+2D+AC+TF-WeM-7 Growth Study of Kagome-structured  $\text{Mn}_3\text{Sn}$  on Gallium Nitride (000\_1) Using Molecular Beam Epitaxy, H. Hall, S. Upadhyay, T. Erickson, A. Shrestha, A. Abbas, Arthur Smith, Ohio University**

Over the past few years, there has been a large amount of interest in Kagome-structured magnetic materials with non-collinear antiferromagnetic ordering [1]. Such materials show interesting magnetic properties including anomalous Hall effect and topological Hall effect [2]. In recent work, we have reported growth of  $\text{Mn}_3\text{Sn}$  on sapphire (0001) which resulted in either *a*-plane or *c*-plane film orientations [3,4]. The substrate however was not ideal, and frequently we observed the disappearance of the diffraction pattern upon opening the Mn and Sn shutters with the pattern reappearing after some amount of resting time. In the case of the *c*-plane orientation, theory suggested this could be due to interfacial disordering of the lattice. This might be due to the ~19% lattice mismatch which also is one reason for the preferred growth of *a*-plane oriented  $\text{Mn}_3\text{Sn}$  on sapphire (0001) due to the much smaller lattice mismatch (<5%) along that direction. Nonetheless, high quality films prove difficult to obtain on sapphire (0001), and a better substrate is desirable. As such, we have investigated the growth of  $\text{Mn}_3\text{Sn}$  films on freshly grown gallium nitride surfaces. The  $\text{Mn}_3\text{Sn}$  growth follows immediately after the growth of N-polar GaN (000 $\bar{1}$ ), thus giving a perfectly clean and well-ordered substrate surface with only ~2.66% lattice mismatch along the 30° line to the high symmetry axis of GaN. We have investigated this as a function of substrate temperature and find an optimal temperature range in which streaky and clear RHEED patterns are obtained from the beginning of the growth. Next plans include studying of this surface with high-resolution STM and spin-polarized STM. This research has been supported by the U.S. Department of Energy, Office of Basic Energy Sciences, Division of Materials Sciences and Engineering under Award No. DE-FG02-06ER46317.

[1] H. Yang *et al.*, *New J. of Physics* **19**, 015008 (2017).

[2] S. Nakatsuji, N. Kiyohara, and T. Higo, *Nature* **527**, 212 (2015).

[3] S. Upadhyay *et al.*, *J. Vac. Sci. & Technol. A* **41**, 042710 (2023).

[4] S. Upadhyay *et al.*, *Surfaces and Interfaces* **42**, 103379 (2023).

9:45am **MI+2D+AC+TF-WeM-8 Exchange Bias Effect in Single-Layer Antiferromagnetic  $\text{Mn}_3\text{GaN}$  Films, Ali Abbas, A. Shrestha, Ohio University; D. Russell, F. Yang, The Ohio State University; A. Smith, Ohio University**

Strain-induced spin structures in non-collinear antiferromagnetic materials like  $\text{Mn}_3\text{GaN}$  can be controlled by an external magnetic field[1][2]. In this work, we report the intrinsic exchange bias in the “single” antiferromagnetic  $\text{Mn}_3\text{GaN}$  films fabricated by epitaxial growth of  $\text{Mn}_3\text{GaN}$  on  $\text{MgO}$  (001) substrate using molecular beam epitaxy under *in-plane* tensile and *out-of-plane* compressive strain. Scanning transmission electron microscopy confirms significant strain at the  $\text{Mn}_3\text{GaN}/\text{MgO}$  interface due to substrate induced tetragonal distortion. Superconducting quantum interference device measurements reveal an exchange bias field ( $H_{\text{eb}}=1225$  Oe) and a vertical magnetization shift below 300 K. Furthermore, magnetization *M* vs. the applied field *H* measurements from 300K down to 50K reveal the consistent horizontal and vertical shift of the hysteresis loop, which are usually observed only in ferro-/antiferromagnetic bilayers. Here, the exchange bias effect may be attributed to strain, leading to canted and uncompensated Mn spins coupled with an upper antiferromagnetic region, as reported in another system [2][3]. The findings of strain-induced exchange bias in antiferromagnetic  $\text{Mn}_3\text{GaN}$  films may open a new route/ novel system for spintronic properties by design. This research has been supported by the U.S. Department of Energy, Office of Basic Energy Sciences, Division of

# Wednesday Morning, November 6, 2024

Materials Sciences and Engineering under Award No. DE-FG02-06ER46317 (work done at Ohio University, not including XRD) and under award No. DE-SC0001304 (XRD and SQUID measurements done at The Ohio State University).

References:

- [1] X.F. Zhou et al., "Exchange Bias in Antiferromagnetic Mn<sub>3</sub>Sn Monolayer Films," *Physical Review Applied*, 14(5), 054037 (2020).
- [2] B. Cui et al., "Strain engineering induced interfacial self-assembly and intrinsic exchange bias in a manganite perovskite film". *Scientific reports*, 3(1), 2542, (2013).
- [3] L. Wang et al., "Exchange bias and vertical shift of the magnetic hysteresis loop in Co/BiFeO<sub>3</sub> bilayers. *Ferroelectrics Letters Section*, 48(4-6), 65-71, (2021).

11:00am **MI+2D+AC+TF-WeM-13 L-Gap Surface Resonance at Pt(111): Influence of Atomic Structure, d Bands, and Spin-Orbit Interaction**, **Markus Donath**, F. Schöttke, P. Krüger, University of Münster, Germany; L. Hammer, T. Kiblinger, M. Schneider, University of Erlangen-Nürnberg, Germany

Pt(111) hosts a surface resonance with peculiar properties concerning energy vs momentum dispersion and spin texture. At variance with the free-electronlike behavior of the L-gap Shockley-type surface states on the fcc(111) surfaces of Au, Ag, and Cu, it splits into several branches with distinct spin polarization around the center of the surface Brillouin zone. Theoretical predictions based on density-functional theory vary depending on the particular functionals used. To clarify this issue, we investigate the atomic structure of Pt(111) by low-energy electron diffraction and the unoccupied electronic structure by spin- and angle-resolved inverse photoemission. The experimental results are backed by theoretical studies using different functionals which show that the characteristics of the surface band depend critically on the lattice constant. We identified a delicate interplay of several contributions: Lattice constant, hybridization with d bands, and the influence of spin-orbit interaction are critical ingredients for understanding the peculiar energy dispersion and spin character of the unoccupied surface resonance.

11:15am **MI+2D+AC+TF-WeM-14 Substrate-Induced Strain Effects on SrFeO<sub>3</sub> Thin Films**, **Lucas Barreto**, University of Pennsylvania; P. Rogge, J. Wang, B. Lefler, Drexel University; D. Puggioni, J. Rondinelli, Northwestern University; S. Koroluk, R. Green, University of Saskatchewan, Canada; S. May, Drexel University

Materials with non-trivial magnetic ordering give rise to exotic topological phenomena that can enhance spin-based devices' performance. In this scenario, the cubic perovskite SrFeO<sub>3</sub> exhibits a rich magnetic ordering, described by a multi-**q** magnetic arrangement. In this work, we evaluate how in-plane lattice stress influences the structural, magnetic, and electronic of SrFeO<sub>3</sub> films. We grow epitaxial SrFeO<sub>3</sub> films on different substrates to induce compressive and tensile strains, characterize them using X-ray diffraction, and probe the electronic transport as a function of temperature. The experimental data are supported by density functional theory calculations, from which we obtain the structural and electronic properties of the strained SrFeO<sub>3</sub> structure. We map the magnetic ordering via resonant x-ray magnetic diffraction and observe shifts in the projection of the magnetic wavevector **q** along the [111] direction. Our results indicate that the lattice strain can tune the magnetic propagation vector on the films while maintaining the SrFeO<sub>3</sub> metallic behavior.

11:30am **MI+2D+AC+TF-WeM-15 Tunable Localized Currents at Crystallographic Domain Boundaries in Altermagnet RuO<sub>2</sub>**, **Gina Pantano**, E. Thareja, University of South Florida; L. Šmejkal, the Czech Academy of Sciences and Johannes Gutenberg Universität Mainz, Germany; J. Sinova, Johannes Gutenberg Universität Mainz, Germany; J. Gayles, University of South Florida

Research on interfacial phenomena in condensed matter physics has garnered significant interest over the last few decades due to the discovery of new properties and phases distinct from the bulk, enabling the manipulation of materials for technological applications. In this work, we investigate the novel effects that arise from the presence of a locally chiral crystallographic domain boundary in the altermagnet ruthenium dioxide (RuO<sub>2</sub>). Altermagnets are characterized by having a substantial non-relativistic spin splitting comparable to ferromagnetic materials but with compensated magnetic ordering. The spin splitting originates from the Heisenberg exchange interaction combined with the anisotropic octahedral crystal field from the surrounding nonmagnetic O atoms, which reduces the symmetry relating the two opposite spin sublattices to an antiunitary

rotation or mirror symmetry. This introduces a new mechanism for controlling spin-dependent transport phenomena by altering the crystal configuration, specifically through its local chirality, such as the crystal Hall effect. Thus, looking at an interface where the local chirality reverses allowed for a more detailed analysis of how the change of symmetry affects electronic transport. RuO<sub>2</sub> was chosen for this study due to its high Néel temperature, metallic nature, and exhibiting one of the largest spin splittings in this new material class. We use first-principle calculations to characterize the interfacial states and their contribution to electronic transport. We observe an induced magnetization at the domain boundary and enhanced anomalous transport along the interface when spin-orbit coupling is considered, due to the change of symmetry. We theorize the localized currents are tunable by the direction of the magnetization at the interface. Our findings will contribute to the understanding of how altermagnetic properties evolve toward interfaces with the reduction in dimensionality and symmetry and contribute to advancements toward the design of sustainable, energy-efficient devices.

## Surface Science

### Room 120 - Session SS+2D+AMS-WeM

#### On-Surface Synthesis: Atomic and Molecular Ensambling on Surfaces

Moderators: Irene Groot, Leiden University, The Netherlands, Nan Jiang, University of Illinois - Chicago

8:30am **SS+2D+AMS-WeM-3 Tailoring Pt-Based Organometallic Nanomesh on Ag(111): A Model System for "Host-Guest" Chemistry**, V. Carreño-Díaz, A. Ceccatto, E. Ferreira, Abner de Sierro, University of Campinas (UNICAMP), Brazil

On-surface synthesis has been extensively used to produce complex functional nanostructures, such as Metal-Organic Frameworks (MOFs). MOFs are composed of highly ordered molecular structures, where metal adatoms act as connecting nodes, generating porous structures that exhibit a long-range order, offering a favorable environment for the adsorption and reaction of molecules in confined spaces, the so-called "host-guest" chemistry [2]. In the present work, we have studied the formation of bidimensional porous networks with hexagonal geometry (nanomesh) resulting from the combination of two molecular precursors: 1,3,5-tris[4-(pyridin-4-yl)-[1,1'-biphenyl]]benzene (TPyPPB) and dichloro-(1,10-phenanthroline)-platinum(II) (Cl<sub>2</sub>PhPt), deposited on the surface of Ag(111). Our results reveal that when the TPyPPB molecules are deposited on the Ag(111) surface, they adopt a porous arrangement with triangular packing mediated by hydrogen bonds [3]. On the other hand, in the presence of the Cl<sub>2</sub>PhPt molecule, the chemical interactions between both molecules change upon annealing at 400K, which leads to various ordering patterns before stabilizing in a network with hexagonal geometry. After dehalogenation, the Cl<sub>2</sub>PhPt molecule is transformed into a new complex, PhPt, maintaining the Pt atom in its structure. The Cl atoms dissociated from the Cl<sub>2</sub>PhPt precursor decorate the periphery of TPyPPB molecules. PhPt molecules can interconnect TPyPPB molecules through metallic coordination between the Pt atom and the N from the pyridyl group (N-Pt-N). The present investigation is based on room temperature scanning-tunneling microscopy (STM) measurements. This experimental approach allows us to explore the properties and structure of these materials at the atomic and molecular levels, opening new perspectives on the design and properties of MOFs.

Acknowledgments:

This work was financially supported by FAPESP (2022/12929-3), CNPq, and CAPES from Brazil.

1. Barth, J., Costantini, G. & Kern, K. Engineering atomic and molecular nanostructures at surfaces. *Nature* 437, 671-679 (2005).
2. Marta Viciano-Chumillas, et al. "Metal-Organic Frameworks as Chemical Nanoreactors: Synthesis and Stabilization of Catalytically Active Metal Species in Confined Spaces". *Accounts of Chemical Research* 53 (2020) 520-531.
3. Alisson C. dos Santos, Vanessa Carreño-Díaz, et al. "On-Surface Design of Two-Dimensional Networks through Nonmetal Atoms" (under preparation).

# Wednesday Morning, November 6, 2024

8:45am **SS+2D+AMS-WeM-4 Modulating the Reactivity of “Single-Atom Catalyst” Sites Within 2D Metal-Organic Frameworks by Small Structural Distortions**, **Zdenek Jakub**, CEITEC - Central European Institute of Technology, Czechia; *J. Planer, D. Hruza, A. Shahsavar, P. Prochazka, J. Cechal*, CEITEC, Czechia

Detailed atomic-scale understanding is a crucial prerequisite for rational design of next-generation single-atom catalysts (SACs). However, the sub-angstrom precision needed for systematic studies is difficult to achieve on working SACs. We present a 2D metal-organic system featuring Fe-N<sub>4</sub> single-atom sites,<sup>1,2</sup> in which the height of the atomically-defined structure is modulated by the 0.4 Å corrugation of the inert graphene/Ir(111) support. We show that the support corrugation significantly affects the system reactivity, as the sites above the support “valleys” bind TCNQ (tetracyanoquinodimethane) much stronger than the sites above the “hills”.<sup>3</sup> The experimental temperature stability of TCNQ varies by more than 60 °C on these seemingly identical sites. We expect that similarly strong effects of sub-angstrom structural distortions will likely take place whenever large molecules interact with neighboring “single-atom catalyst” sites or when multiple reactants co-adsorb on such sites.

## References

- [1] Z. Jakub, A. Shahsavar, et al., *JACS*, **146**, 3471–3482 (2024)
- [2] Z. Jakub, A. Kurowská, et al., *Nanoscale*, **14**, 9507-9515 (2022)
- [3] Z. Jakub, J. Planer, et al., in preparation

9:00am **SS+2D+AMS-WeM-5 On-Surface Synthesis of Polycyclic Heteroatom-Substituted Nanocarbon Materials**, **Willi Auwärter**, Technical University of Munich, Germany **INVITED**

On-surface synthesis protocols provide elegant routes to individual molecular complexes, oligomers, and other nanocarbon materials on metal supports [1]. The resulting structural, physical, and chemical properties can be controlled by heteroatom-substitution.

In this talk, I will present an overview of our activities employing temperature-induced reactions on coinage metal supports in an ultrahigh vacuum environment, affording specific porphyrinoids and BN-substituted nanocarbon materials. On the one hand, routes to unsubstituted, square-type porphyrin tetramers [2] and peripherally O-doped porphyrins are addressed. On the other hand, dehydrogenation processes of borazine [3] and BN-functionalized carbon scaffolds will be discussed, in view of the synthesis and potential transfer of two-dimensional BNC materials.

- [1] Grill, L.; Hecht S. *Nat. Chem.* **2020**, *12*, 115.
- [2] Corral Rascon, E. *et al. J. Am. Chem. Soc.* **2023**, *145*, 967.
- [3] Weiss, T. *et al., Adv. Mat. Interfaces* **2024**, *11*, 2300774

9:30am **SS+2D+AMS-WeM-7 Atomic-Scale Investigation of the Highly Enantiospecific Decomposition of Tartaric Acid on Chiral Cu Surfaces**, **Avery Daniels**, *C. Sykes*, Tufts University

Enantioselectivity is the quintessential form of structure-sensitive surface chemistry, as differences in reactivity arise solely from the lack of mirror symmetry of the surface. Studying enantioselectivity on chiral surfaces provides insight into the design of enantioselective heterogeneous catalysts, which are important in pharmaceutical, agrochemical, and other industries. To determine the optimum surface facet for a given chemical reaction, it is essential to study the reaction on a wide variety of surface facets. Given the serial nature of surface science experiments on single crystals, high-throughput methods to study multiple facets at the same time would circumvent this issue. We have designed surface structure spread single crystals (S4Cs) that expose a vast variety of different surface facets on a single sample. Interestingly, a large portion of these facets are also chiral and therefore the use of S4Cs is ideal for studying for enantioselective surface chemistry. Tartaric acid decomposition on chiral Cu surfaces is known to be highly enantiospecific. With spatially resolved X-ray photoelectron spectroscopy (XPS), we have previously investigated the decomposition of tartaric acid on a Cu(110) ± 14° S4C where surfaces vicinal to Cu(14,17,2)R&S were found to be the most enantiospecific. We have now combined these XPS results with scanning tunneling microscopy (STM) imaging to unveil the atomic-scale origins of the highly enantiospecific decomposition of tartaric acid on chiral Cu surfaces. We found extensive enantiospecific surface restructuring of surfaces vicinal to Cu(110) leading to the formation of facets vicinal to Cu(14,17,2). This reconstruction of the surface depends on both the TA enantiomer and the chirality of the surface itself, and is therefore enantiospecific. These results provide valuable insight into the origins of structure sensitivity for enantioselective

reactions and demonstrate the efficacy of S4Cs in performing high-throughput surface science investigations.

9:45am **SS+2D+AMS-WeM-8 Competition between Hydrogen Bonding and van der Waals Interactions During Binary Self-Assembled Monolayer Formation**, **Rachael Farber**, *L. Penland, H. Hirushan, N. Dissanayake*, University of Kansas

Binary self-assembled monolayers (SAMs) comprised of polar and nonpolar molecules, such as 3-Mercaptopropionic Acid (MPA) and 1-Decanethiol (DT), offer the ability to carefully tune the interfacial properties of Au surfaces. The formation of molecularly precise binary SAMs through the displacement of one molecule with another *via* solution phase processing requires fine control over the structure and composition of the initial SAM. While DT has been extensively characterized using ultra-high vacuum (UHV) surface science techniques, the structural properties of MPA SAMs are less well understood. The relationship between solution phase processing procedures of MPA and island vacancy density, domain size, film uniformity, and the subsequent displacement behavior when exposed to DT, has not been established.

In this work, the effects of solution phase incubation temperature and time on MPA SAM formation and subsequent DT displacement behavior were determined using UHV scanning tunneling microscopy. Three MPA incubation procedures were studied: 3 hr MPA incubation at 35 °C (**MPA-1**), 3 hr MPA incubation at 25 °C (**MPA-2**), and 24 hr MPA incubation at 25 °C (**MPA-3**). While **MPA-1** and **MPA-2** both showed the characteristic MPA lattice, **MPA-1** had fewer domain boundaries and vacancy islands compared to **MPA-2**. **MPA-3**, which had the fewest domain boundaries and vacancy islands, showed regions of an MPA bilayer species across the surface. To determine the consequences of defect density and the presence of an MPA bilayer on DT displacement, **MPA-1**, **MPA-2**, and **MPA-3** were subsequently placed in a 2 μM DT solution for 20 min, 60 min, 3 hr, and 24 hr. **MPA-1** and **MPA-2** had comparable rates of DT displacement, with the formation of a high-density DT film across the surface within 3 hr. **MPA-3** had markedly slower DT displacement. Following a 24 hr incubation of **MPA-3** in the DT solution, small regions of the low-coverage, lying down phase (β) and 2-D gas phase (α) of DT were found across the surface. Only after a 48 hr incubation of **MPA-3** in DT did the high-density DT phase form. These results highlight the significance of the bonding interactions of the initial SAM on displacement kinetics during the formation of binary SAMs.

11:00am **SS+2D+AMS-WeM-13 Paul Holloway Awardee Talk: Learning More with Less: High-Throughput Screening of Molecular Layer Deposition Processes**, **David Bergsman**<sup>1</sup>, University of Washington **INVITED**  
Because of its ability to deposit organic, inorganic, and hybrid ultrathin films with sub-nanometer thickness and compositional control, molecular layer deposition (MLD) has seen growing interest for use in technologies where precise interfacial control is essential, such as in semiconductor processing, membrane separations, and catalysis. However, development of these technologies is inhibited by the relatively slow process times for MLD vs atomic layer deposition and the large number of combinations of inorganic & organic reactants available to MLD.

This presentation will highlight the intrinsic advantages of accelerating MLD process development, both for technology development and for fundamental research. First, previous work in MLD process development will be highlighted, focusing on areas where comparisons between processes yielded fundamental insight into film growth phenomena. Then, an approach for rapidly screening new materials deposited by MLD using a custom-built, high-throughput, multiplexing MLD-style reactor will be discussed. In such a system, multiple reaction chambers are connected to shared reactants and pumping lines, allowing for the elimination of redundant reactor components and reducing capital costs compared to an equivalent number of independent systems. Finally, an example of how this approach can be applied to future technologies, such as EUV photolithography, will be given, demonstrating how materials made using these parallel systems can be screened for their properties of interest and be used to obtain process-structure-property relationships.

<sup>1</sup> TFD Paul Holloway Award Winner

# Wednesday Morning, November 6, 2024

11:30am **SS+2D+AMS-WeM-15 Organic Molecular Architectures Synthesized on Si(001) by Means of Selective Click Reactions**, *T. Glaser, J. Peters*, Justus Liebig University Giessen, Germany; *D. Scharf, U. Koert*, Philipps University Marburg, Germany; *Michael Dürr*, Justus Liebig University Giessen, Germany

The concept of molecular layer deposition on solid surfaces is promising for the synthesis of layers with well-controlled physical and physicochemical properties. Molecules with two functional groups are suitable building blocks for covalent layer-by-layer synthesis. However, with symmetric bifunctional organic molecules, i.e., with two identical functional groups at one molecule, side reactions which hinder the well-controlled layer-by-layer growth, e.g., by chain termination, may occur.

Here we solve this problem using a combination of two selective and orthogonal click reactions for controlled covalent layer-by-layer growth on Si(001). In order to do so, we combine ultrahigh-vacuum- (UHV)-based functionalization of the Si(001) surface with solution-based click chemistry for the attachment of the further layers. The starting point is the Si(001) substrate which is functionalized via selective adsorption of the bifunctional ethynylcyclopropylcyclooctyne (ECCO) molecule under UHV conditions [1]. This first-layer sample is then transferred into solution [2] in order to perform the subsequent layer-by-layer synthesis using the two orthogonal click chemistry reaction steps in an alternating fashion: First, a diazide is coupled in acetonitrile via a copper-catalyzed azide-alkyne click reaction; second, a layer of ECCO molecules is coupled via a catalyst-free, strain-promoted azide-alkyne click reaction. Without contact to ambient conditions, the samples are analyzed by means of X-ray photoelectron spectroscopy in UHV after each reaction step in solution; the N 1s spectra clearly indicated in the first step the selective click reaction of the primary azido group of the diazide molecule, whereas the tertiary azido group stayed intact. In the second step, this tertiary azido group was reacted selectively with the strained triple bond of the ECCO molecule in solution, forming a third layer of organic molecules on Si(001) with the terminal triple bond of ECCO available for further reactions according to this cyclic reaction scheme. Alternating application of the two orthogonal reaction steps then led to a well-controlled layer-by-layer growth up to 11 layers [3]; it opens the possibility for the controlled synthesis of layers with physical or physicochemical properties that alternate on the molecular scale.

[1] C. Länger, J. Heep, P. Nikodemiak, T. Bohamud, P. Kirsten, U. Höfer, U. Koert, and M. Dürr, *J. Phys.: Condens. Matter* 31, 34001 (2019).

[2] T. Glaser, J. Meinecke, C. Länger, J. Heep, U. Koert, and M. Dürr, *J. Phys. Chem. C* 125, 4021 (2021).

[3] T. Glaser, J. A. Peters, D. Scharf, U. Koert, and M. Dürr, *Chem. Mater.* 36, 561 (2024).

11:45am **SS+2D+AMS-WeM-16 Confinement Effects at Surfaces**, *J. Boscoboinik, Dario Stacchiola*, Brookhaven National Laboratory

Nanosized spaces at surfaces offer an interesting playground to understand the effect of confinement in chemistry and physics. Two examples will be described in this talk. In the first one, the water formation from hydrogen and oxygen is studied on a metal surface both in its bare state and also covered with a two-dimensional porous silicate. A change in reaction pathway is observed due to confinement effects. In the second example, nanosized silicate cages supported on a metal are shown to trap single atoms of noble gases through a new ionization-facilitated trapping mechanism. In this case, the gas phase species are first ionized. These ions can then enter the nanocages, at which point they get neutralized by an electron donated by the adjacent metal, resulting a neutral species that are kinetically trapped inside the confined space.

12:00pm **SS+2D+AMS-WeM-17 Facilitating CO<sub>2</sub> Capture Enabled by Weak Intermolecular Interactions Among CO<sub>2</sub>, Water and PEEK-Ionenes Membrane**, *Jennifer Yao, L. Strange, J. Dhas*, PNNL; *S. Ravula, J. Bara*, University of Alabama; *D. Heldebrant, Z. Zhu*, PNNL

Poly (ether ether ketone) (PEEK)-ionene membranes have shown significant potential for direct CO<sub>2</sub> capture due to their high selectivity, durability, and efficiency.<sup>1</sup> Despite their promise, the mechanisms of CO<sub>2</sub> transport through these membranes and the impact of water vapor on its CO<sub>2</sub> capture and diffusion remain poorly understood. Time-of-flight secondary ion mass spectrometry (ToF-SIMS) can detect and distinguish the characteristic molecular ions,<sup>2, 3</sup> making it an ideal tool for studying complex intermolecular interactions of the CO<sub>2</sub>, water and the membrane. In this study, a combination of isotopic labeling and SIMS provides a unique method to track small molecules in organic matrixes at nanoscale. We investigated the interactions of PEEK-ionene membranes with <sup>13</sup>CO<sub>2</sub> and

D<sub>2</sub>O using cryo ToF-SIMS. ToF-SIMS 3D imaging provided chemical mapping of the distribution of these species from the surface down to several micrometers into the membrane. The cryo ToF-SIMS data did not show any significant enhancement of the <sup>13</sup>C/<sup>12</sup>C ratio, implying weak CO<sub>2</sub>-membrane interactions and CO<sub>2</sub> vaporization even at -130 °C in vacuum condition. In contrast, cryo ToF-SIMS revealed a relatively uniform distribution of D<sub>2</sub>O within the heavy water-loaded membrane. This suggests that water-membrane interactions are stronger than CO<sub>2</sub>-membrane interactions. Additionally, the presence of D<sub>2</sub>O in the membrane did not enhance <sup>13</sup>CO<sub>2</sub> retention, indicating weak CO<sub>2</sub>-D<sub>2</sub>O interactions and minimal impact of water vapor on CO<sub>2</sub> diffusion within membrane. For comparison, ToF-SIMS data demonstrated that <sup>13</sup>CO<sub>2</sub> readily reacts with a basic Na<sub>2</sub>CO<sub>3</sub> solution to form NaH<sup>13</sup>CO<sub>3</sub>, highlighting the potential for modifying CO<sub>2</sub>-membrane interactions via functional group modifications. Specifically, introducing basic functional groups may enhance CO<sub>2</sub>-membrane interactions, whereas acidic modifications may reduce them.

## References:

1. K. O'Harra, I. Kammakakam, P. Shinde, C. Giri, Y. Tuan, E. M. Jackson and J. E. Bara, *ACS Applied Polymer Materials*, 2022, 4, 8365-8376.

2. L. E. Strange, S. Ravula, Z. Zhu, J. E. Bara, P. Chen, D. J. Heldebrant and J. Yao, *Surface Science Spectra*, 2024, 31.

3. L. E. Strange, D. J. Heldebrant, S. Ravula, P. Chen, Z. Zhu, J. E. Bara and J. Yao, *Surface Science Spectra*, 2024, 31.

# Wednesday Afternoon, November 6, 2024

## 2D Materials

### Room 122 - Session 2D-WeA

#### 2D Materials: Sensors and Devices

**Moderators:** Vikram Deshpande, University of Utah, Andrey Turchanin, University of Jena

2:15pm **2D-WeA-1 Electric-Field-Sensitive Polymer Electrolytes for Non-Volatile Doping of Two-Dimensional Field-Effect Transistors**, Susan Fullerton Shirey, D. Sarawate, P. Prem, University of Pittsburgh; K. Xu, Rochester Institute of Technology; E. Beckman, University of Pittsburgh  
**INVITED**

Solid polymer electrolyte gating provides access to regimes of transport in two-dimensional (2D) materials that would otherwise be inaccessible using conventional gate dielectrics. The enabling mechanism is the formation of an electric double layer (EDL) at the electrolyte/2D material interface that creates large fields ( $\sim V/nm$ ) and therefore induces large p- and n-type carrier densities in 2D materials ( $\sim 10^{13}$ - $10^{14}$  cm $^{-2}$ ). In this work, we demonstrate a new type of solid polymer electrolyte wherein the electric field created by the ions serves a dual purpose: driving ions to the channel surface to induce heavy doping, and driving chemical reactions that “lock down” the ions at the interface, thereby providing channel doping that persists even after the gate bias is removed (i.e., non-volatile doping). Specifically, the polyethylene oxide (PEO)-based co-polymer is designed with field-sensitive reactive groups to crosslink the polymer and therefore arrest ion mobility, disallowing the ions from diffusing away from the channel surface once the gate is grounded. We demonstrate the non-volatile doping of graphene FETs by applying positive programming gate voltages ( $V_G \geq +2$  V), and then monitoring the Dirac point shift and change in ON/OFF current. The non-volatile doping density is  $\sim 4 \times 10^{12}$  cm $^{-2}$ , estimated by shifts in the Dirac point, which is more than ten times greater than the intrinsic carrier density. Sheet carrier densities measured by Hall effect and chemical/physical characterization of the polymer electrolyte will be presented. The work is supported by the National Science Foundation (NSF, U.S.) under Grant No. ECCS-EPMD-2132006

2:45pm **2D-WeA-3 Systematic Identification of the Optical Characterization of Hexagonal Boron Nitride Thickness on 300-nm Oxide Substrate**, Emily Frederick, K. Lina, University of Central Florida; M. Lodge, Truventic LLC; M. Ishigami, University of Central Florida

This work presents a systematic process to identify the thickness of a hexagonal boron nitride (hBN) flake on 300-nm silicon oxide substrate through optical microscopy data. hBN exhibits periodic optical variations for thickness levels making it difficult for precise thickness determination, necessitating use of other means to accurately determine thickness. Determining the thickness of hBN under optical microscopy integrated with machine learning could significantly reduce the time intensive task of locating and identifying useful flakes alongside reducing potential misidentification of ideal or nonideal flakes. We assigned specific standard red, green, blue color values to theoretical thickness values and incorporated the shadow of the flakes to further distinguish the flake's thickness. By creating a systematic annotation technique, we aim to have a more efficient method for determining flake thickness for all 2D materials to better incorporate machine learning processes.

3:00pm **2D-WeA-4 Selective Etching of Hexagonal Boron Nitride Under Graphene Stack Using Sulfur Hexafluoride Gas in Different Pressure to Create Two-Dimensional Material Devices**, Swastik Ballav, R. Tsuchikawa, R. Ben Khallouq, D. Castro, University of Central Florida; M. Lodge, Truventic; M. Ishigami, University of Central Florida

**Abstract :** Recently, twisted bilayer materials fabricated from two-dimensional (2D) materials have been shown to possess unique electronic and optoelectronic properties. Among these, magic angle graphene sandwiched between hexagonal boron nitride (h-BN) has seen significant interests due to its exotic superconducting properties. Sulfur hexafluoride (SF $_6$ ) gas commonly utilized for its selective h-BN etching, while it stops at graphene to form electronic contact to these devices.

We will discuss the sensitivity of etching parameters for selective etching of h-BN. Specifically, we measured selective etching of h-BN using SF $_6$  as a function of varying pressure from 10 to 80 mTorr in helium environment at 30°C temperature. At higher pressures, graphene acts as an etch stop and leaves underlying h-BN unetched, which can be exploited to make a via for contacts through insulating h-BN. Such pressure-tunable etch selectivity can create unique device structures such as a suspended bridge structure of graphene by etching the underlying h-BN. The selective etching at higher pressures demonstrates the potential of SF $_6$  for fabricating graphene based

superconducting devices stacks which can be used to create highly sensitive bolometric device. These findings can contribute towards fabrication of electronic and optoelectronic devices from other 2D materials.

**Acknowledgement :** This work was supported by U. S. Army OSD Phase II STTR contract W911NF23C0027 and by matching funds from the Florida High Technology Corridor (I-4) Program.

3:15pm **2D-WeA-5 Printed Contacts to Layered Materials**, Sharadh Jois, E. Lee, J. Fleischer, P. Li, T. Esatu, E. Quinn, A. Hanbicki, A. Friedman, Laboratory for Physical Sciences

Over the last decade, there has been an outburst in novel layered materials and devices for advanced computing. The common techniques to create electrical contacts to layered materials rely on electron-beam lithography and photolithography that require polymeric resists that leave behind residues that can be impossible to clean. Several advances in lithography-based contact engineering to improve the quality of electrical contacts to layered materials have been pivotal in enabling basic research. The primary approach taken in these methods was to eliminate polymers from coming in direct contact with the active channel material and reduce defects induced by the deposition of metal films. The encapsulation of the active material with hexagonal boron nitride (h-BN) and creating edge contacts, nano-via contacts, or van der Waals contacts, have given the desirable two-fold benefit. However, these methods require many additional steps that consume several days of fabrication involving dry stamping to make the stack and several steps of lithography to etch undesired areas, deposit metal contacts, and lift-off. Each additional step adds failure modes and reduces device yield, thwarting the rapid prototyping of new devices with layered materials. Direct-write printing is capable of creating microscale metallic contacts in a single step. We demonstrate that printed contacts are an alternate method to achieve high-quality electrical contacts to different layered materials while evading the problems with lithography. We benchmark the printed devices using appropriate measurements, such as gating, resistance vs. temperature, or Hall. Our results show that direct-write printing can be used as an alternative to lithography to fabricate devices of layered materials for rapid testing. Furthermore, our work paves the way for creating printed circuits of layered materials for new applications.

3:30pm **2D-WeA-6 Electrical Transport of High-Quality CVD-Grown MoSe $_2$  Nanoribbons**, Y.-J. Leo Sun, University of Maryland, College Park; O. Ambrozaite, T. Kempa, Johns Hopkins University; T. Murphy, University of Maryland, College Park; A. Friedman, A. Hanbicki, Laboratory for Physical Sciences

Two-dimensional (2D) materials such as transition metal dichalcogenides are excellent candidates for creating novel nano-electronic and photonic devices. Previous research indicates that the edge states of MoS $_2$  could strongly influence its conductivity, and the 2D honeycomb structure enables different electronic performance along the zigzag and armchair edges. Understanding and controlling the conductivity is essential in devices like field effect transistors that use MoS $_2$  as the channel. To date, transport along edge states of MoSe $_2$  nanoribbons, which have substantially reduced dimensionality relative to 2D crystals, has not been explored. In this project, we used chemical vapor deposition (CVD) to synthesize MoSe $_2$  nanoribbons through directed growth on phosphine (PH $_3$ )-treated Si substrates. This approach yields directed growth of monolayer MoSe $_2$  to form narrow ( $< 1\mu m$ ) nanoribbons. Tip-enhanced photoluminescence (TEPL) maps reveal a significant difference between the emission intensity at the edges and center of the nanoribbon. To perform electronic transport measurements, we used e-beam lithography to pattern contacts on the nanoribbons in a Hall bar configuration with the side contacts at the edges and tips of the nanoribbons. The nanoribbon was encapsulated by hBN flakes, and select regions were etched to facilitate the fabrication of edge contacts to reduce contact resistance. The influence of edge states on the electrical performance of MoSe $_2$  nanoribbons was investigated by conductivity and Hall transport measurements. Current flow in the transverse and longitudinal directions of the nanoribbon was compared to analyze the importance of edge states on MoSe $_2$  nanoribbon conductivity.

4:15pm **2D-WeA-9 Ultra-Low Energy Consumption Memory Study Using 2D Materials Heterostructures**, Young-Jun Yu, Chungnam National University, Republic of Korea  
**INVITED**

Van der Waals (vdW) heterostructures using two dimensional (2D) atomic crystals have been attracted intensely for high performance as well as low-power memory applications. Furthermore, floating-gate (FG) memory devices based on 2D heterostructures exhibit stability with dielectric barriers such as hexagonal boron nitride (hBN) between semiconductors

# Wednesday Afternoon, November 6, 2024

and various charge storage layers. However, the reported operation voltage and energy consumption for hBN barriers cannot be reduced below several tens of volts. In this presentation, I will introduce ultrahigh energy efficiency of 2D material heterostructure-based memory devices for approaching to the biological synaptic energy level with employing ultrathin charge-trap layer underneath 2D semiconductor channel.

4:45pm **2D-WeA-11 2D Metal-Dielectric Hybrid Nanostructures via Electrochemical Deposition**, *Chao Dun Tan, M. Buck*, University of St Andrews, UK

Often described as “surfaces without bulk”, carbon nanomembranes (CNMs) are an emerging class of dielectric 2D materials 1-2 nanometers thick. These membranes are derived from aromatic self-assembled monolayers (SAMs) which consist of highly ordered, upright-standing molecules that are formed by spontaneous adsorption at the substrate-liquid interface. By exposing these aromatic SAMs to low energy-electron irradiation, intramolecular bonds are cleaved, resulting in a two-dimensional network by crosslinking of the aromatic molecules. These nanomembranes are sufficiently robust to allow release from the substrate, transfer to other supports, and stacking to multiple layers, thus allowing the tuning from electron tunneling through single CNMs to insulating multilayers. Furthermore, their amorphous structure does not impose limitations with regard to scaling.

It is the electron transfer across monolayers that makes CNMs also an attractive platform for electrodeposition and the design of hybrid structures. The approach taken here contrasts established electrochemical applications of CNMs where they have been employed in area-selective electrodeposition to define passivating regions by exploiting the difference in charge transfer across CNMs and native SAMs. Investigating metal electrodeposition onto CNMs, deposition parameters (e.g. potential and time) allow control of nucleation and growth, thus enabling the morphologies of the deposits to range from individual metal nanoparticles to continuous layers. Moreover, exploiting the transferability of CNMs, the scheme offers the prospect to produce hybrid nanostructures defined by electrode structures which serve as reusable master patterns. Since CNMs are chemically inert, they have a large potential window and, thus, provide flexibility as regards electrolytes used and materials deposited. The possibility of generating templated metal/dielectric nanostructures may open pathways for the implementation of CNMs as nanocircuit boards in combination with other 2D materials, metamaterials, or nano-electromechanical systems (NEMS).

5:00pm **2D-WeA-12 Disentangling Anisotropic Resistivities of the Topological Insulator  $\text{Bi}_4\text{Br}_4$** , *Bert Voigtländer, J. Hofmann, S. Kovalchuk, V. Cherepanov, T. Balashov, F. Lüpke*, Forschungszentrum Juelich GmbH, Germany; *Z. Wang, Y. Yao*, Beijing Institute of Technology, China; *S. Tautz*, Forschungszentrum Juelich GmbH, Germany

$\text{Bi}_4\text{Br}_4$  is a promising higher-order topological insulator with a highly anisotropic crystal structure. In this material, topological edge states have been observed at room temperature. As a step towards nanoscale electric transport measurements through possible ballistic edge channels at step edges, we disentangle the resistivities of this material in all directions. We combine four-point resistance measurements in the square geometry on a bulk sample of  $\text{Bi}_4\text{Br}_4$  with four-point resistance measurements on thin 2D flakes of this material in the linear configuration. These measurements give sufficient information to disentangle the two lateral resistivities along and perpendicular to the quasi-one-dimensional crystal structure, the latter being seven times lower than the conductivity along the atomic rows. Moreover, we can as well disentangle the vertical resistivity, which is much larger (~ 500 times) than the in-plane components. Due to degradation of this material under ambient conditions, we performed the electrical measurements under UHV conditions. Further, due to the micrometer sizes of the thin flakes of this material, a multi-tip scanning tunneling microscope was used to perform the four-point measurements on the micrometer scale.

5:15pm **2D-WeA-13 Electrical Breakdown of 2D Ruddlesden-Popper Metal Halide Perovskites**, *Mengru Jin*, Texas A&M University; *E. Vasileiadou*, Northwestern University; *I. Spanopoulos*, University of South Florida; *K. Lee*, Texas A&M University; *M. Kanatzidis*, Northwestern University; *Q. Tu*, Texas A&M University

## Abstract

2D Ruddlesden-Popper (RP) metal halide perovskites (MHPs) have emerged as promising low-cost, high-performance direct bandgap semiconductor materials in a plethora of energy and electronic applications, offering

enhanced environmental stability compared to their conventional 3D analogues. Electrical breakdown (BD) in such devices signifies the cumulative degradation of the internal structure of the 2D MHPs, leading to loss of device functionality. Understanding the BD process, its mechanisms and inducements are critical for the commercialization of the semiconductor devices based on 2D MHPs. Here, we investigate the electrical BD behavior of a prototypical family of 2D RP MHPs,  $(\text{BA})_2\text{MA}_{n-1}\text{Pb}_{n+1}\text{I}_{3n+1}$  (BA = butylammonium, MA = methylammonium cation, and n indicates the number of  $\text{PbI}_6^{4-}$  octahedra in one repeating unit), using conductive atomic force microscopy (C-AFM). Thin 2D MHP flakes were mechanically exfoliated onto conductive substrate directly from solution-grown single crystals using the scotch-tape method. I-V curves were obtained from flakes to quantify the breakdown strengths as a function of n, thickness and the ramping rate in a dry environment. When the applied bias surpasses a threshold voltage (defined as  $V_{\text{BD}}$ ), the current will increase rapidly, which indicates the electrical BD and a hole will be burnt into the flake. Analysis of the hole depth revealed a layer-by-layer breakdown process very similar to that found in boron nitride (BN). The  $V_{\text{BD}}$  decreases with reductions in either the thickness or the sweep rate. Conversely, the BD strength exhibits an opposing trend, escalating as the thickness decreases. Furthermore, the BD strength increases with n, which reaches  $\sim 5.45 \times 10^8$  V/m for a monolayer 2D MHP with  $n = 5$  at a ramping rate of 1 V/s. The BD strength is comparable to those of BN and self-assembled monolayer, implying good intrinsic reliability of 2D MHPs under electrical field. Our work provides the first systematic investigation of the electrical BD of 2D MHPs, which generates indispensable insights into guiding the 2D MHP materials and device design toward long-term durable applications.

## Magnetic Interfaces and Nanostructures

### Room 121 - Session MI+2D+AC+TF-WeA

#### 2D Magnetism and Magnetic Nanostructures

**Moderators:** *Mikel Holcomb*, West Virginia University, *Tiffany Kaspar*, Pacific Northwest National Laboratory

2:15pm **MI+2D+AC+TF-WeA-1 Interface Tunable Magnetism in Transition Metal Telluride Thin Films and Heterostructures**, *Hang Chi*, University of Ottawa, Canada

INVITED

Novel quasi-2D magnets are attracting much attention recently. In situ prepared sharp interfaces are desirable for strain engineering and/or hybridizing with other quantum systems, enabling fundamentally new phenomena and opportunities for spintronics [1]. Ferromagnetic  $\text{Cr}_2\text{Te}_3$  ultrathin films, optimally grown on  $\text{Al}_2\text{O}_3(0001)$  and  $\text{SrTiO}_3(111)$  using molecular beam epitaxy, manifest an extraordinary sign reversal in the anomalous Hall conductivity as temperature and/or strain are modulated. The nontrivial Berry curvature in the electronic-structure momentum space is believed to be responsible for this behavior [2]. Furthermore, when proximitized with  $(\text{Bi,Sb})_2\text{Te}_3$ -type topological insulator, via the Bloembergen-Rowland interaction, magnetic ordering in monolayer  $\text{Cr}_2\text{Te}_3$  is favorably enhanced, displaying an increased Curie temperature [3]. Combining ab initio simulation, advanced scanning tunneling microscopy, magnetic force microscopy, transmission electron microscopy, magneto transport and particularly depth-sensitive polarized neutron reflectometry,  $\text{Cr}_2\text{Te}_3$  has been established as a far-reaching platform for further investigating the marriage of magnetism and topology. These findings provide new perspectives to the magnetic topological materials in general, that are topical for the future development of topological spintronics.

## References

- [1] H. Chi and J. S. Moodera, "Progress and prospects in the quantum anomalous Hall effect", *APL Mater.* 10, 090903 (2022). <https://doi.org/10.1063/5.0100989>
- [2] H. Chi, Y. Ou, T. B. Eldred, W. Gao, S. Kwon, J. Murray, M. Dreyer, R. E. Butera, . . . J. S. Moodera, "Strain-tunable Berry curvature in quasi-two-dimensional chromium telluride", *Nat. Commun.* 14, 3222 (2023). <https://doi.org/10.1038/s41467-023-38995-4>
- [3] Y. Ou, M. Mirzhalilov, N. M. Nemes, J. L. Martinez, M. Rocci, A. Akey, W. Ge, D. Suri, . . . H. Chi, "Enhanced Ferromagnetism in Monolayer  $\text{Cr}_2\text{Te}_3$  via Topological Insulator Coupling", *arXiv:2312.15028* (2024). <https://doi.org/10.48550/arXiv.2312.15028>

## Acknowledgment

We acknowledge the support of the Natural Sciences and Engineering Research Council of Canada (NSERC) Discovery Grant RGPIN-2024-06497.



# Wednesday Afternoon, November 6, 2024

2:45pm **MI+2D+AC+TF-WeA-3 AVS National Student Awardee Talk/Falicov Student Award Finalist Talk: Probing Intrinsic Magnetization Dynamics of the  $\text{Y}_3\text{Fe}_5\text{O}_{12}/\text{Bi}_2\text{Te}_3$  Interface at Low Temperature**, A. Willcole, Sandia National Laboratories, USA; V. Lauter, Oak Ridge National Laboratory, USA; A. Grutter, National Institute of Standards and Technology (NIST); C. Dubs, INNOVENT e.V. Technologieentwicklung, Germany; D. Lidsky, Sandia National Laboratories, USA; Bin Luo<sup>1,2</sup>, Northeastern University, US; M. Lindner, T. Reimann, INNOVENT e.V. Technologieentwicklung, Germany; N. Bhattacharjee, Northeastern University, US; T. Lu, P. Sharma, N. Valdez, C. Pearce, T. Monson, Sandia National Laboratories, USA; M. Matzelle, A. Bansil, D. Heiman, N. Sun, Northeastern University, US

Topological insulator-magnetic insulator (TI-MI) heterostructures are essential in spintronics, enabling magnetization control via topological surface state-induced spin orbit torque. However, many TI-MI interfaces often face issues like contamination in the magnetic insulator and a low-density transitional region in the topological insulator, which obscure the system's intrinsic properties. In this study, we addressed these challenges by depositing sputtered  $\text{Bi}_2\text{Te}_3$  (BT) on liquid phase epitaxy grown  $\text{Y}_3\text{Fe}_5\text{O}_{12}$  (YIG)/ $\text{Gd}_3\text{Ga}_5\text{O}_{12}$ . The liquid phase epitaxy grown YIG exhibits exceptional interface quality, without an extended transient layer derived from interdiffusion processes of the substrate or impurity ions, thereby eliminating rare-earth impurity-related losses in the MI at low temperatures. At the TI-MI interface, high resolution depth-sensitive polarized neutron reflectometry confirmed the absence of a low-density transitional growth region of the TI. The demonstrated BT/YIG system is uniquely suited to elucidate the intrinsic TI-magnetic insulator magnetization dynamics due to the lack of an extended transient layer in the magnetic insulator at the magnetic insulator-substrate interface and lack of a low density, intergrowth region of the TI at the TI-magnetic insulator interface.

By overcoming these undesirable interfacial effects, we isolate and probe the intrinsic low-temperature magnetization dynamics and transport properties of the TI-MI interface. Using temperature dependent ferromagnetic resonance (FMR) we found a strong damping enhancement at low temperature due to the topologically protected Dirac surface states (TSS) in the  $\text{Bi}_2\text{Te}_3$  film – a signature of significant spin pumping. Accompanying the damping enhancement, we also observed a large induced in-plane magnetic anisotropy for the BT/YIG heterostructure. We explain this by spin-pumping and spin-momentum locking, due to which the precessing spins of the YIG are forced to align with the spins pumped into the TSS and therefore remain locked in the plane of the BT/YIG interface. The temperature dependence of the magnetotransport which supports the suppression of bulk conduction, and the emergence of weak-antilocalization is consistent with the low temperature enhanced spin pumping in the BT/YIG that we observed, highlighting the interplay between the transport and spin pumping behavior in the TI-MI system. Further study of TI-magnetic insulator interfaces, specifically magnetic insulators with perpendicular magnetic anisotropy, are pertinent to potentially unlock high temperature quantum anomalous hall effect (QAHE) heterostructures, and the next generation of low power spintronics.

3:00pm **MI+2D+AC+TF-WeA-4 Falicov Student Award Finalist Talk: Surface Investigation of  $\epsilon$ -phase  $\text{Mn}_3\text{Ga}$  on GaN (0001) Substrate using Scanning Tunneling Microscopy**, Ashok Shrestha<sup>3</sup>, A. Abbas, D. Ingram, A. Smith, Ohio University

Antiferromagnetic materials have garnered significant attention due to their exotic properties and possible applications in next generation spintronic memory and computing devices [1]. In recent years, research on non-collinear antiferromagnetic materials such as  $\text{Mn}_3\text{X}$  (X: Ir, Ge, Sn, Ga) has heightened due to non-trivial, topological properties of these materials with unique spin textures [2]. Among these Mn-based antiferromagnets,  $\text{Mn}_3\text{Ir}$  has been commonly employed for applications [3]. As Ir is an expensive metal, efforts have been made to explore Ir-free antiferromagnets. Particularly,  $\text{Mn}_3\text{Ga}$  emerges as a promising candidate due to its versatile texture, magnetic ordering, and properties akin to  $\text{Mn}_3\text{Ir}$  [4]. Among the three distinct phases of  $\text{Mn}_3\text{Ga}$ , one of the most intriguing yet less explored is the  $\epsilon$ -phase ( $\text{D}_{019}$ - $\text{Mn}_3\text{Ga}$ ), which exhibits anomalous Hall effect and topological Hall effect in distinct temperature ranges [3]. In this presentation, we will delve into the growth and surface studies of a thin film of  $\text{D}_{019}$ - $\text{Mn}_3\text{Ga}$  on a Ga polar- GaN (0001) substrate.

We have successfully grown an epitaxial  $\epsilon$ -phase  $\text{Mn}_3\text{Ga}$  layer using molecular beam epitaxy. The sample quality, lattice constants and crystal structure of the grown film were determined by *in-situ* reflection high energy electron diffraction and *ex-situ* X-ray diffraction. Upon examination with scanning tunneling microscopy, the surface revealed multiple terraces and row-like structures. Notably, the edges of the terraces form  $120^\circ$  angles with each other, consistent with the hexagonal crystal structure of the  $\epsilon$ -phase  $\text{Mn}_3\text{Ga}$ . Additionally, we observed several stackings of just a monolayer, with their heights matching the  $c/2$  value of  $\text{Mn}_3\text{Ga}$ . These measurements are further confirmed by X-ray diffraction. At atomic resolution, hexagonally arranged atoms with a  $1 \times 1$  crystal structure were observed. The measured average *in-plane* atomic spacing was  $5.37 \pm 0.05$  Å, deviating only -0.56% from theoretical predictions (5.40 Å). However, atomic spacing exhibited local variations. Other interesting structures were also observed in the scanning tunneling microscopy images, which will be discussed in the presentation. Chemical analysis via Rutherford backscattering confirmed the sample's Mn:Ga ratio as 3.2:1.0, which depends on the growth temperature. Further research will involve exploring non-collinear antiferromagnetism using spin-polarized scanning tunneling microscopy, with results to be presented at the conference.

References:

Chen et al., APL Mater.**11**, 111026 (2023).

Qin et al., Nature **613**(7944), 48 (2023).

Hernandez et al., Surf. and Interface **41**, 103167 (2023).

1. Liu et al., Sci. Rep. **7**(1), 515 (2017).

3:15pm **MI+2D+AC+TF-WeA-5 Thermally Generated Spin Transport Across Magnetic Interfaces**, Hari Srikanth, USF Tampa **INVITED**

Spin-heat coupling and thermo-spin transport are topical areas of interest for the spintronics community. The origin of longitudinal Spin Seebeck effect (LSSE) and its relationship with magnetic anisotropy as well as magnon propagation across magnetic insulator/heavy metal interfaces have remained challenging issues. LSSE induces incoherent magnon excitations with the application of a temperature gradient across the thickness of a magnetic material. Although the ferrimagnetic insulator  $\text{Y}_3\text{Fe}_5\text{O}_{12}$  (YIG) is known as the benchmark system for LSSE, other members of the insulating rare earth iron garnet family, e.g. the compensated ferrimagnet  $\text{Gd}_3\text{Fe}_5\text{O}_{12}$  (GdIG), ferrimagnet insulator  $\text{Tm}_3\text{Fe}_5\text{O}_{12}$  (TmIG) etc., are of interest and have received less attention from the point of view of spin-caloritronics. We have pioneered the technique of RF transverse susceptibility to probe the effective magnetic anisotropy in magnetic materials and heterostructures. Combining the RF transverse susceptibility with LSSE measurements, we have shown correlation between bulk and surface anisotropy with the field and temperature dependence of LSSE in YIG/Pt heterostructures and other compensated ferrimagnets like GdIG. Our recent work on TmIG/Pt heterostructures with varying film thickness reveals the clear role of anisotropy and Gilbert damping on the LSSE. From RF susceptibility, LSSE and broadband FMR experiments, quantitative analysis of the magnon propagation length and its correlation with magnetic anisotropy and Gilbert damping has been done. Overall, this talk would present new results in the thermal spin transport of garnet heterostructures which are of fundamental importance in spin transport across magnetic interfaces.

4:15pm **MI+2D+AC+TF-WeA-9 Spin Switchable 2D-Superlattice Metal-Halide Perovskite Film via Multiferroic Interface Coupling**, Bogdan Dryzhakov, Oak Ridge National Laboratory; B. Hu, University of Tennessee Knoxville; V. Lauter, Oak Ridge Natinal Laboratory

Solution-processible 2D-phase metal-halide perovskites have emerged as a remarkable class of semiconducting, exhibiting a wide-range of optoelectronic properties and multi-functionalities. In this work, interfacing ferromagnetic spins with this semiconductor's Rashba band yields magnetic field control over the excited state spin degrees of freedom, as demonstrated through optical analogues that resolve the spin polarization in steady-state and dynamics, and *in-situ* neutron scattering methods, where a photo-ferromagnetic profile is depth-resolved. The 2D-superlattice perovskite films are prepared using an optimized, low-cost spin-cast method, resulting in highly crystalline and smooth thin films with a well-defined alternating layered structure of self-assembled organic cations and lead-iodide octahedra. Within the anisotropic 2D-planes of MHPs, fluorinated A-site ligands distort the lattice, yielding robust ferroelectricity and Rashba bands arising from broken inversion symmetry and strong spin-orbit coupling. Spin-switchable circularly polarized photoluminescence (CPL) between  $\sigma^+$  and  $\sigma^-$  polarizations is achieved at the multiferroic perovskite/Co interface by manipulating the ferromagnetic spins on the Co

<sup>1</sup> AVS National Student Awardee

<sup>2</sup> Falicov Student Award Finalist

<sup>3</sup> Falicov Student Award Finalist

# Wednesday Afternoon, November 6, 2024

surface between positive and negative magnetic field directions. This switching behavior arises from selective interactions between the ferromagnetic spins on the Co surface and the circularly polarized  $\sigma^+$  and  $\sigma^-$  orbitals within the perovskite's Rashba band structures. Polarized neutron reflectometry measurements reveal long-range interactions of the Co magnetism to the perovskite's spin-polarized excitons, with chemical (NSLD) and magnetization (MSLD) depth profiles indicating optically induced magnetization through the perovskite's thickness. This work presents a fundamental platform for exploring spin selectivity effects within Rashba band structures using CPL studies in multiferroic perovskite/ferromagnetic interfaces.

4:30pm **MI+2D+AC+TF-WeA-10 Engineering the Hybrid Nanocolumnar Metamaterial Platforms for Advanced Optical and Magnetic Applications**, *Ufuk Kilic*, C. Briley, University of Nebraska-Lincoln; R. Feder, Fraunhofer Institute for Microstructure of Materials and Systems, Germany; D. Sekora, University of Nebraska-Lincoln; A. Ullah, University of Nebraska - Lincoln; A. Mock, Weber State University; C. Binek, University of Nebraska - Lincoln; H. Schmidt, Friedrich Schiller University, Germany; C. Argyropoulos, The Pennsylvania State University; E. Schubert, M. Schubert, University of Nebraska - Lincoln

The hybrid metamaterial platforms have garnered remarkable attention in various subdisciplines of physics, chemistry, and biology due to their wide range of advanced functionalities including strong tunable optical and magnetic anisotropies, the ability to confine, modulate, and control of light, to engineer new permanent nanomagnets, for example. In this study, we employed a custom-built ultra-high vacuum electron-beam glancing angle deposition technique [1] to fabricate spatially-coherent, super lattice type nanocolumnar heterostructure metamaterial platforms from both hard (cobalt) and soft (permalloy) magnetic materials. Furthermore, by using atomic layer deposition technique, we incorporate ultrathin interface layer (~1.4 nm) of Al<sub>2</sub>O<sub>3</sub> between the magnetic nano-columnar subsegments. This interface engineering at nanoscale provides another angle of freedom to tune both the magnetic and optical properties of hybrid nanocolumnar metamaterial platforms.

By taking the advantage of the generalized spectroscopic ellipsometry technique, we reached out the complex anisotropic dielectric properties of the fabricated structures. Our analysis involves widely used anisotropic Bruggeman effective medium model approach which provides to extract optical and structural properties, accordingly [2]. Moreover, to perform magnetic characterization of our fabricated metamaterial design, we employed both generalized vector magneto-optic ellipsometry and vibrating sample magnetometer measurements [3]. In order to delve into the fundamental driving mechanisms behind the anisotropic tunable magneto-optic responses from the proposed metamaterial platforms, we conducted a series of systematic micromagnetic and finite element modeling simulations, as well. We believe that these new structural metamaterial designs can result in the development of next-generation sensing devices, permanent nanomagnets, magnetic recording technologies, on-chip nanophotonic and opto-magnetic device applications.

References:

- [1] Kilic, U., et al. *Sci Rep* 9, 71 (2019).
- [2] Schmidt, D., and Schubert, M., *J. Appl. Phys.* 114.8 (2013).
- [3] Briley, Chad, et al. *Appl. Phys. Lett.* 106.13 (2015).

4:45pm **MI+2D+AC+TF-WeA-11 Magnetic Field Affects Oxygen Evolution Reaction Only in Metal Oxy-Hydroxides**, *Filippo Longo*, Chemical Energy Carriers and Vehicle Systems Laboratory, Empa, Swiss Federal Laboratories for Materials Science and Technology, Switzerland; R. Peremadathil Pradeep, E. Darwin, H. Hug, Magnetic and Functional Thin Films Laboratory, Empa, Swiss Federal Laboratories for Materials Science and Technology, Switzerland; A. Borgschulte, Chemical Energy Carriers and Vehicle Systems Laboratory, Empa, Swiss Federal Laboratories for Materials Science and Technology, Switzerland

Ni-based electrodes have been largely employed in alkaline electrolyzers for the production of H<sub>2</sub> and O<sub>2</sub> [1]. Due to the sluggish kinetics of the oxygen evolution reaction (OER), many experimental approaches have been employed to boost the catalytic performance of such electrodes [2]. The application of an external magnetic field during OER has shown outstanding catalytic improvement [3]. Despite considerable research effort, the understanding of its origin is still object of debate [4,5]. In this work we show how the Ni-based electrodes improve their catalytic activity towards OER during the application of an external magnetic field. We investigate in detail the catalytically active surface, the microscopic, electronic, and

magnetic structures by soft- and hard X-ray photoelectron spectroscopy combined with impedance spectroscopy and magneto-optical measurements. It is relevant in this context that the oxy-hydroxide formed during OER is the catalytically active compound, and is thus likely also the origin of the magnetic effect. To underline the importance of the oxy-hydroxide formation, we employ a multilayered system made of Co-Pt-Ru multi-lattices, exhibiting much more favorable magnetic properties (such as strong perpendicular magnetic anisotropy) than nickel. Interestingly, hardly any improvement of OER is found. The various findings corroborate the picture of spin-exchange interaction of metal-oxide bonds as the underlying mechanism of the magneto-chemical effect.

- [1] S. W. Sharshir et al., *International Journal of Hydrogen Energy* (2023).[2] J. S. Kim et al., *Adv. Energy Mater.* (2018), 8, 1702774.[3] F.A. Garcés-Pineda et al., *Nat Energy* 4, 519–525 (2019).[4] T. Wu et al., *Nat Commun* 12, 3634 (2021).[5] X. Ren et al., *Nat Commun* 14, 2482 (2023).

## Surface Science

### Room 120 - Session SS+2D+AMS-WeA

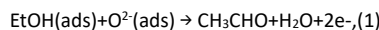
#### Defects Nanoarchitecture and Complex Systems

**Moderators: Dario Stacchiola**, Brookhaven National Laboratory, **Zhenrong Zhang**, Baylor University

2:30pm **SS+2D+AMS-WeA-2 Molecular Sensing ZnO Surfaces Studied by Operando Low-Energy Ion Beam Analysis**, *Taku Suzuki*, Y. Adachi, T. Ogaki, I. Sakaguchi, National Institute for Materials Science, Japan

#### 1. Introduction

The basic mechanism of the resistive gas sensing has been established; it is essentially a redox reaction of the surface mediated by the negatively charged oxygen adsorbate. For example, the sensing of ethanol (EtOH) with the ionosorbed oxygen of O<sup>2-</sup> is written as,



where (ads) denotes an adsorbate. It is reasonable to assume that the gas sensing properties differ between crystallographic atomic planes. Indeed, the crystal plane dependent gas sensing response has been studied by many research groups in the last decade for EtOH sensing by ZnO, which is one of the most intensively studied target gas – sensing material combinations. The specific knowledge of the crystal plane dependence of gas sensing is useful for the development of sensing materials.

The ZnO crystal plane dependence of the gas sensing properties has typically been studied using a nanocrystal. However, the effect resulting from the contact between the particles has hindered straightforward interpretation. To overcome this problem, the ZnO crystal plane dependence of the EtOH sensing was investigated using an analytical approach in the present study, namely low-energy ion scattering spectroscopy (LEIS) combined with the pulsed jet technique.

#### 2. Method: LEIS combined with pulsed jet

We applied a newly developed He<sup>+</sup> LEIS combined with the pulsed jet technique to analyze the surface structure of ZnO during the EtOH sensing. In this novel technique, the free gas jet is periodically blown onto the sample surface to simulate the gas sensing surface in a vacuum as one under the realistic working condition, while the background pressure is kept low enough for the operation of He<sup>+</sup> LEIS.

The sample was ZnO single crystals with an atomically flat mirror-polished surface. Four dominant low-index surfaces, which are Zn-terminated (0001) (c+), O-terminated (0001) (c-), (10-10) (m), and (11-20) (a), were used to evaluate the crystal orientation dependent gas sensing properties.

References

- [1] N. Saito et al., *Chemical Sensors* 39(2023)108. (Japanese)
- [2] T. Suzuki et al., *Surfaces and Interfaces* 35(2022)102371.
- [3] T. Suzuki et al., *Appl.Surf.Sci.*538(2021)148102.

2:45pm **SS+2D+AMS-WeA-3 Finding Surface Defects in Electronic Materials**, *Sujitra Pookpanratana*, National Institute of Standards and Technology

**INVITED**

All electronic materials contain a wide range of defects ranging in length scales from point defects to micrometer (or sub-millimeter) scale features. Some defects can be beneficial, benign, or detrimental to the functionality of the material. It's critical to identify and locate defects, and determine their impact in the host material. Here, I will highlight the identification of defects and their impact in 2D graphene-based systems and wide

# Wednesday Afternoon, November 6, 2024

bandgap semiconductors using photoemission electron microscopy (PEEM). PEEM is a nanoscale, surface-sensitive, full-field imaging technique based on the photoelectric effect. PEEM provides real space imaging of surfaces with enhanced contrast mechanism based on topographic and electronic properties, and measurement of electronic properties. In the first example, we image epitaxial graphene (EG) topography in real space and measure the electronic structure of monolayer EG regions with micrometer-scale angle resolved photoemission ( $\mu$ -ARPES). We detect characteristic electronic features of graphene such as the Dirac points and the  $\pi$ -band, and the electronic flat band at region with different contrast [1]. Through Raman spectroscopy on the same regions that were analyzed by PEEM, and we estimated a significant amount of compressive strain ( $\sim 1.2\%$ ) coinciding with the flat band region [1]. In the second example, we highlight the full-field PEEM capability by following the deintercalation and re-intercalation of 2D Ag within EG under heating conditions. For the 2D Ag system, we find Ag clusters initially diffuse to the top EG surface and finally re-intercalate through defects with the Ag intercalation front to be  $0.5 \text{ nm s}^{-1} \pm 0.2 \text{ nm s}^{-1}$  [2]. The EG defects serve as intercalation “doors.” Lastly, we will show extended surface defects propagating through epitaxy GaN and  $\beta$ -Ga<sub>2</sub>O<sub>3</sub> which also induce the presence of bandgap states.

[1] F. Niefind, H. G. Bell, T. Mai, A. W. Hight Walker, R. E. Elmquist, S. Pookpanratana, *J. Appl. Phys.* 131, 015303 (2022).

[2] F. Niefind, Q. Mao, N. Nayir, M. Kowalik, J. J. Ahn, A. Winchester, C. Dong, R. A. Maniyara, J. Robinson, A. van Duin, and S. Pookpanratana, *Small* 20, 2306554 (2024).

3:15pm **SS+2D+AMS-WeA-5 SSD Morton S. Traum Award Finalist Talk: Silver Iodide – Surface Structure and Ice Nucleation Investigated by Noncontact AFM**, *Johanna Hütner*<sup>1</sup>, *D. Kugler*, Vienna University of Technology, Austria; *F. Sabath*, Bielefeld University, Germany; *M. Schmid*, Vienna University of Technology, Austria; *A. Kühnle*, Bielefeld University, Germany; *U. Diebold*, *J. Balajka*, Vienna University of Technology, Austria  
Silver iodide (AgI) is used as a cloud seeding material due to its ability to nucleate ice efficiently, which is explained by the good lattice match between AgI and hexagonal ice. The basal (0001) cleavage plane of AgI deviates from the lattice of hexagonal ice by as little as 2.5%. However, AgI consists of stacked planes of positively charged Ag<sup>+</sup> alternating with negatively charged I<sup>-</sup>. Cleaving a AgI crystal along the (0001) plane thus exposes Ag<sup>+</sup> and I<sup>-</sup> terminated surfaces. Both terminations are polar and inherently unstable.

We present atomically resolved noncontact atomic force microscopy (NC-AFM) images that show how AgI(0001) surfaces compensate for this non-zero electric dipole perpendicular to the surface. Both Ag and I terminated surfaces form reconstructions, whose structure affects their ice nucleating abilities. NC-AFM images of UHV cleaved surfaces exposed to water vapor reveal that ice forms an epitaxial layer only on the Ag terminated surface, whereas on the I termination ice forms three-dimensional clusters.

These atomic-level observations could enhance our understanding of ice formation processes in the atmosphere.

3:30pm **SS+2D+AMS-WeA-6 SSD Morton S. Traum Award Finalist Talk: Reversible Non-Metal to Metal Transition and Effective Debye Temperatures of Highly Crystalline NiFe<sub>2</sub>O<sub>4</sub> Thin Films**, *Arjun Subedi*<sup>2</sup>, *D. Yang*, *X. Xu*, *P. Dowben*, University of Nebraska-Lincoln, USA

The surface of NiFe<sub>2</sub>O<sub>4</sub> thin film undergoes a conductivity change with temperature. X-ray photoelectron spectroscopy (XPS) of NiFe<sub>2</sub>O<sub>4</sub> thin film at room temperature showed large binding energy shifts in Ni 2p<sub>3/2</sub>, Fe 2p<sub>3/2</sub>, and O 1s core levels, due to photovoltaic surface charging indicating that prepared NiFe<sub>2</sub>O<sub>4</sub> thin film was dielectric or non-metallic at room temperature. The core level binding energy shifts, due to photovoltaic surface charging, were found to be around 5 eV for each of the core levels at room temperature. The core level binding energy shifts decreased when the thin film was annealed in vacuum. The XPS core level binding energy shifts from the expected values became negligible at an elevated temperature of 410 K and beyond. This suggests that NiFe<sub>2</sub>O<sub>4</sub> thin film became metallic at the temperature of 410 K and beyond. When the sample cooled down to room temperature, the sample reversibly became more dielectric, showing again the same core level binding energy shifts of 5 eV. Such reversible phase change of the thin film was further supported by the reversible Fermi edge shift with temperature. Low energy electron diffraction (LEED) images, taken for the NiFe<sub>2</sub>O<sub>4</sub> thin film surface, showed

that the surface was highly crystalline throughout the reversible temperature controlled non-metal to metal transition. The XPS spectra of Ni 2p<sub>3/2</sub>, Fe 2p<sub>3/2</sub>, and O 1s core levels taken at different temperatures showed that the changes in core level binding energies followed a proposed Arrhenius-type model with temperature. The effective bulk Debye temperatures of  $629.10 \pm 58.22 \text{ K}$  and  $787.03 \pm 52.81 \text{ K}$  were estimated using temperature dependent intensities of Fe 2p<sub>3/2</sub> and Ni 2p<sub>3/2</sub> XPS spectra respectively indicative of different sites for Fe and Ni. The effective surface Debye temperature of  $249.7 \pm 11.1 \text{ K}$  was estimated using temperature dependent intensities of LEED. Lower effective Debye temperature was observed for surface, as expected. The phase transition, the estimates of the effective Debye temperatures, and the model applied to the core level binding changes with temperature altogether shed light on the fundamental properties of the material with temperature.

4:15pm **SS+2D+AMS-WeA-9 In situ Structure Study of a MnO<sub>x</sub>-Na<sub>2</sub>WO<sub>4</sub>/SiO<sub>2</sub> Catalyst for OCM under Na<sub>2</sub>WO<sub>4</sub> Melting Conditions**, *Yang Yang*, ShanghaiTech University, China; *D. Wang*, *E. Vovk*, ShanghaiTech.edu.cn, China; *Y. Liu*, *J. Lang*, ShanghaiTech University, China  
MnO<sub>x</sub>-Na<sub>2</sub>WO<sub>4</sub>/SiO<sub>2</sub> catalyst exhibited notable C<sub>2</sub> selectivity/yield in the oxidative coupling of methane (OCM), a promised green chemistry reaction<sup>[1,2]</sup>. Nevertheless, the reaction mechanism of this catalyst remains a subject of contention, particularly regarding the role of Na<sub>2</sub>WO<sub>4</sub> in the activation<sup>[3,4]</sup>. In this study, *in situ* characterizations of a TiO<sub>2</sub>-modified MnO<sub>x</sub>-Na<sub>2</sub>WO<sub>4</sub>/SiO<sub>2</sub> catalyst, are conducted by XRD and XPS correlating to the OCM reaction condition, focusing on the simultaneous phase transition of catalyst components within its activation temperature zone. The online MS along with XPS/XRD coupled activity study confirm that transition from Mn<sup>3+</sup> to Mn<sup>2+</sup> stands as a pivotal factor influencing the reactivity. *In situ* XRD further revealed that in this narrow temperature window there is a particular three-step Na<sub>2</sub>WO<sub>4</sub> phase change, ending as molten salt, right before the substantial Mn<sup>3+</sup> to Mn<sup>2+</sup> transfer initiated. In addition, the rarely observed Na<sub>2</sub>WO<sub>4</sub> behavior as molten salt is obtained by *in situ* XPS with rapid spectra collected during an on-stage heating process. A sensitive self-reduction of the tungsten upon heating to melting point is found. These comprehensive *in situ* catalyst characterizations, covering the extensive structure-activity relationship from solid state to partial molten salt condition, providing a interlocking pathway for the reactive oxygen species transferring at high temperature. The results provides new important insight into the complex MnO<sub>x</sub>-Na<sub>2</sub>WO<sub>4</sub>/SiO<sub>2</sub> catalyst as a key to understand the activation mechanism of NaWMnSi catalyst in OCM.

[1] Lunsford JH, Catalytic conversion of methane to more useful chemicals and fuels: a challenge for the 21st century. *Catalysis today* 63 (2000) 165-174;

[2] Lunsford JH The Catalytic Oxidative Coupling of Methane. *Angewandte Chemie International Edition in English* 34 (1995) 970-980;

[3] Si J, Zhao G, Sun W, Liu J, Guan C, Yang Y, Shi XR, Lu Y Oxidative Coupling of Methane: Examining the Inactivity of the MnO<sub>x</sub>-Na<sub>2</sub>WO<sub>4</sub>/SiO<sub>2</sub> Catalyst at Low Temperature. *Angewandte Chemie International Edition* 61 (2022) e202117201

[4] Fang X, Li S, Gu J, Yang D Preparation and characterization of W-Mn catalyst for oxidative coupling of methane. *J Mol Catal* 6 (1992) 255-261

4:30pm **SS+2D+AMS-WeA-10 Characterization of Nanoplastics Samples**, *T. Roorda*, *M. Brohet*, *S. Campos Jara*, *Irene Groot*, Leiden University, Netherlands

Plastic particles in the ocean have become a contaminant of emerging concern due to their damage to humans and marine animals. Of all plastic production, which is increasing still, it has been shown that more than 99% of plastic waste which ends up in the oceans cannot be accounted for. The belief is that all of this plastic degrades to a nano-sized scale which is extremely hard to detect. In order to understand the fate of nanoplastics in aquatic environments, we must have a better understanding of the degradation mechanisms at an atomic and chemical level. In this project, we have developed procedures to evaporate powdered materials and deposit them onto a prepared surface. The deposition of nanoplastics is confirmed by mass spectrometry, Auger electron spectroscopy, and X-ray photoelectron spectroscopy. Using atomic force microscopy combined with scanning tunneling microscopy, the deposited plastics are investigated.

We also investigate plastics samples after several degradation mechanisms, such as oxygenation, hydrogenation, UV exposure, and thermal annealing. After degradation, the plastics samples are studied in ultra-high vacuum with atomic force microscopy combined with scanning tunneling microscopy and with X-ray photoelectron spectroscopy.

<sup>1</sup> SSD Morton S. Traum Award Finalist

<sup>2</sup> SSD Morton S. Traum Award Finalist

# Wednesday Afternoon, November 6, 2024

4:45pm **SS+2D+AMS-WeA-11 Oxidation of NiCr and NiCrMo- Unraveling the Role of Mo with XPEEM Studies**, *Keithen Orson*, *D. Jessup*, University of Virginia; *W. Blades*, Juniata College; *J. Sadowski*, Brookhaven National Laboratory; *Y. Niu*, *A. Zakharov*, Lund University, Sweden; *P. Reinke*, University of Virginia

Nickel-chromium based superalloys combine good mechanical strength with excellent resistance to corrosion over a wide range of conditions. Passivity stems primarily from a thin layer of chromium oxides and hydroxides and increasing Cr content above a threshold of 11-15wt% results in a protective passive layer. Adding minor alloying elements like Mo has an outsized impact on corrosion resistance, but there is debate in literature over the mechanism of this action. To investigate the interplay of Cr concentration and Mo alloying, the early-stage oxidation (0-65 Langmuir of O<sub>2</sub>) of Ni22Cr, Ni5Cr, and Ni22Cr6Mo were studied on a clean metal surface and moderate temperatures (450-500 °C). The oxidization was studied in-situ using x-ray photoelectron microscopy (XPEEM), which yields x-ray absorption hyperspectral images at 0, 5, 20, and 65 L of exposure, and a timeseries observing the oxide evolution from 0 to 65L at a single photon energy representative of Cr<sub>2</sub>O<sub>3</sub>. XPEEM valence band spectra, and conventional XPS study of the same samples complement the experiment. To analyze the ~10<sup>7</sup> spectra produced by hyperspectral imaging, several data dimensionality reduction techniques including principal component analysis and non-negative matrix analysis were used to gain insight into the oxide evolution, the species present, and their spatial distribution. The amounts of each species present in the hyperspectral images were quantified using cosine similarity. Oxidation of Ni22Cr produces islands of Cr<sub>2</sub>O<sub>3</sub> along with a surface oxide, while on Ni5Cr larger, sparser islands are observed. For both binary alloys the oxide grows in a layer-plus-island morphology. The oxide island chemistry of Ni5Cr appears to include some NiO as well as Cr<sub>2</sub>O<sub>3</sub>. Ni22Cr6Mo, on the other hand, does not nucleate oxide islands visible with XPEEM but instead forms a continuous oxide layer whose thickness increases over time. This is commensurate with a layer-by-layer growth mode which is a significant advantage for protective function. This observation has implications for Mo's protective mechanism in the passive film, suggesting that Mo may be protecting from localized breakdown by altering the morphology of the oxide to produce a more uniformly protective oxide layer.

5:00pm **SS+2D+AMS-WeA-12 An Investigation of Local Distortions on High Entropy Alloy Surfaces**, *Lauren Kim*, University of Wyoming; *P. Sharma*, Lehigh University; *G. Balasubramanian*, Lehigh University; *T. Chien*, University of Wyoming

High entropy alloys (HEAs) are a widely studied family of materials that typically contain five or more elements. There are many combinations of elements that can create HEAs, and material properties can be tuned simply by changing elemental compositions. These properties of HEAs result in numerous applications, such as catalysis, energy storage, and aerospace engineering refractory materials. Severe-lattice-distortion is identified as one of the four core effects impacting the physical properties in HEAs. In this work, we demonstrate atomic resolution images of the surface of a CrMnFeCoNi HEA (Cantor alloy) using scanning tunneling microscopy (STM). This data allows us to determine lattice local distortions unambiguously. Additionally, we report our findings on the types of local defects on the surface, such as grain boundaries, phase changes, and amorphization, and how these defects can impact local distortions of the crystals nearby.

5:15pm **SS+2D+AMS-WeA-13 Grain Boundary and Twin Boundary Solute Segregations in Nanocrystalline Al-Mg Alloy**, *Xuanyu Shang*, *z. Shang*, *A. Shang*, Purdue University, China; *H. Wang*, *X. Zhang*, Purdue University  
Chemical segregations at grain boundaries (GBs) have been broadly investigated in Al alloys. However, there are limited experimental evidence demonstrating the dependence of solute segregation on GB characteristics. Here, we quantified solute segregation at GBs in nanocrystalline Al-1Mg (at.%) alloy by combining energy-dispersive X-ray spectroscopy, high-resolution scanning transmission electron microscopy and automated crystallographic indexing and orientation mapping. The dependence of solute segregation on the grain boundary misorientation angle is analyzed. Due to their higher excess free volume, high angle grain boundaries contain more Mg solutes than the low angle grain boundaries. Furthermore, coherent twin boundaries (CTBs) exhibit low solute segregation. However, incoherent twin boundaries (ITBs) display greater solute concentration. The different solute segregation behavior between CTBs and ITBs originates from their grain boundary structure. The solute segregation behavior reported here may shed light on the GB engineering of Al alloys.

5:30pm **SS+2D+AMS-WeA-14 Charge Ordering Phase Transition in Bilayer Sn on Si(111)**, *Nathan Guisinger*, *M. Chan*, Argonne National Laboratory; *C. Lilley*, University of Illinois - Chicago

The atomic-scale investigation of the "bilayer" reconstruction of Sn on heavily doped n-type Si(111) was performed with scanning tunneling microscopy. When cooled to 55K, the bilayer reconstruction undergoes both a structural and electronic transition. Structurally, the dimer units of the bilayer shift to form a herringbone pattern with a rhombohedral ordering. The electronic structure transitions into a very uniform square lattice with similar dimensions to the structural dimers. There are distinct differences between the structural and electronic spacing that resolves itself when counting multiple periods. This ordering is like behavior observed in materials that exhibit charge density waves. Furthermore, STS point spectra show a transition from a small gap to a large insulating gap at low temperature that is consistent with a transition to a Mott insulating ground state. The charge ordering coupled with the relaxation to a Mott insulating phase upon cooling the Sn bilayer presents unique physics when the dimensionality is reduced from the bulk.

5:45pm **SS+2D+AMS-WeA-15 SSD Morton S. Traum Award Finalist Talk: On-Surface Design of Highly-Ordered Two-Dimensional Networks Stabilized by Nonmetal Atoms**, *Alisson Ceccatto*<sup>1</sup>, University of Campinas (UNICAMP), Brazil; *G. Campi*, Yachay Tech University, Ecuador; *V. Carreño*, *E. Ferreira*, University of Campinas (UNICAMP), Brazil; *N. Waleska-Wellenhofer*, *E. Freiburger*, *S. Jaekel*, Friedrich-Alexander-University Erlangen-Nürnberg (FAU), Germany; *C. Papp*, Freie Universität Berlin, Germany; *H. Steinrück*, Friedrich-Alexander-University Erlangen-Nürnberg (FAU), Germany; *D. Mowbray*, Yachay Tech University, Ecuador; *A. de Siervo*, University of Campinas (UNICAMP), Brazil

Supramolecular nanoarchitectures have been widely explored to precisely design low-dimensional materials at atomic and molecular levels [1]. Such control is mainly based on bottom-up fabrication methods, e.g. on-surface synthesis, by combining molecular building blocks and atoms to engineer novel nanomaterials [2]. Particularly, the self-assembled monolayers (SAMs) of organic molecules present the potential for applications in nanoelectronics due to their reversible non-covalent interactions [3]. Such intermolecular interactions allow the fabrication of almost defect-free supramolecular nanostructures. Typically, the geometry of these nanoarchitectures can be controlled by the insertion of metal and non-metal atoms in the reaction process. To date, the adatom-mediated SAM fabrication concentrates on the use of metal adatoms, especially d metals (Cu, Co, Au, and Fe) [4]. Herein, by combining scanning tunneling microscopy (STM) measurements and density functional theory (DFT) calculations, we report the 2D self-assembled of 1,3,5-tris[4-(pyridin-4-yl)-[1,1'-biphenyl]]benzene (TPyPPB) molecules on Ag(111) in the presence of Cl adatoms. The adsorption of the TPyPPB molecules on the clean Ag(111) surface forms an almost defect-free porous SAM stabilized by hydrogen bonds, so-called triangular packing. Such packing can be explored as a host-guest material for atom/molecular confinement. However, in the presence of Cl adatoms, the molecular arrangement changes dramatically. The molecular assembly changes its geometry, forming a non-porous SAM stabilized by H...Cl...H bonds. Such halogen-mediated SAM presents the advantage that the adatom used to stabilize the nanostructure has less influence on the electronic density compared to the typical metal adatoms.

Keywords: On-surface synthesis, STM, Self-assembly monolayer, Nanoporous networks.

Acknowledgments: This work was financially supported by FAPESP (2021/04411-1), FAPESP (2022/12929-3), CNPq, and CAPES (627946/2021-00).

References

1. Fan, Q. et al. *Accounts of Chemical Research* 48, 2484–2494 (2015).
2. Pawlak, R. et al. *Journal of the American Chemical Society* 142, 12568–12573 (2020)
3. Casalini, S. et al. *Chemical Society Reviews* 46, 40–71 (2017)
4. Shi, Z. et al. *Journal of the American Chemical Society* 133, 6150–6153 (2011)

<sup>1</sup> SSD Morton S. Traum Award Finalist

## 2D Materials

### Room 122 - Session 2D-ThM

#### 2D Materials: Defects, Dopants, Edges, Functionalization, and Intercalation

Moderator: Young Hee Lee, Sungkyunkwan University

8:00am **2D-ThM-1 Electronic and Magnetic Properties of Intrinsic Defects in  $\text{TiS}_2$** , *P. Keeney*, university of North Florida; *A. Evans, T. Pekarek, J. Haraldsen, Paula Mariel Coelho*, University of North Florida

Transition metal dichalcogenides (TMDCs) are materials with unique electronic properties due to their two-dimensional nature. Recently, there is a large and growing interest in synthesizing ferromagnetic TMDCs for applications in electronic devices and spintronics. Apart from intrinsically magnetic examples, modification via either intrinsic defects or external dopants may induce ferromagnetism in non-magnetic TMDCs [1-2]. Our study focuses on intrinsic defects in  $\text{TiS}_2$ , which is a system known for potential applications in energy storage. We use scanning tunneling microscopy (STM) and superconducting quantum interference device (SQUID) magnetometry to characterize the crystal structure and magnetic properties of  $\text{TiS}_2$  crystals. Atomically resolved STM images suggest the formation of sulfur vacancies and possibly interstitial defects creating brighter triangular shape regions. Preliminary analysis of magnetic data indicates low-spin paramagnetic response, with a saturated magnetization of  $\sim 0.16$  emu/g and 80% saturation by  $\sim 2.5$  T. To rule out ferromagnetism, hysteresis loops were analyzed and showed the coercive field to be zero within experimental error. Concurrently, DFT calculations on formation energy and electronic density were also being performed for proper identification of defect formations. Additionally, simulated STM images were generated by calculations that map the electronic density of the surface for the energetically favorable defects. An initial comparison to experimental STM images corroborates with the initial hypothesis of sulfur vacancies and titanium interstitial defects. Further studies include doping of  $\text{TiS}_2$  with transition metals and further investigation of the electronic and magnetic properties of these doped TMDC systems.

[1] Magnetic doping in transition metal dichalcogenides, *PM Coelho, J. Phys.: Condens. Matter* 36 203001 (2024).

[2] Room-Temperature Ferromagnetism in  $\text{MoTe}_2$  by Post-Growth Incorporation of Vanadium Impurities, *PM Coelho, HP Komsa, K Lasek, V Kalappattil, J Karthikeyan, MH Phan, AV Krashennnikov, and M Batzill, Adv. Electron. Mater.*, 1900044 (2019).

8:15am **2D-ThM-2 DFT-Based Investigation of Formation Energies and Properties of 2D  $\text{TiS}_2$  with Various Defects**, *Patrick Keeney, P. Coelho, J. Haraldsen*, University of North Florida

Titanium disulfide ( $\text{TiS}_2$ ) belongs to a family of materials known as transition metal dichalcogenides (TMDs). These materials exhibit relatively weak van der Waals forces between layers, allowing them to be reduced down to thin films and even one monolayer in thickness. While graphene is the most well researched 2D material, it does not possess a bandgap and thus has limited applications with regard to electronic devices. TMDs often have tunable bandgaps, filling a clear need within 2D materials. They also exhibit sandwich-like structures, with one layer of transition metal atoms sandwiched by two layers of chalcogen atoms.

The most researched applications of 2D  $\text{TiS}_2$  are those regarding ion batteries, photovoltaic devices, and spintronics. This study investigates the effects of intrinsic point defects within a 2D ( $\text{TiS}_2$ ) lattice on the electronic and magnetic properties. By comparing post-annealed scanning tunneling microscopy (STM) images with SGGGA+U-based density functional theory (DFT) calculations, we examine which defects are more likely to occur by connecting specific geometries that arise from typical intrinsic defects. We also compare a base, benchmarked 2D  $\text{TiS}_2$  supercell with supercells containing various point defects, allowing us to interpret the total energy differences and identify which are most energetically favorable.

8:30am **2D-ThM-3 Role of Chalcogen Vacancies and Hydrogen in Bulk and Monolayer Transition-Metal Dichalcogenides**, *Shoaib Khalid*, Princeton University Plasma Physics Lab; *A. Janotti*, University of Delaware; *B. Medasani*, Princeton University Plasma Physics Lab

Like in any other semiconductor, point defects in transition-metal dichalcogenides (TMDs) are expected to strongly impact their electronic and optical properties. However, identifying defects in these layered two-dimensional materials has been quite challenging with controversial conclusions despite the extensive literature in the past decade. Using first-principles calculations, we revisit the role of chalcogen vacancies and

hydrogen impurity in bulk TMDs, reporting formation energies and thermodynamic and optical transition levels. We show that the S vacancy can explain recently observed cathodoluminescence spectra of  $\text{MoS}_2$  flakes and predict similar optical levels in the other bulk TMDs. In the case of the H impurity, we find it more stable sitting on an interstitial site in the Mo plane, acting as a shallow donor, and possibly explaining the often observed n-type conductivity in some bulk TMDs. We also predict the frequencies of the local vibration modes for the H impurity, aiding its identification through Raman or infrared spectroscopy.

Our results show that the chalcogen vacancies are deep acceptors and cannot lead to n-type or p-type conductivity in monolayer TMDs. Both the (0/-1) and (-1/-2) transition levels occur in the gap, leading to paramagnetic charge states  $S=1/2$  and  $S=1$ , respectively, in a collinear-spin representation. We discuss trends in terms of the band alignments between the TMDs, which can serve as a guide to future experimental studies of vacancy behavior.

8:45am **2D-ThM-4 Defect-engineered High-gain  $\text{WS}_2$  Photodetector after 10 MeV Proton Irradiations**, *Joonyup Bae, D. Lee, S. Kwak, J. Kim, W. Lee*, Seoul National University, Republic of Korea

As silicon-based electronics approach their physical limitations, two-dimensional (2D) transition-metal dichalcogenides (TMDs) have emerged as potential alternatives due to their unique mechanical and electrical properties. Among TMDs,  $\text{WS}_2$  exhibits layer-dependent bandgaps and impressive electron and hole mobilities. However, to effectively integrate 2D TMDs into advanced applications, reliable doping strategies must be developed.

Conventional ion implantation doping methods used in silicon and GaAs-based semiconductors are not suitable for 2D TMDs due to lattice damage and high post-annealing temperatures. Alternative techniques, such as substitutional doping and charge transfer doping, have been explored but face limitations related to high-temperature processes and dopant carrier concentration control.

This study investigates the n-type doping effect of high-energy proton beam irradiation on intrinsic n- $\text{WS}_2$  using various fluences. Previous studies have focused on post-fabricated devices, making it difficult to isolate the specific interactions between the substrate and TMD materials. By examining the effects of proton irradiation on bulk  $\text{WS}_2$  crystals, this study aims to understand the intrinsic impacts with different proton fluences on 2D  $\text{WS}_2$ .

Electrical properties, defect state formation, and work function variations were assessed using transmission line measurement, Raman spectroscopy, low-temperature photoluminescence spectroscopy, and Kelvin probe force microscopy. Density Functional Theory (DFT) calculations suggest that sulfur vacancies generated by proton irradiation contribute to the formation of defect states near the conduction band, facilitating an n-type doping effect.

To validate the effects of proton beam irradiation-induced defects, multilayer  $\text{WS}_2$  photodetectors exposed to varying proton fluences were fabricated. Increasing proton fluence led to a significant improvement in internal photo-gain under 530 nm wavelength illumination, attributable to the creation of mid-gap states. This proton-mediated doping technique offers insights into the direct effects of high-energy protons on  $\text{WS}_2$ , potentially informing the development of advanced ultra-large-scale integration devices with controllable proton irradiations.

This work was supported by the Korea Research Institute for defense Technology planning and advancement (KRIT) grant funded by Defense Acquisition Program Administration (DAPA) (KRIT-CT-21-034).

9:00am **2D-ThM-5 Doping Transition Metal Dichalcogenides by Low Energy Ion Irradiation**, *W. Blades*, Juniata College; *F. Bastani, E. Truhart, K. Burns, Petra Reinke*, University of Virginia

Transition metal dichalcogenides (TMD)  $\text{MX}_2$  offer unique and versatile functionality for a wide range of electronic, photonic, and quantum devices. It remains a significant challenge to achieve electronic or magnetic doping. In conventional semiconductors such as Si, or III-V materials ion implantation is well-established as a versatile method of doping but TMDs are much more susceptible to damage. We introduce a new concept termed "backdoor doping" which mimics low energy ion irradiation with an energy below 50 eV with the goal of doping of the metal sub-lattice with a wide range of elements while at the same time minimizing damage.

We combine experimental studies of defects in TMDs with computational models describing the ion-matter interactions, and defect signatures using DFT. We will compare defects created by (i) annealing, (ii) ion irradiation, and (iii) plasma exposure in a semiconducting and a metallic TMD (e.g.

# Thursday Morning, November 7, 2024

MoS<sub>2</sub>, TaS<sub>2</sub>). We observed defects created by annealing in WSe<sub>2</sub> with scanning tunneling microscopy and spectroscopy (STM, STS) and density functional theory (DFT). Initially chalcogen vacancies dominate but larger, extended defects with multiple damaged bonds develop rapidly. The defects introduce numerous states in the gap and damage the structural and bonding integrity of the TMD layer. A small background pressure of the chalcogen might help to repair broken M-X bonds and offer a path to defect repair. We will systematically compare the different modes of defect formation using experiment and DFT modeling. If time permits, STEM (scanning transmission electron microscopy) will be included for detailed structural and phase information.

The low energy ion irradiation is achieved by using a “sandwich structure” made of a TMD layer which is capped with a thin metal layer made of the desired dopant. For proof of concept we are using Au and Fe metal layers. The sandwich structure is irradiated from the metal layer side and the projectile (a noble gas ion with an energy <5 keV) will initiate a collision cascade. The collision cascade is adjusted to eject metal atoms from the thin layer into the TMD while limiting transmission of the projectile. The defect formation in the metal is modeled with SRIM/TRIM (stopping and range of ions in matter) and SDTrimSP which are Monte Carlo simulations of collision events in matter. These simulations predict the energy of ions leaving the metal layer and entering the TMD. The TMD layer is then studied with STM to assess the defect inventory, XPS to understand compositional variations, and other methods to fully characterize the TMD.

9:15am **2D-ThM-6 Atomic-scale Manipulation of Two-dimensional Materials with Ion Beams: From Aberration-corrected STEM to Monochromated EELS**, *Kory Burns, T. Alem, E. Truhart*, University of Virginia, USA; *C. Smyth*, Sandia National Laboratories, USA; *S. McDonnell*, University of Virginia, USA; *T. Ohta*, Sandia National Laboratories, USA; *J. Hachtel*, Oak Ridge National Laboratory, USA

Heterogeneities can be selectively engineered in 2D materials from the interaction of charged projectiles at varying velocities, angle of incidences, and stage temperatures. These heterogeneities exist as intrinsic structural defects, impurities in lattice sites, topological disorder, and strain-driven interfaces. So, how can we study these defects in detail to correlate their impact on materials properties? In this talk, aberration-corrected scanning transmission electron microscopy (STEM) is combined with monochromatic electron energy loss spectroscopy (EELS) to combine unprecedented spatial resolution with world-class energy resolution from an electron probe to decouple the nature of bosons arising from subtle heterogeneities. On-axis EELS, where our bright field disc is perfectly aligned with the EELS entrance aperture, leaves our signal being dominated by dipole scattering, so we get a delocalized signal. To get a localized signal from adatoms and vacancies in our material, we must go off-axis to suppress the long-range signals and highlight hyperbolic phonon polaritons. Hereby, off-axis EELS is employed, where a bright-field disc is electrically shifted outside of the EELS entrance aperture by the projector lenses such that a portion of the dark field disc now enters the spectrometer window to give information on the impact scattering in the off-axis regime. We use the selection rules inside an electron microscope to decouple the optical transitions arising from single anomalies in 2D materials. Ultimately, this work not only pushes boundaries in electron microscopy, but provides avenues to the entire scientific landscape on decoupling the defect-property relationship in solids for the better design of next-generation nanoelectronics.

9:30am **2D-ThM-7 MoS<sub>2</sub>/MoSe<sub>2</sub> Janus Crystals: Nanoscale Defects and Composition Misconceptions Revealed Through Cross-Correlated AFM and TERS Imaging**, *Andrey Krayev*, HORIBA Scientific; *T. Zhang*, MIT; *L. Hoang*, Stanford University; *N. Mao*, MIT; *A. Mannix*, *E. Pop*, Stanford University; *J. Kong*, MIT

In this talk we'll present the results of an extensive collaborative project aimed at the cross-correlated nanoscale AFM (atomic force microscopy) and TERS (tip enhanced Raman scattering) characterization of various defects appearing in the course of synthesis of Janus transition metal dichalcogenides (TMDs). Optoelectronic and catalytic properties of Janus TMDs differ from normal TMDs, thus Janus materials are of great interest for the research community.

In the course of our study, we characterized MoS<sub>2</sub> and MoSe<sub>2</sub> Janus materials derived from MoS<sub>2</sub> and MoSe<sub>2</sub> correspondingly via the cold plasma-assisted replacement of the top chalcogen layer. Preliminary Raman characterization of the as-synthesized crystal performed in a single point with the single excitation wavelength (532nm) showed weak Raman peaks of the precursors, what was misinterpreted as incomplete conversion to Janus material.

Cross-correlated AFM and TERS imaging revealed that the precursor monolayers, both MoS<sub>2</sub> and MoSe<sub>2</sub> featured noticeable number of nanoscale bi-, tri- and higher number of layer islands. These islands have been identified in the Janus crystals transferred to gold or silver via the Kelvin probe imaging and their composition was confirmed by TERS imaging even for the islands of just 20-30 nm in diameter. It was these multi-layer islands which were responsible for the weak Raman bands of the precursor.

The morphology of the Janus crystals derived from MoS<sub>2</sub> and MoSe<sub>2</sub> was also fundamentally different. In the course of conversion of MoSe<sub>2</sub> to MoSeS pre-existing tensile strain in MoSe<sub>2</sub> was complemented by additional tensile strain resulting from the replacement of the selenium atoms with sulfur which led to physical breakage of the crystals. TERS imaging demonstrated that the gaps between the domains in MoSeS monolayers seen in topography and the surface potential images were physical cracks.

Conversely, compressive strain appearing in MoS<sub>2</sub> Janus crystals converted from MoS<sub>2</sub> results in the formation of wrinkles that after the transfer to gold or silver looked like cracks in MoSeS, but in reality there was no physical breakage in these crystals. Interestingly, by varying the substrate on which the precursor crystals are grown, nice wrinkle- and crack-free Janus monolayers can be produced.

Finally, we'll briefly discuss the TERS spectral peculiarities with 785 nm and 473 nm excitation.

9:45am **2D-ThM-8 Modulating Epitaxy and Film Domain Morphology of MBE-grown 2D Transition Metal Tellurides (TMTe<sub>x</sub>) through Engineering the Deposition Sequence and Substrate Selection**, *Ossie Douglas, D. Zamora Alvarez, M. Rafique, D. Wei, Z. Yin*, University of South Florida; *P. Snapp*, NASA Goddard Space Flight Center; *M. Wang*, University of South Florida

With increasing interest in transition metal tellurides (TMTe<sub>x</sub>) for optoelectronic applications, physical vapor deposition (PVD) thin film growth techniques offer unique opportunities to decouple factors influencing material characteristics during growth. TMTe<sub>x</sub> thin films are commonly engineered via modulation of their domain morphology and dimensionality through deposition process controls for regulating the crystallinity. Film crystallinity regulation can be achieved using PVD techniques, like molecular beam epitaxy (MBE), through its unique co-deposition process controls. While co-deposition, or simultaneous deposition, of both the transition metal and tellurium (Te) is a common approach, this process obscures the influence of individual precursors due to the complex thermodynamic and kinetic growth conditions. The simultaneous release of precursors directly influences the vapor flux which is correlated to the film roughness and thickness. Thin film growth is further dictated by the interaction between adatoms and the substrate surface. Particularly, lattice mismatch at the film-substrate interface is influenced by the crystalline/amorphous surface nature of Asaro-Tiller-Grinfeld instability, indicating a significant impact on the grown crystalline domain size and morphology. We demonstrated sequential deposition of precursors on substrates with varying crystal structure and chemical composition to decouple the influence of different factors, yielding TMTe<sub>x</sub> with distinguishable morphology.

Specifically, we demonstrated control over the film morphology which is dependent on the initial precursor (TM/Te) deposited on either crystalline or amorphous substrates. Initial deposition of either of the precursors on muscovite mica (crystalline) resulted in the formation of fully oriented nanoribbon films with significantly different domain morphology. In contrast, either TM-initiated or Te-initiated deposition on oxidized/nitrided silicon (amorphous) surfaces, led to either disordered films or randomly oriented nanoribbons, respectively. This demonstrates that MBE-grown domain morphology of TMTe<sub>x</sub> thin films is highly dependent on precursor sequence and substrate selection, permitting transition between uniform and nanoribbon films for future applications in field-effect transistor or gas sensor device development.

11:15am **2D-ThM-14 Oxidation Stability of SnSe Under Atmospheric Conditions**, *Jonathan Chin, B. Gardner, M. Frye*, Georgia Institute of Technology; *D. Liu*, Applied Materials; *S. Marini*, Cornell University; *J. Shallenberger*, The Pennsylvania State University; *M. McDowell*, Georgia Institute of Technology; *M. Hilse, S. Law*, The Pennsylvania State University; *L. Garten*, Georgia Institute of Technology

Tin selenide (SnSe) is predicted to exhibit a d<sub>11</sub> piezoelectric response of 250 pm/V when scaled down to the monolayer limit [1], but as the film thickness is decreased surface interactions can have a greater impact on performance. For example, in 2D transition metal dichalcogenides (TMDs),

oxides form not only on the surface but also propagate between layers, degrading the thin film [2]. Oxide layers have been shown to form at the surface of bulk SnSe above 200 °C [3], but the impact of oxygen on the surface and layer stability at room temperature has yet to be fully explored. Therefore, it is critical to understand the stability of the surface and interlayer structure in SnSe under standard operating condition.

This talk describes the chemical and structural stability of SnSe thin films to atmospheric exposure. The structure and composition of thin films of SnSe grown by molecular beam epitaxy is compared immediately upon growth and after a two-year exposure to ambient atmosphere. X-ray diffraction (XRD) taken before and after atmospheric exposure shows no measurable change in the crystallographic phase, orientation, or layer spacing. Similarly, the characteristic Raman vibrational modes of SnSe are unchanged with exposure, and there are no indications of modes corresponding to SnSe<sub>2</sub>, SnO or SnO<sub>2</sub>. These measurements show that the bulk of the SnSe thin film is not degrading over time as incorporating oxygen between layers would have changed the peak spacing in XRD and Raman spectroscopy. The chemical stability of the bulk phase is further supported by x-ray photoelectron spectroscopy (XPS) measurements that show that the film maintains a 1:1 Sn:Se stoichiometry. XPS cross-sections show indications of SnO<sub>2</sub> but only at the surface of the SnSe film. The oxide layer was limited to the surface within approximately 3.5 nm, as confirmed via x-ray reflectivity (XRR) measurements of the layer thicknesses. Resistivity measurements show an electrical response dominated by SnSe, not SnO<sub>2</sub>. These XPS, Raman, XRR, and resistivity results suggest that exposure to atmosphere creates a passivated layer of SnO<sub>2</sub> on the surface of SnSe but does not impact the bulk. Overall, SnSe demonstrates long-term chemical stability under atmospheric conditions, rendering it a suitable option for device applications that employ the protective metal oxide layer found in SnSe and possibly other layered chalcogenide structures.

1. Fei, W. Li, J. Li, L. Yang, *Appl. Phys. Lett.* **107**, 173104 (2015).
2. Y. Guo, S. Zhou, J. Zhao, *ChemNanoMat* **6**, 838–849 (2020).
3. *Sci.* **21**, 3333–3338 (1986).

11:30am **2D-ThM-15 Nucleation of Ald Grown Gate Dielectrics on WS<sub>2</sub> Using Low Temperature Oxygen Plasma Pretreatment**, *Robert K. Grubbs, T. van Pelt, S. Nemeth, D. Cott, B. Groven, P. Morin, C. de la Rosa, G. Kar, J. Swerts*, IMEC Belgium

Due to the ever decreasing device size driven by the electronics industry, the future of channel materials for small transistors is heading toward the use of two dimensional transitional metal dichalcogenide (2d TMD) materials. 2d TMDs are beneficial in the short channel regime because of their potential high on-to-off current ratios and because of their potentially high channel mobilities, or conductance, between the source and the drain. Beyond TMD electrical and structural quality, two large challenges exist for the implementation of TMDs into transistors. First is the electrical contact of source and drain metals to the TMD and second is the deposition of a nanometer thin, high quality, high k, defect free dielectric material on top of the TMD to form the critical transistor gate dielectric. To tackle the second challenge, the surface of WS<sub>2</sub> TMD was functionalized with a low temperature remote oxygen plasma which enabled nucleation sites to form on the surface of multi-layer WS<sub>2</sub> without catastrophic destruction of the long-range order of the WS<sub>2</sub>. From these nucleation sites, ALD HfO<sub>2</sub> and Al<sub>2</sub>O<sub>3</sub> using TMEAH (tetrakis(methylethylamido)hafnium)/H<sub>2</sub>O and TMA (trimethylaluminum)/H<sub>2</sub>O at 200°C was deposited as the gate dielectric and a 5 nm thin layer with 100% coverage could be achieved at increased oxygen plasma exposures. This WS<sub>2</sub> functionalization / nucleation process was explored by measuring the effects of oxygen exposure and temperature and their resulting effect on the ALD deposited gate dielectric film. The ALD gate dielectric coverage and its effects on the underlying 2D material was quantified with AFM, XPS, photoluminescence and Raman spectroscopy. This research has led to a process where multi-layer WS<sub>2</sub> can be functionalized and a high-quality gate dielectric can be successfully deposited on the TMD channel materials.

11:45am **2D-ThM-16 Direct Synthesis of Few Layer Graphene on 3D Printed Metal Alloy Substrates for Medical Applications**, *Irma Kuljanishvili, Y. Kim*, Saint Louis University, Department of Physics; *W. King*, Saint Louis University, School of Medicine; *A. Roe, Z. Wang*, Saint Louis University, Department of Physics

Single- and double-layer graphene, as well as few layered graphene films continue to attract significant attention due to their unique properties and wide variety of applications, including many in biomedical fields. Synthesis of high-quality graphene films on various metal substrates has been successfully demonstrated to date. In many applications large areas

graphene has been prepared by chemical vapor deposition (CVD) on catalytic metal surfaces and subsequently transferred onto target substrates or devices, which include either flat, rigid or flexible substrates. However, an increased interest in the use of graphene in medical applications often requires its direct fabrication on the substrates other than common metal surfaces such as Cu, Ni, Co, etc.

Here we report on CVD synthesis/fabrication of quality two- to three-layered graphene films with controlled morphologies on 3D printed metal alloy substrates. The number of layers, homogeneity and crystallinity of graphene grown on a large area 3D printed samples was studied with Raman spectroscopy, while microstructure, morphology and chemical make up of the graphene films was investigated by atomic force microscopy (AFM), scanning electron microscopy (SEM), X-ray photoelectron microscopy (XPS), respectively. We demonstrate correlation between growth temperature and hydrophobic properties of as-growth graphene films, with highest surface contact angle approaching superhydrophobic characteristics in the optimized growth conditions. Our results demonstrate a viable and robust process of direct growth of graphene film on non-traditional flat and arbitrary shaped 3D printed metal alloy structures. This approach could potentially be applied to the synthesis of other 2D materials which are becoming increasingly popular and viable in biomedical fields. It also opens new opportunities for other arbitrary designs of 3D printed metal constructs being developed for a variety of medical applications including but not limited to medical implants, mechanical prosthetics, electrical stimulation probes, and other.

## Electronic Materials and Photonics

### Room 114 - Session EM+2D+AP+QS+TF-ThM

#### Epitaxy: Advances in Materials Integration and Devices

Moderator: Somil Rathi, Arizona State University

8:00am **EM+2D+AP+QS+TF-ThM-1 Electronic and Photonic Integrated Devices Enabled by Local III-V on Si Heteroepitaxy**, *M. Scherrer*, IBM Research GmbH, Zurich Research Laboratory, Switzerland; *K. Moselund*, Paul Scherrer Institute, Switzerland; *Heinz Schmid*, IBM Research GmbH, Zurich Research Laboratory, Switzerland

Heterogeneous integration of electronic chipllets is one of the key performance drivers in today's HPC and consumer products. Similarly, a performance benefit can be envisioned by heterogeneous integration of preferred materials at the device level. Here we explore this bottom-up path and report on local growth of III-V compound semiconductors on silicon for electronic and photonic applications. For electronic applications the high charge carrier mobility in III-V materials is particularly interesting, while for optical devices, the direct bandgap and in-plane coupling to Si waveguides are key benefits. We will detail the epitaxial growth of III-Vs on Si by template-assisted selective epitaxy using MOCVD and highlight this method's uses by discussing selected device characteristics for field-effect transistors [1] and pin photodetectors directly integrated to Si waveguides [2]. The dense and precise co-placement of III-V gain material with Si allows for novel device designs, which will be illustrated by recent results on lasers based on hybrid III-V/Si photonic crystal cavity designs [3].

This research is supported by EU Grant 860095, 678567, 735008 and SNF grant 188173.

[1] C. Convertino et al. *Nat. Electron.* (2021) doi.org/10.1038/s41928-020-00531-3

[2] P. Wen et al. *Nat. Comm.* (2022) doi.org/10.1038/s41467-022-28502-6.

[3] M. Scherrer et al. *ACS Photonics* (2024) doi.org/10.1021/acsp Photonics.3c01372

8:15am **EM+2D+AP+QS+TF-ThM-2 In situ Graphene Barriers for Remote Epitaxy of SiC**, *Daniel Pennachio, J. Hajzus, R. Myers-Ward*, US Naval Research Laboratory

Remote epitaxy (RE) is a thin film growth technique where epitaxial alignment is directed by interactions with a substrate despite it being covered by a top layer of material.[1] This top layer must be inert and atomically thin for the underlying substrate's potential field to dominate the epitaxial alignment. Since the intermediate layer is inert, the epitaxial thin film is weakly bonded to the substrate and can be removed as a freestanding membrane and the substrate can be reused, without the damage associated with other transfer techniques such as controlled cleaving or ion implantation. Transferred 2D two-dimensional (2D) material,

such as graphene, is commonly used for a layer, but the transfer can degrade the film and increase process complexity. To avoid this, we aim to grow in situ graphene in the same chemical vapor deposition (CVD) RE growth as SiC. RE SiC is advantageous since the high cost of SiC makes substrate reuse appealing and isolated SiC membranes are excellent for quantum photonics. Despite these benefits, SiC's high-temperature hydrogen-containing CVD environment can easily damage graphene, making RE difficult.

This study established growth windows for in situ graphene via propane-based hot wall CVD followed by subsequent SiC deposition. Growing at 1620 °C in 20 slm H<sub>2</sub> with 20 sccm propane flow produced predominantly monolayer (ML) graphene films on on-axis 6H-SiC(0001) substrates and 2-3 ML films on 4° off-axis 4H-SiC(0001) substrates with minimal defects found in Raman spectral maps. These films exhibited increased uniformity over graphene grown via Si sublimation from the SiC substrate, as determined by atomic force microscopy (AFM) and Raman spectral maps. This optimal graphene growth condition was used for subsequent RE attempts to study the effect of SiC growth temperature, precursor C/Si ratio, and growth rate on epilayer crystallinity and graphene barrier damage. Nomarski microscopy, scanning electron microscopy (SEM), and AFM found SiC growth at 1620°C with a C/Si ratio of 1.55 to have the smoothest surface morphology and fewest polytype inclusions. SiC crystalline quality appeared correlated to growth rate, with lower growth rates producing smoother films with fewer polytype inclusions. Single-crystalline, polytype-pure SiC epilayers was achieved on 4° off-axis CVD graphene/4H-SiC(0001). Cross-sectional transmission electron microscopy (TEM) of some growth interfaces in this study exhibited non-uniform multilayer graphitic carbon, motivating further study of this growth system to improve boundary uniformity and SiC epilayer quality.

[1] Kim, Y., Cruz, S., Lee, K. et al. *Nature* 544, 340–343 (2017).

8:30am **EM+2D+AP+QS+TF-ThM-3 Basal Plane Dislocation Mitigation via Annealing and Growth Interrupts**, *Rachael Myers-Ward, N. Mahadik, D. Scheiman, J. Hajzus, S. White, D. Pennachio*, Naval Research Laboratory

Basal plane dislocations (BPD) in SiC are high-voltage bipolar device killers that source Shockley-type stacking faults in the presence of an electron-hole plasma [1]. Multiple research groups have been successful in mitigating their propagation from the substrate into the epitaxial layer [2-5]. While these are sufficient for typical SiC devices, for high pulsed power current density or high surge current capability applications, the injected carrier concentration is significant enough to expand converted BPDs. Here, we will report results from comparisons of H<sub>2</sub> etching to Ar annealing and the use of H<sub>2</sub> versus Ar during growth interrupts to prevent BPD expansion.

SiC epitaxial layers were grown using a CVD reactor on 4° off-axis substrates toward the [11-20] that are known to have BPDs. A H<sub>2</sub> etch or Ar anneal was performed before the buffer layer (BL) growth while a growth interrupt in H<sub>2</sub> or Ar was conducted prior to the intentionally low doped drift layer. Ultraviolet photoluminescence (UVPL) imaging was used to image the samples before and after UV stressing up to 13 kWcm<sup>-2</sup>.

The H<sub>2</sub> etch and H<sub>2</sub> growth interrupt prevented BPDs from expanding under UV stress of 13kWcm<sup>-2</sup> and it is believed that the H<sub>2</sub> treatment specifically inhibited this expansion. To confirm the role of H<sub>2</sub>, we performed a growth using the same conditions as the H<sub>2</sub> etch/interrupt, however, an Ar anneal was used instead of a H<sub>2</sub> etch and the growth interrupt was conducted in an Ar atmosphere instead of H<sub>2</sub>. The sample was UV stressed up to 1000 Wcm<sup>-2</sup> and it was found that four BPD expanded from the substrate into the epilayer. For comparison, a sample grown with a double H<sub>2</sub> etch (before the buffer layer growth and drift layer) and a sample grown with a H<sub>2</sub> etch plus H<sub>2</sub> growth interrupt did not produce faulting at the same power density. This indicates that H<sub>2</sub> influences BPD expansion. We will present detailed parametric results of samples grown with various etching/ annealing, growth interrupts, anneal times, buffer layer thickness, gas flow rates and interrupt temperature, both in H<sub>2</sub> and Ar.

[1] J.P. Bergman, et al., *Mater. Sci. Forum* Vol. 353-356, 299 (2001).

[2] N.A. Mahadik et al., *Mater Sci Forum* 858, 233 (2016).

[3] R. E. Stahlbush, et al., *Appl. Phys. Lett.* 94, 041916 (2009).

[4] M. Kato, et al., *Sci. Rep.*, 12, 18790 (2022).

[5] N.A. Mahadik et al., *Appl. Phys. Lett.*, 100, 042102 (2012).

8:45am **EM+2D+AP+QS+TF-ThM-4 Shadow Mask Molecular Beam Epitaxy**, *S. Mukherjee, R. Sitaram, X. Wang*, University of Delaware; *Stephanie Law*, Pennsylvania State University

Shadow mask molecular beam epitaxy (SMMBE) is a form of selective area epitaxy (SAE) which uses a mask either directly fabricated on or placed in contact with the substrate. During film deposition, epitaxial layers are grown on the substrate through apertures in the mask. In addition to selective area growth, SMMBE also produces a shadowing effect near the mask edges in which elemental fluxes vary as a function of position. This results in a gradient of film thickness and/or composition near the mask edges. The steepness of the gradient can be controlled by varying the mask thickness and/or the angle of the mask edges. In this paper, we demonstrate the potential of the SMMBE technique to create in-plane gradient permittivity materials (GPMs) by taking advantage of the shadowing effect. A GPM is a material in which the permittivity varies as a function of location. Our aim is to synthesize in-plane GPMs, in which the permittivity varies in the lateral in-plane direction rather than in the vertical growth direction. In an in-plane GPM, different wavelengths of light can be confined at different in-plane locations on the chip. We are interested in creating an infrared GPM, so we chose Si:InAs as our material. To create our GPMs, we use the SMMBE approach: by creating flux gradients of both indium and silicon near the edges of the mask, we can control the doping density and thus the permittivity of Si:InAs in the lateral in-plane direction. We started with reusable Si masks that are 200 μm thick and 1 cm x 1 cm in dimension. Each mask has an aperture at its center which has a dimension of 0.5 cm x 0.5 cm at the top and 0.528 cm x 0.528 cm at the bottom. Nano-FTIR spectra obtained via s-SNOM using a mid-IR nano-FTIR module demonstrates that we successfully synthesized infrared GPMs. The GPM grown using a 200 μm mask can confine light with wavenumbers 650 cm<sup>-1</sup> to 900 cm<sup>-1</sup> over an in-plane distance of 13 μm. In this talk, I will discuss the influence of several growth parameters in controlling the in-plane permittivity of the GPMs, including the growth temperature, mask thickness, and As:In ratio. In particular, the 500 μm mask provides a larger shadowing effect in comparison to 200 μm mask. This leads to a larger gradient in permittivity over a longer in-plane distance in the GPM: light with wavenumbers 650 cm<sup>-1</sup> to 1400 cm<sup>-1</sup> can be confined over an in-plane distance of 30 μm. This provides a larger surface area for the construction of an ultracompact spectrometer. Tailored mask designs can be employed to synthesize in-plane GPMs with tailored permittivity gradients in the future.

9:00am **EM+2D+AP+QS+TF-ThM-5 Impact of Excess Ga on Electronic Properties in Plasma-assisted MBE-grown β-Ga<sub>2</sub>O<sub>3</sub>**, *Thaddeus Asel, B. Noesges, J. Li, Y. Kim, A. Neal, S. Mou*, Air Force Research Laboratory, Materials and Manufacturing Directorate, USA

β-Ga<sub>2</sub>O<sub>3</sub> has been of significant interest due to its high electric breakdown field, commercially available native substrate, and shallow n-type donors. However, β-Ga<sub>2</sub>O<sub>3</sub> differs from other Ga-based semiconductors where metal-rich growth conditions are utilized to achieve adsorption-controlled growth by consuming the Ga flux entirely. Instead, β-Ga<sub>2</sub>O<sub>3</sub> growth must balance the incorporation of Ga with the desorption of a volatile suboxide species, Ga<sub>2</sub>O where this suboxide is a limiting step when growing β-Ga<sub>2</sub>O<sub>3</sub> via molecular beam epitaxy (MBE) with a traditional Ga source. Increased Ga<sub>2</sub>O desorption causes the growth rate of β-Ga<sub>2</sub>O<sub>3</sub> to decrease as the Ga flux is increased beyond the stoichiometric point of the material and can impact the stoichiometry of the grown film. In this work, we explore the impact of O-rich and Ga-rich conditions on electronic properties in films of β-Ga<sub>2</sub>O<sub>3</sub> grown via plasma-assisted MBE (PAMBE). Initial results comparing two samples under O-rich and Ga-rich conditions showed a large difference in peak low-temperature mobility. The O-rich sample showed a peak low temperature mobility of 793 cm<sup>2</sup>/V·s while Ga-rich sample peaked at only 198 cm<sup>2</sup>/V·s. The mobility and volume carrier density versus temperature data was fit using a model to extract out donor and compensating acceptor density. The Ga-rich sample showed an acceptor concentration of 2.0×10<sup>16</sup> cm<sup>-3</sup> compared to the O-rich sample that was measured to have an acceptor concentration of 3.0×10<sup>15</sup>, and order of magnitude lower. This is possibly due to the formation of V<sub>Ga</sub> during the Ga<sub>2</sub>O desorption process during the growth of the films. Another series of films were grown across a wider range of O- to Ga-rich conditions to further establish a trend between growth conditions and compensating acceptor density. Only Ga flux varied between samples and substrate temperature, Si source temperature and RF oxygen plasma conditions were held constant. Si concentration in each film was anti-correlated with the growth rate which is expected. Conversely, compensating acceptor density increased with increasing Ga-rich conditions and does not follow the trend of the growth rate. The best peak



low-temperature mobility occurred for the sample grown in the most O-rich conditions ( $789.6 \text{ cm}^2/\text{Vs}$ ) and mobility decreased with increasing compensating acceptor concentration. Overall, these results indicate the importance of Ga:O ratios in  $\beta\text{-Ga}_2\text{O}_3$  films grown via MBE with conventional Ga sources. These results demonstrate how improved electronical performance can be achieved in  $\beta\text{-Ga}_2\text{O}_3$  by growing under O-rich conditions and limiting the formation of  $\text{V}_{\text{Ga}}$  due to suboxide desorption.

9:15am **EM+2D+AP+QS+TF-ThM-6 Advancing Single-Crystalline Oxide Membrane Growth via Molecular Beam Epitaxy**, *Shivasheesh Varshney, S. Choo*, University of Minnesota; *M. Ramis*, Institute of Materials Science of Barcelona (ICMAB-CSIC), Spain; *L. Thompson, J. Shah, Z. Yang, J. Wen, S. J. Koester, K. Mkhoyan, A. S. McLeod*, University of Minnesota; *M. Coll*, Institute of Materials Science of Barcelona (ICMAB-CSIC), Spain; *B. Jalan*, University of Minnesota

A sacrificial layer method has proven to be an effective route for synthesizing free-standing membranes. In this approach, a crystalline sacrificial layer is selectively dissolved in water, allowing the target film to be transferred onto a host substrate. However, commonly used sacrificial layers (such as  $\text{SrCa}_2\text{Al}_2\text{O}_6$ ) have complex stoichiometry, posing synthesis challenges in molecular beam epitaxy (MBE). In this presentation, we will discuss two distinct but MBE-friendly, fast and facile approaches to synthesize single-crystalline oxide nanomembranes using hybrid MBE [1,2]. In particular, we synthesize epitaxially, single-crystalline  $\text{SrTiO}_3$  membranes, ranging from a few unit cells to several hundred nanometers in thickness, using an SrO sacrificial layer, and a solution-processed amorphous  $\text{SrCa}_2\text{Al}_2\text{O}_6$  sacrificial layer. Films grown in a layer-by-layer growth mode on a solution-processed amorphous  $\text{SrCa}_2\text{Al}_2\text{O}_6$  whereas in a step-flow growth mode on SrO sacrificial layer. Films grown on SrO layer dissolve rapidly ( $< 5$  minutes) in water, resulting in millimeter-sized membranes. Combining structural characterization using x-ray diffraction (XRD), atomic force microscopy (AFM), piezo force microscopy (PFM), and scanning transmission electron microscopy (STEM), we will present the structure-property relationships in these membranes with particular emphasis on investigating the role of non-stoichiometry on dielectric properties. Using PFM, we demonstrate that Sr-deficient films exhibit robust polarization at room temperature, while stoichiometric films remain consistent with the paraelectric phase. Finally, we will present the growth of single crystalline complex oxide films on a compliant substrate consisting of a few unit-cell  $\text{SrTiO}_3$  seed layers onto an amorphous  $\text{SiO}_2$  wafer.

1. S. Varshney, S. Choo, L. Thompson, Z. Yang, J. Shah, J. Wen, S. J. Koester, K. A. Mkhoyan, A. McLeod, and B. Jalan, "**Hybrid Molecular Beam Epitaxy for Single Crystalline Oxide Membranes with Binary Oxide Sacrificial Layers**" *ACS Nano* 8, 18, 6348-6358 (2024).
2. S. Varshney, M. Ramis, S. Choo, M. Coll, and B. Jalan, "**Epitaxially Grown Single-Crystalline  $\text{SrTiO}_3$  Membranes Using a Solution-Processed, Amorphous  $\text{SrCa}_2\text{Al}_2\text{O}_6$  Sacrificial Layer**" under review (2024) <http://arxiv.org/abs/2405.10464>

## 2D Materials

### Room 122 - Session 2D+EM+QS-ThA

#### 2D Materials: Applications

**Moderators:** Matthias Batzill, University of South Florida, Fei Yao, University at Buffalo

2:45pm **2D+EM+QS-ThA-3 New Graphene Oxide-based Nanozymes for Cancer Theranostics**, A. Foti, S. Sciacca, G. Tranchida, S. Petralia, R. Fiorenza, S. Scirè, L. D'Urso, C. Bonaccorso, A. Fraix, University of Catania, Catania, Italy; A. De Bonis, University of Basilicata, Italy; **Cristina Satriano**, University of Catania, Catania, Italy

Graphene oxide (GO) and plasmonic nanoparticles (Pd, Au, Ag NP) nanocomposites were scrutinized in this study as combinative multimodal platform with enzyme-like, photocatalytic and photothermal properties. A green one-pot chemical reduction method by using D-glucose as reducing agent and polyvinylpyrrolidone (PVP) as capping agent, was used to fabricate the hybrid 2D platforms (NP@G) and the reference plasmonic nanoparticles alone. Different molar ratios of the metal precursor/reducing agent were tested to get the best results in terms of stability, reproducibility and reaction yield, as monitored by the plasmonic band of the NPs. The physicochemical characterization of the morphological, compositional, structural, and functional properties of NP@G nanozymes was carried out in terms of X-ray photoelectron spectroscopy (XPS), X-ray diffraction (XRD), transmission electron microscopy (TEM), UV-visible, Raman spectroscopy, Fourier Transformed Infrared Spectroscopy (FTIR), thermocamera, atomic force microscopy (AFM), dynamic light scattering (DLS) and zeta potential (ZP). The enzyme-like activity was tested by colorimetric assays in a cell-free environment to confirm the maintenance of the nanozymes capability in the NP@G samples. The photocatalytic properties were tested in the H<sub>2</sub> evolution by water splitting reaction under simulated solar light. Further, the nanoplatfoms were tested in prostate cancer cells (PC-3 line) in terms of cytotoxicity, cell migration and reactive oxygen species (ROS) production, to prove the antitumoral action of the developed nanomedicine. Cell imaging by laser scanning confocal microscopy (LSM) demonstrated the theranostic capability of the developed platforms, including dynamic processes at the level of sub-cellular compartments.

**Acknowledgements:** ADB and CS acknowledge the financial supported by MUR in the framework of PRIN2022-PNRR call under project CoMu4CaT.

3:00pm **2D+EM+QS-ThA-4 Engineering Novel Hybrid Membranes for Battery Separators from Sustainable Sources**, **Suvash Ghimire**, P. Makkar, M. Islam, K. Mukhopadhyay, University of Central Florida

The surge in device use in transportation, biomedical sectors, and other industries is escalating at an alarming rate, coupled with grave concerns about pollution and global warming that underscores the urgency for developing efficient, safe, and environmentally friendly energy storage devices. There is a growing urgency to reduce planet-warming pollution through mining and other activities at the federal level to drop carbon emissions by half this decade and reach close to zero by the middle of the century to prevent some of the most devastating effects of climate change. Research groups worldwide are developing metal-based substitutes that address sustainability by eliminating the use and generation of hazardous substances during the synthesis and developing cheap, recyclable substitutes for electrode materials, electrolytes, membranes, and separators that are the pivotal components of energy storage devices.

Materials and their interfaces play an essential role in energy storage devices by facilitating ion transports and impeding short circuits by separating anode and cathode. Ion exchange membranes have broad applications in water electrolysis, fuel cells, and flow batteries. To date, Nafion® membranes and polyolefin-based separators are considered the industrial standards due to their excellent proton conductivity and high chemical stability. However, high cost, poor strength, shrinkage at high temperatures, and use of fluorinated chemicals hinder their widespread use. Therefore, there is an urgent need to develop membranes that can be alternatives to existing membranes without compromising the cost and environmental impact. Leveraging their porosity, properties, low cost, and thermal and chemical stabilities, clay-based membranes could be a new alternative for new-generation materials for such applications.

Our research presents a novel pathway for developing flexible and durable hybrid clay membranes by modifying them with zwitterions. The ionic conductivity of the membranes, measured using electrochemical impedance spectroscopy in a non-aqueous electrolyte solution, was found to be in the range of 10<sup>-4</sup> S/cm, which is comparable to the ionic

conductivities of related membranes used in electrochemical energy storage devices; this is a significant new development considering clay ion-exchange membranes. Our study exhibits a new avenue to engineer highly efficient ion-conducting membranes with high thermal stability (300 °C) that can provide an efficient and recycle-free approach to developing a new generation of separators from sustainable sources for energy applications, especially for battery technology.

3:15pm **2D+EM+QS-ThA-5 Unveiling Composition-Structure Relationships for the Discovery of Novel High-Entropy 2D Materials Using the Mixed Enthalpy-Entropy Descriptor**, **Dibyendu Dey**, University of Central Florida; O. Ogunbiyi, University of Missouri; B. Ball, University of Central Florida; L. Liang, M. Zachman, Oak Ridge National Laboratory; Y. Yang, University of Missouri; L. Yu, University of Central Florida

High-entropy two-dimensional materials (HE-2DMs) represent an emerging class of materials that show promise for numerous functional applications. These materials inherit the distinctive features of conventional 2D materials, such as reduced dimensionality, exceptional flexibility, and a large surface-to-volume ratio, while introducing a high configurational entropy of mixing to the system. Despite their immense potential, the experimental realm of HE-2DMs has thus far been limited to a few materials, leaving the complex interplay between their composition, structure, and synthesizability largely unexplored. In this work, by utilizing the Mixed Enthalpy Entropy Descriptor (MEED) [1], the material space of high-entropy 2D chalcogenides, including Group IV (Ti, Zr, Hf), Group V (V, Nb, Ta), and Group VI (Cr, Mo, W) metals in their 2H, 1T, and 1T' phases, has been systematically explored. MEED uniquely encapsulates the chemical and structural attributes critical for synthesizing HE-2DMs in their diverse polymorphs, demonstrating capabilities beyond any existing descriptor. Guided by MEED predictions, several top-candidate high-entropy tellurides and selenides, which exhibit extraordinary potential for applications in flexible electronic devices and advanced batteries, have been synthesized.

**Acknowledgments:** This work is supported by the US Department of Energy (DOE) Basic Energy Sciences (BES) under Award Number DE-SC0021127.

#### Reference:

1. Dibyendu Dey, Liangbo Liang, Liping Yu, Journal of the American Chemical Society 146, 5142 (2024).

3:30pm **2D+EM+QS-ThA-6 Antenna-Coupled Magic-Angle-Twist-Graphene Josephson Junction Millimeter Wave Detector**, **David Castro**, University of Central Florida

We designed a sensitive detector of THz and mm waves using an antenna-coupled magic-angle-twist-graphene Josephson junctions. Magic angle twisted bilayer graphene superconducts at a transition temperature of ~2K. We can create a lateral Josephson junction by selectively gating different sections of a single sheet of magic angle graphene. The detection mechanism in our design is based on the change in maximum zero-voltage DC current in response to an applied AC signal at the junction. We expect it to be faster than bolometric detection mechanisms while maintaining high sensitivity. We determined that the bowtie antenna would work best for this device by using finite element electrodynamic simulations. We estimated the responsivity, noise-equivalent-power, and the prospects for single-photon detection. This detector device can be used in the future for sensing applications and quantum information systems.

#### Acknowledgments

This work was supported by U. S. Army OSD Phase II STTR contract W911NF23C0027 and by matching funds from the Florida High Technology Corridor (I-4) Program.

## 2D Materials

### Room Central Hall - Session 2D-ThP

#### 2D Materials Poster Session

##### 2D-ThP-2 Topotactical Reaction of NiTe<sub>2</sub> Films with Excess Ni, *Nirosha Rajapakse, M. Batzill, K. Lasek, University of South Florida*

Compositional control of layered materials has the potential for creating new 2D materials with desirable properties. Certain transition metal dichalcogenides (TMDs) may be modified by incorporating excess metals in between the 2D sheets and covalently linking them. Such an incorporation of metals may be achieved in a topotaxy approach. Topotaxy is a solid-state reaction in which the crystal structure of a starting material is modified by incorporation of elements into the existing crystal structure. Here this is explored for NiTe<sub>2</sub> by reacting it with excess Ni. In our study, NiTe<sub>2</sub> thin films were synthesized by molecular beam epitaxy. Subsequently, the composition of these films can be modified by two different approaches; (i) by thermal annealing inducing loss of Te and (ii) by reaction with excess Ni. In both cases the change in the Ni:Te ratio is monitored by XPS and a structural transformation of the film is observed by LEED and STM. With an increase in the Ni-content a ( $\sqrt{3} \times \sqrt{3}$ ) R30 superstructure is observed. In STM it can be shown that this new superstructure phase forms separate domains from the pure NiTe<sub>2</sub>, suggesting that it is compositional line phase in the Ni-Te phase diagram. The superstructure can be explained by Ni insertion in between NiTe<sub>2</sub> layers. From XPS measurements, the Ni-concentration in the intercalation layer is close to 2/3 of the Ni concentration of a NiTe<sub>2</sub> layer. The structural models for the intercalation are discussed based on DFT calculations. In STM nanoscale stripe like ripple networks are observed, which may indicate stacking faults in the intercalation layer due to lattice expansion. This study demonstrates a controlled approach to modify the composition of 2D NiTe<sub>2</sub>, which may help to control proposed properties of the layered Ni-telluride system, such as superconducting phases [1] or make it a more efficient electrocatalyst [2]. In general, the approach of modifying NiTe<sub>2</sub> by topotaxy may also allow to modify it with other transition metals than Ni and this will be studied in future work.

#### Reference:

1. Pan, S. *et al.* On-Site Synthesis and Characterizations of Atomically-Thin Nickel Tellurides with Versatile Stoichiometric Phases through Self-Intercalation. *ACS Nano* **16**, 11444–11454 (2022).
2. Nappini, S. *et al.* Transition-Metal Dichalcogenide NiTe<sub>2</sub>: An Ambient-Stable Material for Catalysis and Nanoelectronics. *Adv. Funct. Mater.* **30**, (2020).

##### 2D-ThP-3 Compositional Phase Control of MoTe<sub>2-x</sub> via Growth Temperature, Post-Growth Annealing, and Post-Growth Metal Incorporation, *Onyedikachi Alanwoko, M. Batzill, University of South Florida*

The ability to control and create different phases of two-dimensional(2D) materials like 2D transition metal dichalcogenides (TMDs) is a promising way of realizing new electronic and chemical properties of 2D materials. MoTe<sub>2</sub> has a small formation energy difference (~0.04eV) between its two competing 1H and 1T' phases. In MBE growth it has been shown that low growth temperatures favor the 1T' phase while at higher growth temperatures the 1H phase is preferentially obtained. However, the 1H phase is generally tellurium deficient resulting in the formation of Mo-rich mirror twin grain boundaries (MTBs). This tellurium deficiency at higher growth temperatures may be related to the preferential formation of the 1H phase. Here we show through scanning tunneling microscopy (STM) that the Te-deficiency in the monolayer film can be tuned and a new ordered 2D Mo-telluride phase is obtained. With increasing Te-deficiency the structures change from a disordered MTB network to superstructures with  $2(\sqrt{7} \times \sqrt{7})R19.1$  and  $2(\sqrt{3} \times \sqrt{3})R30$  periodicity. Some of these phases can be assigned to periodic MTB networks. However, the different phases require different synthesis procedures, and once formed these phases appear thermally stable in vacuum to 500°C when they all transform into a tubular Mo<sub>6</sub>Te<sub>6</sub> phase. In this study, we systematically investigate the preparation conditions (which include the variation of the growth temperature, Te-desorption by post-growth vacuum annealing, and vapor deposition of Mo) enabling the controlled synthesis of these new phases. Particularly promising is the observation that we can react MoTe<sub>2</sub> with vapor-deposited Mo to obtain new ordered Te-deficient phase, this opens the possibility in future studies to react MoTe<sub>2</sub> with dissimilar TM to create new doped or alloyed 2D materials with potentially desirable properties.

##### 2D-ThP-4 Influence of Fluorination and Oxygenation Sources on the Thermal Atomic Layer Etching of MoS<sub>2</sub>, *Jacob Tenorio, Boise State University*

Atomic layer etching (ALE) has emerged as a pivotal technique in the precise fabrication of two-dimensional (2D) materials, particularly molybdenum disulfide (MoS<sub>2</sub>), which holds promise in the semiconductor industry due to its high mobility in monolayer form. The ability to precisely etch amorphous and crystalline MoS<sub>2</sub> films provides a pathway for controlling thickness, which is critical to achieving desired electrical and optical properties. Previous studies used MoF<sub>6</sub> and H<sub>2</sub>O in thermal ALE of MoS<sub>2</sub>. Here, we report studies of alternate sources of fluorination and oxygenation and evaluate their impact on thermal ALE of MoS<sub>2</sub>. Oxygen sources include water and ozone and fluorine sources include HF/Pyridine and MoF<sub>6</sub>. Etch rates, uniformity, and surface chemistry post ALE were characterized using spectroscopic ellipsometry, atomic force microscopy, and X-ray photoelectron spectroscopy. Preliminary results indicate etch per cycle values of 0.5 Å/cycle for MoF<sub>6</sub>+H<sub>2</sub>O at 200 °C, 0.32 Å/cycle for HF+H<sub>2</sub>O at 250 °C, and 0.26 Å/cycle for HF+O<sub>3</sub> at 250 °C. Additionally, ALE processes were combined with ALD to demonstrate thickness control for achieving few-layer MoS<sub>2</sub>.

##### 2D-ThP-5 SCTD Through Ultraviolet Ozone Treatment for 2D Semiconductor Based Field Effect Transistors, *J. Park, Juwon Lee, Sungkyunkwan University (SKKU), Republic of Korea*

The semiconductor industry is increasingly demanding high-performance, highly integrated circuits and the downscaling of conventional cell size has reached its limits. However, using silicon-based technology into downscaled technology has faced diverse challenges in ensuring high cell transistor performance. Therefore, many researchers are exploring the application of next generation semiconductor materials, such as two-dimensional(2D) metal dichalcogenides (TMDs). TMDs have received significant attention as a novel alternative to silicon in the semiconductor industry because of their excellent electrical, mechanical properties.

To achieve the performance of TMD-based devices, it is very important and essential to have good ohmic contact with Schottky barrier (SB) control. The SB is typically controlled by doping such as ion implantation and thermal diffusion. However, these conventional doping methods are impossible to TMDs because they can damage the crystal lattice or cause defects. This is due to the characteristics of TMDs having a thin layer structure.

Several doping schemes have been investigated to reduce contact resistance in TMD-based devices, including edge contact, interlayer depinning, and surface charge transfer doping (SCTD). Among them, SCTD is an effective doping technique for 2D semiconductors due to its non-destructiveness and simplicity. The SCTD mechanism follows an alignment of Fermi level at the semiconductor and dopant material interface. The difference in work function (WF) between semiconductors and metal oxides is the main factor in charge transfer. When the WF of the metal oxide is larger than that of the semiconductor, the electrons in the semiconductor spontaneously move to the metal oxide, the holes accumulate in the semiconductor, and the energy band at the interface bends upward, eventually the semiconductor is doped p-type. In this study, we introduce a method to oxidize WSe<sub>2</sub> to WO<sub>x</sub> using ultraviolet (UV) ozone treatment. By this method, the surface of WSe<sub>2</sub> is changed to WO<sub>x</sub>, and WO<sub>x</sub> is a substance having a larger WF than WSe<sub>2</sub>, and acts as a dopant material to perform p-type doping of WSe<sub>2</sub>. As a result, we confirmed that the device characteristics of 2D WSe<sub>2</sub>-based field effect transistor (FET) were improved.

The SB formed at the interface between the 2D semiconductors and the metals obstructs carrier injection and causes contact resistance to increase. Regardless of metals, an unintended high SB exists due to the Fermi level pinning effect. SCTD can selectively dope 2D semiconductors around metal contacts. Contact doping using SCTD is an effective way to lower the SB and improve the contact characteristics of 2D FETs.

##### 2D-ThP-6 Plasma Assisted Etching of MoS<sub>2</sub>: An Ab-Initio Molecular Dynamics(AIMD) Study, *Shoaib Khalid, Y. Barsukov, S. Ethier, I. Kaganovich, Princeton University Plasma Physics Lab*

Molybdenum disulfide (MoS<sub>2</sub>) in its two-dimensional form represents a leading contender for the fabrication of advanced semiconductors. A critical attribute of MoS<sub>2</sub> is its adjustable bandgap, which varies with material thickness. This characteristic is vital for the tailored production of nanoelectronics devices, aligning with industry requirements for precision and flexibility. In this study, we employ ab initio molecular dynamics (AIMD) to investigate the etching mechanisms of Molybdenum disulfide (MoS<sub>2</sub>).

Our results provide a basic understanding of plasma assisted etching process. By simulating the interaction of plasma with MoS<sub>2</sub> surfaces, we identify the critical factors that can influence the etching rates and patterns. Our calculations indicate that fluorinating the MoS<sub>2</sub> surface before subjecting it to Ar plasma bombardment can enhance etching yield and improve surface roughness. The presence of fluorine (F) at the surface forms a stronger F-S bond compared to the Mo-S bond, facilitating etching of the surface sulfur (S) atoms without significant damage to the underlying layers. This process is crucial for reducing the surface roughness of the unetched layers. Furthermore, the effect of Ar ion energy on etching yield and surface roughness is also addressed.

**2D-ThP-7 The Relationship between the Adhesion Strength and the Anodization Time for the Formation of Titanium Oxide Nanotubes on Ti-6Al-4V**, ITZEL PAMELA TORRES AVILA, M. VARGAS LÓPEZ, A. CHINO ULLOA, J. CASTREJÓN FLORES, Unidad Profesional Interdisciplinaria de Biotecnología, Mexico

In this work, an anodic oxidation process was applied to the surface of Ti-6Al-4V in order to form titanium oxide nanotubes (TONs). This titanium alloy is the most studied due to its  $\alpha/\beta$  microstructure, which provides different mechanical properties. The anodic oxidation was carried out at a constant voltage of 60 V using an electrolyte based on ethylene glycol (EG), 0.5 wt.% ammonium fluoride, and 1 wt.% distilled water. The established anodization time were 10, 20, 30, 40, 50, and 60 min. The adhesion strength of the different TONs layers to the Ti-6Al-4V surface was evaluated by nanoscratch test and the critical load was determined from the analysis of the groove of the nanoindenter path. It ranged from 0 mN for 10 min samples to  $47 \pm 3$  mN for 50 min samples. The results showed that the TONS formed at 50 min presented the best adhesion strength to the titanium alloy sample.

Keywords: nanotubes adhesion strength, titanium

**2D-ThP-8 Characteristics of Composites of Expanded Graphite and Silver Nanoparticles Prepared by Thermal Decomposition**, Won Gyu Lee, Kangwon National University, Republic of Korea

The dispersibility of the metallic Ag nanomaterial on the surface of the graphite carbon material was significantly reduced, and depending on the process conditions, it aggregated on the surface of the specific carbon material, making it difficult to construct the carbon/nanomaterial composite with the expected uniform structure. It was concluded that this result was based on the poor dispersibility of nanometals in solvents. In addition, the adhesion between the synthesized carbon/metal nanocomposite materials was poor, making it difficult to produce sheets for sample characterization. In particular, in the case of expanded graphite, it was judged to be due to interlayer shrinkage due to capillary force during the material drying process after composite synthesis in aqueous solution. Therefore, it can be seen that a synthesis method with the low surface tension of nanometal dispersion solvent is essential.

Therefore, in this study, a process environment that excludes surface tension was required to increase dispersibility by using the supercritical properties to improve the dispersibility of nano metals and to increase processability due to the shrinkage of the material. Supercritical carbon dioxide uses supercritical carbon dioxide, in which the surface tension of the fluid disappears at temperatures above 31.0°C and pressures above 73.8 bar, and nanometals are evenly dispersed and evenly attached to the surface of carbon materials from which hydrophobic properties have been removed. The research focuses on synthesizing carbon composites to improve the physical properties of a single material and realize high functionality through networking between materials. Therefore, it is expected that synthesizing a carbon/nanomaterial composite under supercritical process conditions will enable the synthesis of a homogeneous and highly processable composite material. Carbon materials such as graphene, which have high thermal conductivity and excellent mechanical properties, do not change their thermal conductivity characteristics even when bent, thereby overcoming the physical and functional limitations of existing heat dissipation materials and providing high-performance, lightweight, and environmentally friendly properties. In addition, it is attracting attention as a new material with optimal characteristics as a high heat dissipation material that can achieve energy savings.

**2D-ThP-9 Momentum Dependent Charge Density Wave Gap in an Antiferromagnetic Metal**, Nathan Valdez, University of Central Florida; S. Regmi, Idaho National Laboratory; I. Bin Elias, A. Pradhan Sakhya, D. Jeff, M. Sprague, M. Islam Mondal, D. Jarret, A. Agosto, University of Central Florida; T. Romanova, Polish Academy of Sciences, Poland; J. Chu, University of Washington; S. Khondaker, University of Central Florida; A. Ptok, D. Kaczorowski, Polish Academy of Sciences, Poland; M. Neupane, University of Central Florida

Charge density wave (CDW) ordering has been an important topic of study for a long time owing to its connection with other exotic phases such as superconductivity and magnetism. The RTe<sub>3</sub> (R = rare-earth elements) family of materials provides a fertile ground to study the dynamics of CDW in van der Waals layered materials, and the presence of magnetism in these materials allows to explore the interplay among CDW and long range magnetic ordering. Here, we have carried out a high-resolution angle-resolved photoemission spectroscopy (ARPES) study of a CDW material GdTe<sub>3</sub>, which is antiferromagnetic below  $\sim 12$  K, along with thermodynamic, electrical transport, magnetic, and Raman measurements. Our ARPES data show a two-fold symmetric Fermi surface with both gapped and ungapped regions indicative of the partial nesting. The gap is momentum dependent, maximum along  $\Gamma$ -Z and gradually decreases going towards  $\Gamma$ -X. Our study provides a platform to study the dynamics of CDW and its interaction with other physical orders in two- and three-dimensions.

\*This work is supported by the National Science Foundation under CAREER award DMR-1847962, the NSF Partnerships for Research and Education in Materials Grant DMR-2121953, and the Air Force Office of Scientific Research MURI Grant No. FA9550-20-1-0322.

**2D-ThP-10 Investigating the Electronic Structure of Bilayer Graphene/RuCl<sub>3</sub> Heterostructure**, Aalok Tiwari, S. Sasmal, I. Koo, Carnegie Mellon University, USA; C. Jozwiak, E. Rotenberg, Advanced Light Source, Lawrence Berkeley National Laboratory; A. Bostwick, advanced light Source, Lawrence Berkeley National Laboratory; S. Singh, J. Katoch, Carnegie Mellon University, USA

The stacking of two-dimensional materials to form van der Waals (vdW) heterostructures provides an unprecedented ability to tune electronic structure and engineer interfaces. RuCl<sub>3</sub> has recently attracted significant attention as it is a Mott insulator, Kitaev material, and interfacing with graphene results in massive charge transfer, modifying their electronic properties. This can be exploited to create low-power devices for novel optoelectronic applications. In this talk, I will present a comparison of the electronic structure of bilayer graphene on interfacing with  $\alpha$ -RuCl<sub>3</sub> and hBN, using angle-resolved photoemission spectroscopy with nanoscale spatial resolution (nanoARPES). We can directly explore the charge transfer at the interface due to different work function of the bilayer graphene and RuCl<sub>3</sub>. I will discuss tuning the electronic structure in bilayer graphene/RuCl<sub>3</sub> using electron doping via potassium atom deposition.

**2D-ThP-11 2D Materials for Energy-Efficient Nanoelectronics**, F. Yao, Huamin Li, University at Buffalo - SUNY

With the rise of graphene (Gr) since 2004, two-dimensional (2D) have been extensively explored for energy-efficient nanoelectronics due to their novel charge transport properties compared to conventional three-dimensional (3D) bulk materials. However, there are still challenges and issues for practical implementation of 2D materials. Here we take 2D semiconducting MoS<sub>2</sub> as an example to review our recent research of energy-efficient nanoelectronics, ranging from materials synthesis to structure engineering and device demonstration. First, by functionalizing the growth substrate, we can achieve on-demand selective-growth of 2D MoS<sub>2</sub> using chemical vapor deposition (CVD) and the electron mobility can be up to 20 cm<sup>2</sup>/Vs at room temperature. At the interface between MoS<sub>2</sub> and SiO<sub>2</sub> substrates, an interfacial tension can be induced due to a mismatch of thermal expansion coefficients, which creates an anisotropy of in-plane charge transport [1, 2] as well as a self-formed nanoscroll structure [3]. Second, at the interface between MoS<sub>2</sub> and metal contact, a monolayer h-BN decoration can enable novel manipulation of charge transport through quantum tunneling, in contrast with conventional thermionic emission [3]. The contact resistance can be suppressed by both localized and generalized doping using transition metals [4]. Third, at the interface between MoS<sub>2</sub> and other 2D materials, band-to-band Zener tunneling and cold-source charge injection can be enabled, giving rise to a superior transport factor (<60 meV/decade) in field-effect transistor (FET) configurations. These novel charge transport can be utilized to overcome the fundamental limit of "Boltzmann tyranny", and realize tunnel FETs and cold-source FETs with sub-60-mV/decade subthreshold swings [5-7] or novel anti-ambipolar FETs [8]. Fourth, at the

interface between MoS<sub>2</sub> and ferroelectric or ionic dielectrics, excellent electrostatic gating leads to a superior body factor (<1), and also improves the energy efficiency for transistor operation [9].

## Reference

1. H. Li and co-workers, under review by Nature Communication.
2. H. Li and co-workers, DRC, Ann Arbor, MI, p. 133, 2019.
3. H. Li and co-workers, Adv. Mater., vol. 32, no. 2002716, 2020.
4. H. Li and co-workers, Nanoscale, vol. 12, pp. 17253, 2020.
5. H. Li and co-workers, IEEE IEDM, virtual, p.251, 2020.
6. H. Li and co-workers, ACS Nano, vol. 15, pp. 5762, 2021.
7. H. Li and co-workers, ACS Nano, vol. 11, pp. 9143, 2017.
8. H. Li and co-workers, JVST B, vol. 41, no. 053202, 2023.
9. H. Li and co-workers, Nano Express, vol. 4, no. 035002, 2023.

## 2D-ThP-12 Unique Nanowire and 2D Material Device Fabrication by Nanofrazor Technology, *Nicholas Hendricks, F. Yang, E. Clerc, J. Chaaban, E. Çağın*, Heidelberg Instruments Nano AG, Switzerland

Thermal scanning probe lithography (t-SPL), enabled by the NanoFrazor technology, is a nanolithography technique particularly suitable for patterning, contacting, and modifying 2D materials and nanowires [1-6]. t-SPL generates patterns by scanning a heated ultrasharp tip over a sample surface to induce local changes. By using thermal energy as a stimulus, it is possible to perform various modifications to the sample via removal, conversion, or addition of/to the sample surface. Along with an ultrasharp tip, the t-SPL cantilever contains several other important functions such as an integrated thermal height sensor and an integrated heating element both of which are advantageous for generating devices from nanowires and 2D materials.

Nanowires and 2D materials have been the focus of intense academic and industrial research as these materials provide great promise as next generation electronic devices. However, when patterning electrical contacts to nanowires and 2D materials with conventional fabrication techniques (photolithography, electron beam lithography), the fabrication process becomes challenging and time consuming due to overlay requirements. These techniques can also lead to less than desired device performance due to damage from charged particles or ultraviolet irradiation, as well as contamination from residual resist. The issue of time intensive processing comes from the random positioning of nanowires and 2D material flakes on substrates which makes overlay challenging. This point of overlay is addressed with t-SPL by having an integrated thermal height sensor that allows for a non-invasive, in-situ measurement technique to detect buried nanowires or 2D materials prior to patterning. Such capabilities allow for real-time imaging and markerless overlay with high precision.

Within this presentation, the background and workings of t-SPL will be briefly introduced, nanostructuring on nanowires and 2D materials will be discussed along with electrical and optical device performance for nanowire and 2D material-based devices fabricated using t-SPL.

- [1] X. Zheng et al., Nat. Commun., 11, 3463 (2020)
- [2] X. Liu et al., APL Mater., 9, 011107 (2021)
- [3] A. Conde-Rubio et al., ACS Applied Materials & Interfaces, 14, 37 (2022)
- [4] S. Ghosh et al., ACS Appl. Mater. Interfaces, 15, 40709-40718 (2023)
- [5] H. Ying et al., Device, 1, 100069 (2023)
- [6] L. Shani et al., Nanotechnology, 35, 255302 (2024)

## 2D-ThP-13 Engineering Surface Termination of Ti<sub>2</sub>C<sub>3</sub>T<sub>x</sub> MXene for Enhanced Soft Actuator Performance, *D. Silva Quinones, Haozhe Wang*, Duke University

Ti<sub>2</sub>C<sub>3</sub>T<sub>x</sub>, the pioneer MXene, has attracted attention for its unique properties such as adjustable electrical conductivity, high mechanical stability, and versatile responsiveness, thus holding immense potential for advancing soft robotics and sensing applications. However, the performance of the MXene-based soft actuator is limited by uncontrollable surface terminations (-OH, -F, etc) induced in the synthesis process. Modifying these surface functional groups allows for customizing Ti<sub>2</sub>C<sub>3</sub>T<sub>x</sub> to possess desired properties.

This study introduces an innovative methodology to manipulate the surface termination of Ti<sub>2</sub>C<sub>3</sub>T<sub>x</sub> through plasma treatment. Various plasma conditions were applied to Ti<sub>2</sub>C<sub>3</sub>T<sub>x</sub> flakes, with resultant alterations in surface termination analyzed via X-ray Photoelectron Spectroscopy (XPS). Additionally, changes in structure were evaluated using X-ray Diffraction

(XRD) and Raman Spectroscopy. Furthermore, Ti<sub>2</sub>C<sub>3</sub>T<sub>x</sub>/cellulose actuators were fabricated utilizing Ti<sub>2</sub>C<sub>3</sub>T<sub>x</sub> with controlled surface terminations. Nanocrystal and nanofiber phases of cellulose were employed and compared to optimize actuation performance. Remarkably, the Ti<sub>2</sub>C<sub>3</sub>T<sub>x</sub>/cellulose actuator exhibited robust responses to Near-Infrared (NIR) light, showcasing potential applications in soft robotics and sensing. The mechanism of controlled surface terminations contributing to the multi-responsive actuator will also be discussed.

## 2D-ThP-14 Graphene-Based Hybrid Nanoparticle for the Chemotherapy Treatment of Prostate Cancer, *Diego La Mendola, L. Chiaverini, R. Di Leo, C. Giorgieri*, University of Pisa, Italy; *C. Satriano*, University of Catania, Italy; *T. Marzo*, University of Pisa, Italy

Prostate cancer (PC) is a frequent malignancy in men with a poor prognosis in the case of relapse or disease detected at the advanced stage with metastasis. It is ascertained as the levels of angiogenin (Ang) a potent angiogenic factor involved in cancer cells spreading- dramatically increase in PC patients, positively correlating with the disease progression and prognosis. Accordingly, Ang and angiogenesis-related processes represent a promising target. On the other hand, though taxanes represent the standard chemotherapy, their combinations with platinum anticancer drugs show advantages. Based on these premises we aim to improve the combination chemotherapy for PC developing PLGA-PEG fluorescent biocompatible nanovectors (NVs) for drugs loading decorated with angiogenin-mimicking peptides, and deposited onto reduced form of graphene oxide (rGO).

These new graphene-based hybrid nanoparticle have been characterized by means of UV-visible spectroscopy, Zeta potential, Atomic Force Microscopy. Biological tests showed that the synthesized systems are able to carry out taxanes, platinum complexes into specific target leading to impairment of cancer cells angiogenesis.

Acknowledgments: The financial support from Ministero Italiano dell'Università e della Ricerca under the program PRIN 2022 - Progetti di Rilevante Interesse Nazionale, project code: 2022ALJRPL "Biocompatible nanostructures for the chemotherapy treatment of prostate cancer"

## 2D-ThP-15 Investigating the Interaction between MXene and Silane through High-Resolution X-ray Photoelectron Spectroscopy (XPS), *Mohamed Nejjib Hedhili, M. Ali, S. Barman, D. Alsulaiman, H. Alshareef*, KAUST, Saudi Arabia

MXene grafted with silane combines the distinctive properties of MXene nanosheets with the functional advantages of silane molecules, thereby enhancing versatility and performance across various applications, from materials science to biomedical engineering. The modification of MXene with silane involves chemically bonding silane molecules onto the surface of MXene nanosheets. Despite this, the bonding mechanism between silane and MXene remains incompletely understood. This study introduces an XPS-based methodology to unequivocally determine the silane-MXene coupling. The approach involves comparing XPS results of pristine MXene with silane-modified MXene and MXene modified with silane-free agents like alcohol. The XPS data reveal the formation of Ti-O-Si bonds exclusively following silanization of MXene, with no such bonds observed in alcohol-modified MXene. Therefore, this analysis underscores the capability of XPS in identifying the bonding nature between silane and MXene.

## 2D-ThP-17 Study of Electronic and Optical Properties of TMD Heterostructures Grown by CVD, *Elycia Wright*, Clark Atlanta University; *K. Johnson*, Morehouse College; *S. Coye, M. Senevirathna, M. Williams*, Clark Atlanta University

Transition metal dichalcogenides (TMDs) have attracted significant attention in the semiconductor field due to their unique properties. These properties, such as having a direct bandgap in the visible-infrared range, rich valley physical properties, and strong spin-orbit coupling, make them promising for various applications in electronics, optoelectronics, spintronics, and valleytronics. Furthermore, the distinct physical properties of 2D TMD heterostructures further enhance their potential, leading to a growing interest in researching heterostructures composed of different TMD materials.

Chemical vapor deposition (CVD) techniques have proven advantageous in producing TMD materials and their heterostructures with controlled thickness due to their low cost, high yield, and industrial compatibility. However, challenges, such as different growth windows among different TMD materials when growing high-quality large-area TMD heterostructures, need to be addressed.

# Thursday Evening, November 7, 2024

This work will investigate new strategies for producing large-area TMD heterostructures, such as MoSe<sub>2</sub>/WS<sub>2</sub>, using various chemical vapor deposition (CVD) techniques. We will analyze the properties of these materials, including their band gap, optical phonon modes, and excitons, using Raman and photoluminescence spectroscopy.

**2D-ThP-18 Synthesis, Fabrication and Mechanical Testing of Freestanding Few-Layer Draphene/Boron Nitride/Polymer Heterostacks Investigated Using Local and Non-Local Measurement Techniques, Yoosuk Kim, M. Lespasio, Saint Louis University, Department of Physics; E. Missale, University of Trento, Department of Civil, Environmental and Mechanical Engineering, Italy; B. Aziz, Saint Louis University, Department of Physics; G. Speranza, University of Trento, Department of Industrial Engineering,, Italy; R. Divan, D. Gosztola, Argonne National Laboratory, Center for Nanoscale Materials; C. Lei, University of Scranton, Department of Physics and Engineering; M. Pantano, University of Trento, Department of Civil, Environmental and Mechanical Engineering, Italy; I. Kuljanishvili, Saint Louis University, Department of Physics**

Two-dimensional (2D) van der Waals materials and their heterostructures have gained significant interest in the past two decades due to their unique characteristics, including high aspect ratio and specific physical, electrical, and mechanical properties. Heterostructures composed of two or more 2D materials have emerged as key components for applications in metaphotonics, energy storage, transistors, photodiodes, memory, and photovoltaics. Understanding the mechanical properties of multilayered 2D materials is essential for practical applications which often involve advanced synthesis methods, developing new transfer techniques and designing custom platforms and architectures for their reliable evaluation and measurements. Techniques such as buckling or bending metrology, nanoindentation, bulge testing, atomic force microscopy (AFM) deflection tests, and tensile testing are necessary to measure these properties. Expanding the mechanical characterization of heterostructures like graphene and boron nitride, especially when capped with a polymeric layer, is vital for practical applications.

This study presents the synthesis, fabrication and mechanical testing of 2D hybrid heterostacks, consisting of few-layer boron nitride and two-three layered graphene heterostructures synthesized via chemical vapor deposition, capped with polymethyl methacrylate layer and suspended across ~200 μm wide trenches using a combined wet-dry transfer method. The mechanical characterization of the heterostacks was performed using two independent approaches: (a) non-local tensile testing (b) local load-displacement testing employing atomic force microscopy probes, complemented by finite element simulations. Both approaches provided new results, which are in good agreement with each other. Our findings offer new insights into a combined load capacity in complex multi-material two-dimensional hybrid systems, and underscore the potential of 2D hybrid heterostructures for advancing micro- and nano-scale device designs, particularly in applications requiring large-area mechanical stability.

## 2D Materials

### Room 122 - Session 2D+EM+MN+TF-FrM

#### 2D NEMS and Strain Engineering

Moderator: Matthias Batzill, University of South Florida

8:45am **2D+EM+MN+TF-FrM-3 Longitudinal Sound Speed Determination in 2D Semiconducting Crystal of GaS by Broadband Time-Domain Brillouin Scattering**, *Watheq Al-Basheer*, King Fahd University of Petroleum & Minerals, Saudi Arabia; *C. Viernes, R. Zheng, S. Netzke, K. Pichugin, G. Sciaini*, University of Waterloo, Canada

Due to their unique structure and exceptional physicochemical characteristics, 2D semiconducting materials like GaS have recently attracted significant interest, making them viable options for numerous photonic industries and applications. In this study, time-domain broadband Brillouin scattering measurements were performed on a single, flake-like gallium sulfide (GaS) crystal to determine the out-of-plane longitudinal sound speed, evaluated at  $(3140 \pm 20)$  m/s. As a member of the group-III monochalcogenide semiconductors, GaS has recently attracted significant attention owing to its remarkable semiconducting properties. Moreover, its high absorption coefficient and efficient carrier mobility have made it a perfect candidate in many photonic and optoelectronic applications and industries, such as fast UV photodetectors, hydrogen evolution catalysis, field-effect transistors, energy storage, gas sensing, and nonlinear optics. The reported results demonstrate the effectiveness of this non-destructive, all-optical technique for investigating the elastic properties of fragile 2D layered materials and provide the value of the out-of-plane compressive elastic constant.

#### Keywords

Time-domain Brillouin scattering, coherent acoustic phonons, broadband transient spectroscopy,

elastic constant, sound speed, 2D semiconductors, GaS, layered materials.

9:00am **2D+EM+MN+TF-FrM-4 Laser-Induced Strain Tuning in Monolayer Graphene Nanomechanical Resonators**, *Muhammad Ashar Naveed, S. Pandit, Y. Wang*, University of Nebraska - Lincoln

Graphene, as the paradigm-shifting two-dimensional (2D) material, has demonstrated great potential in micro-/nano-electromechanical systems (MEMS/NEMS) due to its extraordinary mechanical properties, ultimate device thicknesses, and unparalleled flexibility in integration. On the other hand, the atomic thickness and the transfer process employed in device fabrication pose challenges to achieving uniform strain over the entire device. In this work, we utilize Raman spectroscopy and investigate the strain distribution in drumhead resonators based on the mechanically exfoliated graphene monolayers suspended over patterned oxidized silicon ( $\text{SiO}_2/\text{Si}$ ) substrates. Moreover, the effects of laser-induced heating and consequential strain tuning have been systematically explored by combining Raman spectroscopy and mechanical resonance measurements. This study sheds light on the strain engineering of monolayer graphene nanomechanical resonators, and the methodology developed is readily applied to other 2D materials and heterostructures.

9:15am **2D+EM+MN+TF-FrM-5 Developing 2D SnSe for Piezoelectric Applications**, *J. Chin, M. Frye, B. Gardner*, Georgia Institute of Technology; *D. Liu*, Penn State University; *M. Hulse*, Pennsylvania State University; *I. Graham*, Georgia Institute of Technology; *J. Shallenberger, K. Wang, M. Wang, Y. Shin, N. Nayir, A. can Duin, S. Law*, Pennsylvania State University; *Lauren Garten*, Georgia Institute of Technology

Unique functionalities can arise when 2D materials are scaled down near the monolayer limit. Tin selenide (SnSe) is one such 2D material which is centrosymmetric in bulk but becomes non-centrosymmetric when reduced to the monolayer limit, enabling piezoelectricity, and potentially, ferroelectricity. Developing 2D piezoelectric and ferroelectric materials is critical for the scaling of efficient sensors and electronics, such as ferroelectric field effect transistors. However, unlike other 2D materials, the strong interlayer bonding makes exfoliating a monolayer of SnSe challenging. Therefore, direct film growth is necessary to control the layer thickness and promote lateral growth large enough for device testing. This talk will focus on the development of processing routes to control the morphology and layering of SnSe thin films grown by molecular beam epitaxy (MBE) for piezoelectric devices. The bulk *Pnma* phase of SnSe is stabilized over a broad range of Sn:Se flux ratios from 250 – 300 °C on (100) MgO and (0001)  $\text{Al}_2\text{O}_3$  substrates. Changing the flux ratio did not affect the SnSe film stoichiometry; increasing the flux ratio only changes the predominant crystallographic orientation. ReaxFF molecular dynamics (MD)

show that the limited stoichiometric change is due to the formation of Se clusters that weakly interact with the surface of the SnSe particles. Changing the temperature, flux ratios, and flux timing had a significant impact on the morphology and orientation of the SnSe thin films. Machine learning was used to infer the critical processing parameters that are needed for creating an oriented, wafer-scale thin film. Overall, this study identifies the conditions for the growth of monolayer SnSe thin films necessary for the development of 2D piezoelectric devices.

9:30am **2D+EM+MN+TF-FrM-6 Two-Dimensional (2D)  $\text{FePS}_3$  Nanoelectromechanical Resonators with Local-Gate Electrostatic Tuning**, *Yunong Wang, S. Yousuf, X. Zhang, P. Feng*, University of Florida

Nanoelectromechanical systems (NEMS) based on 2D magnetic materials are promising candidates for exploring ultrasensitive detection and magnetostrictive phenomena due to their high mechanical stiffness, high strength, and low mass. The resonance frequency of the suspended membrane resonator can be probed optically and manipulated mechanically via electrostatically induced strain. This makes electrostatic frequency tuning of the 2D magnetic NEMS resonator a promising way for exploring the novel magneto-mechanical coupling mechanism. Towards building magneto-mechanical coupling NEMS devices, we fabricated circular drumhead  $\text{FePS}_3$  NEMS resonators with different cavity-diameter sizes (3 $\mu\text{m}$  to 7 $\mu\text{m}$ ). In this work, we report on experimental demonstrations of high-performance antiferromagnet  $\text{FePS}_3$  drumhead resonators with the highest frequency tuning range up to 31.62%. We further perform analytical modeling to gain insight and quantitative understanding of the frequency scaling law for  $\text{FePS}_3$  drumhead resonators. Combining our experimental results and analytical modeling of the resonances, we resolved the elastic behavior of  $\text{FePS}_3$ , including the transition from ‘membrane-like’ regime to ‘plate-like’ regime, with built-in tension ( $\gamma$ ) ranging from 0.1 to 2N/m. This study not only offers methods for characterizing the mechanical properties of ultrathin membranes of magnetic 2D materials but also provides important guidelines for designing high-performance magnetic NEMS resonator devices and opens possibilities for building drumhead resonator devices to exploit strain- and dynamics-engineered applications based on ultrathin magnetic 2D crystals.

9:45am **2D+EM+MN+TF-FrM-7 Tunable Phononic Frequency Combs in Atomically Thin Resonators**, *S M Enamul Hoque Yousuf, T. Kaisar*, University of Florida; *J. Lee*, University of Central Florida; *S. Shaw*, Florida Institute of Technology; *P. Feng*, University of Florida

Phononic frequency comb (PnFC), the analogue of optical frequency comb in the radio frequency (RF) regime, has attracted significant research interest due to its potential applications in sensing and computing. In this abstract, we report on PnFCs generation via an atomically thin molybdenum disulfide ( $\text{MoS}_2$ ) nanoelectromechanical resonator. We first measure the nonlinear mode coupling coefficient ( $\lambda$ ) due to 1:1 internal resonance from the first-principles approach. To describe the energy exchange between the coupled modes, we employ two resonator equations with a single dispersive coupling term to model the response. The coupled mode equations are solved using the method of averaging to derive a closed form expression for the nonlinear mode coupling coefficient. To calibrate the vibration amplitude of both modes in the displacement domain, we measure the undriven thermomechanical noise. The nonlinear shift of the resonance frequency of mode 1 ( $f_1$ ) that results from the dispersive coupling to mode 2 is measured as we drive mode 2 near its natural frequency ( $f_2$ ). We estimate the mode coupling coefficient using our derived model. Additionally, we investigate the impact of Duffing nonlinearity on the energy cycling of the modes.

We utilize the 1:1 internal resonance to couple energy between two modes. The resonator response can be tuned from stable periodic response to quasi-periodic response by controlling external perturbation signals, such as DC gate voltage, RF drive voltage and frequency. The resonator exhibits three unique comb regions with well-defined comb structure. We observe that the periodic and quasiperiodic branches exist for a particular drive voltage and frequency, based on distinct initial conditions. Our demonstration leads the way to achieving tunable PnFCs in nanoscale devices to study nonlinear modal interactions and build ultrasensitive sensors and computing devices.

**Bold page numbers indicate presenter**

— A —

Abbas, Ali: MI+2D+AC+TF-WeA-4, 17;  
MI+2D+AC+TF-WeM-7, 11; MI+2D+AC+TF-WeM-8, **11**  
Adachi, Yutaka: SS+2D+AMS-WeA-2, 18  
Agosto, Alexis: 2D-ThP-9, 28  
Ahmed, Asma: 2D+AP+EM+QS+SS+TF-TuM-6, 3  
Akande, Wisdom: EM+2D+BI+QS+TF-TuA-4, **7**  
Alanwoko, Onyedikachi:  
2D+AP+EM+QS+SS+TF-TuM-14, 4; 2D-ThP-3, **27**  
Al-Basheer, Watheq: 2D+EM+MN+TF-FrM-3, **31**  
Alcer, David: EM+2D+BI+QS+TF-TuA-3, 7  
Alem, Tinsae: 2D-ThM-6, 22  
Ali, Muhsin: 2D-ThP-15, 29  
Alshareef, Husam Niman: 2D-ThP-15, 29  
Alsulaiman, Dana: 2D-ThP-15, 29  
Ambrozaite, Ona: 2D-WeA-6, 15  
Argyropoulos, Christos: MI+2D+AC+TF-WeA-10, 18  
Asel, Thaddeus: EM+2D+AP+QS+TF-ThM-5, **24**  
Asselberghs, Inge: 2D+EM+MI+QS-WeM-4, 9  
Auwärter, Willi: SS+2D+AMS-WeM-5, **13**  
Azcatl, Angelica: 2D+EM+MI+QS-WeM-13, 10  
Aziz, Bashar: 2D-ThP-18, 30

— B —

Bae, Joonyup: 2D-ThM-4, **21**  
Balajka, Jan: SS+2D+AMS-WeA-5, 19  
Balashov, Timofey: 2D-WeA-12, 16  
Balasubramanian, Ganesh: SS+2D+AMS-WeA-12, 20  
Balicas, Luis: 2D+EM+MI+QS-WeM-15, **10**  
Ball, Biswajit: 2D+EM+QS-ThA-5, 26  
Ballav, Swastik: 2D-WeA-4, **15**  
Banerjee, Parag: EM+2D+BI+QS+TF-TuA-11, 8; EM+2D+BI+QS+TF-TuA-9, 8  
Bansil, Arun: MI+2D+AC+TF-WeA-3, 17  
Bara, Jason: SS+2D+AMS-WeM-17, 14  
Barman, Sharat Chandra: 2D-ThP-15, 29  
Barreto, Lucas: MI+2D+AC+TF-WeM-14, **12**  
Barsukov, Yuri: 2D-ThP-6, 27  
Bastani, Farzad: 2D-ThM-5, 21  
Batziil, Matthias: 2D+AP+EM+QS+SS+TF-TuM-13, **3**; 2D+AP+EM+QS+SS+TF-TuM-14, 4; 2D-ThP-2, 27; 2D-ThP-3, 27  
Beckman, Eric: 2D-WeA-1, 15  
Ben Khallouq, Rachid: 2D-WeA-4, 15  
Bentmann, Hendrik: MI+2D+AC+TF-WeM-1, 10  
Bergsman, David: SS+2D+AMS-WeM-13, **13**  
Bhandari, Ghadendra: MI+2D+AC+TF-WeM-4, **11**  
Bhattacharjee, Nirjhar: MI+2D+AC+TF-WeA-3, 17  
Bilal, Laiba: 2D+LS+NS+SS-TuA-12, **6**  
Bin Elius, Iftakhar: 2D-ThP-9, 28  
Binek, Christian: MI+2D+AC+TF-WeA-10, 18  
Birmingham, Blake: EM+2D+BI+QS+TF-TuA-5, 7  
Bissel, Eric: EM+2D+BI+QS+TF-TuA-11, 8  
Bissell, Eric: EM+2D+BI+QS+TF-TuA-9, 8  
Blades, Will: SS+2D+AMS-WeA-11, 20  
Blades, William: 2D-ThM-5, 21  
Boehm, Alex: 2D+LS+NS+SS-TuA-11, 6  
Bonaccorso, Carmela: 2D+EM+QS-ThA-3, 26  
Borgschulze, Andreas: MI+2D+AC+TF-WeA-11, 18  
Borgström, Magnus: EM+2D+BI+QS+TF-TuA-3, 7  
Borys, Nicholas J.: 2D+LS+NS+SS-TuA-5, 5

Boscoboinik, Anibal: 2D+LS+NS+SS-TuA-12, 6  
Boscoboinik, J. Anibal: SS+2D+AMS-WeM-16, 14  
Bostwick, Aaron: 2D+LS+NS+SS-TuA-1, 5; 2D+LS+NS+SS-TuA-3, 5; 2D-ThP-10, 28  
Bowman, William: EM+2D+BI+QS+TF-TuA-10, **8**  
Briley, Chad: MI+2D+AC+TF-WeA-10, 18  
Brohet, Maxime: SS+2D+AMS-WeA-10, 19  
Buck, Manfred: 2D-WeA-11, 16  
Burns, Kory: 2D-ThM-5, 21; 2D-ThM-6, **22**  
Butler, Anthony: 2D+AP+EM+QS+SS+TF-TuM-6, 3

— C —

Cabanillas, Anthony: 2D+AP+EM+QS+SS+TF-TuM-6, 3  
Çağın, Emine: 2D-ThP-12, 29  
Callahan, Dennis: EM+2D+BI+QS+TF-TuA-9, 8  
Campi, Gustavo: SS+2D+AMS-WeA-15, 20  
Campos Jara, Sergi: SS+2D+AMS-WeA-10, 19  
can Duin, Adri: 2D+EM+MN+TF-FrM-5, 31  
Canto, Barbara: 2D+EM+MI+QS-WeM-4, 9  
Carreño, Vanessa: SS+2D+AMS-WeA-15, 20  
Carreño-Díaz, Vanessa: SS+2D+AMS-WeM-3, 12  
CASTREJÓN FLORES, JOSÉ LUIS: 2D-ThP-7, 28  
Castro, David: 2D+EM+QS-ThA-6, **26**; 2D-WeA-4, 15  
Ceccatto, Alisson: SS+2D+AMS-WeA-15, **20**; SS+2D+AMS-WeM-3, 12  
Cechal, Jan: SS+2D+AMS-WeM-4, 13  
Chaaban, Jana: 2D-ThP-12, 29  
Chakravarty, Anindita:  
2D+AP+EM+QS+SS+TF-TuM-6, 3  
Chan, Maria: SS+2D+AMS-WeA-14, 20  
Chen, Charlene: 2D+EM+MI+QS-WeM-13, 10  
Chen, Chu-Te: 2D+AP+EM+QS+SS+TF-TuM-6, **3**  
Chen, Pengyu: EM+2D+BI+QS+TF-TuA-8, 7  
Cheng, Ching-Jung: 2D+EM+MI+QS-WeM-13, 10  
Cherepanov, Vasily: 2D-WeA-12, 16  
Cherono, Sheilah: EM+2D+BI+QS+TF-TuA-4, 7  
Chi, Hang: MI+2D+AC+TF-WeA-1, **16**  
Chiaverini, Lorenzo: 2D-ThP-14, 29  
Chien, TeYu: SS+2D+AMS-WeA-12, 20  
Chin, Jonathan: 2D+EM+MN+TF-FrM-5, 31; 2D-ThM-14, **22**  
CHINO ULLOA, ALEXIS: 2D-ThP-7, 28  
Choo, Sooho: EM+2D+AP+QS+TF-ThM-6, 25  
Chris-Okoro, Ikenna: EM+2D+BI+QS+TF-TuA-4, 7  
Chu, Jiun-Haw: 2D-ThP-9, 28  
Churchill, Hugh: 2D+LS+NS+SS-TuA-5, 5  
Clark, Mark: 2D+EM+MI+QS-WeM-13, 10  
Clerc, Elliott: 2D-ThP-12, 29  
Coelho, Paula M.: 2D-ThM-2, 21  
Coelho, Paula Mariel: 2D-ThM-1, **21**  
Coll, Mariona: EM+2D+AP+QS+TF-ThM-6, 25  
Constantin Popescu, Cosmin:  
EM+2D+BI+QS+TF-TuA-9, 8  
Cott, Daire: 2D-ThM-15, 23  
Counsell, Jonathan: 2D+LS+NS+SS-TuA-4, **5**  
Coye, Selena: 2D+AP+EM+QS+SS+TF-TuM-7, 3; 2D-ThP-17, 29  
Craciun, Valentin: EM+2D+BI+QS+TF-TuA-4, 7  
Crumlin, Ethan: EM+2D+BI+QS+TF-TuA-4, 7  
Cui, Alex: 2D+EM+MI+QS-WeM-7, 9  
Cunha, Carlos: 2D+EM+MI+QS-WeM-4, 9  
Currie, Taylor: 2D+AP+EM+QS+SS+TF-TuM-17, **4**

— D —

D. Schlosser, Rasmus: EM+2D+BI+QS+TF-TuA-3, 7

Daniels, Avery: SS+2D+AMS-WeM-7, **13**  
Darwin, Emily: MI+2D+AC+TF-WeA-11, 18  
Das, Abhijit: EM+2D+BI+QS+TF-TuA-3, 7  
De Bonis, Angela: 2D+EM+QS-ThA-3, 26  
De Gendt, Stefan: 2D+EM+MI+QS-WeM-4, 9  
de la Rosa, Cesar: 2D-ThM-15, 23  
de Marneffe, Jean-Francois: 2D+EM+MI+QS-WeM-4, **9**  
de Siervo, Abner: SS+2D+AMS-WeA-15, 20; SS+2D+AMS-WeM-3, **12**  
Deshpande, Vikram: 2D+EM+MI+QS-WeM-5, **9**  
Dewasurendra, Vikum: MI+2D+AC+TF-WeM-4, 11  
Dey, Dibyendu: 2D+EM+QS-ThA-5, **26**  
Dhas, Jeffrey: SS+2D+AMS-WeM-17, 14  
Di Leo, Riccardo: 2D-ThP-14, 29  
Diebold, Ulrike: SS+2D+AMS-WeA-5, 19  
Dissanayake, N.: SS+2D+AMS-WeM-8, 13  
Divan, Ralu: 2D-ThP-18, 30  
Donath, Markus: MI+2D+AC+TF-WeM-13, **12**  
Dorfman, Kevin: EM+2D+BI+QS+TF-TuA-8, 7  
Douglas, Ossie: 2D-ThM-8, **22**  
Dowben, Peter: SS+2D+AMS-WeA-6, 19  
Dryzhakov, Bogdan: MI+2D+AC+TF-WeA-9, **17**  
Dubs, Carsten: MI+2D+AC+TF-WeA-3, 17  
Dürr, Michael: SS+2D+AMS-WeM-15, **14**  
D'Urso, Luisa: 2D+EM+QS-ThA-3, 26

— E —

E. Sestoft, Joachim: EM+2D+BI+QS+TF-TuA-3, 7  
Ellison, Christopher: EM+2D+BI+QS+TF-TuA-8, 7  
Eres, Gyula: 2D+AP+EM+QS+SS+TF-TuM-8, 3  
Erickson, Tyler: MI+2D+AC+TF-WeM-7, 11  
Esatu, Tsegereda: 2D-WeA-5, 15  
Ethier, Stephane: 2D-ThP-6, 27  
Evans, Anne: 2D-ThM-1, 21

— F —

Farber, Rachael: SS+2D+AMS-WeM-8, **13**  
Feder, Rene: MI+2D+AC+TF-WeA-10, 18  
Feng, Philip: 2D+EM+MN+TF-FrM-7, 31  
Feng, Philip X.-L.: 2D+EM+MN+TF-FrM-6, 31  
Ferreira, Eidsa: SS+2D+AMS-WeA-15, 20  
Ferreira, Eidsa Brenda da Costa: SS+2D+AMS-WeM-3, 12  
Ferry, Vivian: EM+2D+BI+QS+TF-TuA-1, **6**; EM+2D+BI+QS+TF-TuA-8, 7  
Figgemeier, Tim: MI+2D+AC+TF-WeM-1, 10  
Fiorenza, Roberto: 2D+EM+QS-ThA-3, 26  
Fleischer, Jason: 2D-WeA-5, 15  
Flodgren, Vidar: EM+2D+BI+QS+TF-TuA-3, 7  
Fonseca Vega, Jose: 2D+LS+NS+SS-TuA-11, 6  
Foti, Alice: 2D+EM+QS-ThA-3, 26  
Fraix, Aurore: 2D+EM+QS-ThA-3, 26  
Frederick, Emily: 2D-WeA-3, **15**  
Freiberger, Eva Marie: SS+2D+AMS-WeA-15, 20  
Friedman, Adam: 2D-WeA-5, 15; NS1+2D+QS-MoA-3, 1  
Friedman, Adam L.: 2D+EM+MI+QS-WeM-3, 9; 2D-WeA-6, 15  
Fritz, Torsten: 2D+AP+EM+QS+SS+TF-TuM-5, 2  
Frye, Marshall: 2D+EM+MN+TF-FrM-5, 31; 2D-ThM-14, 22  
Fu, Yu: 2D+AP+EM+QS+SS+TF-TuM-6, 3  
Fukazawa, Atsuki: 2D+AP+EM+QS+SS+TF-TuM-3, 2  
Fullerton Shirey, Susan: 2D-WeA-1, **15**

— G —

Gai, Zheng: MI+2D+AC+TF-WeM-3, 10  
Gao, Zhi: EM+2D+BI+QS+TF-TuA-5, 7



## Author Index

- Gardner, Bonnie: 2D+EM+MN+TF-FrM-5, 31; 2D-ThM-14, 22  
Garten, Lauren: 2D+EM+MN+TF-FrM-5, **31**; 2D-ThM-14, 22  
Gaume, Romain: EM+2D+BI+QS+TF-TuA-10, 8  
Gayles, Jacob: MI+2D+AC+TF-WeM-15, 12  
Geldiyev, Begmuhammet: MI+2D+AC+TF-WeM-1, 10  
Geohegan, David: 2D+AP+EM+QS+SS+TF-TuM-4, 2  
Geohegan, David B.: 2D+AP+EM+QS+SS+TF-TuM-8, 3  
George, Antony: 2D+AP+EM+QS+SS+TF-TuM-5, 2  
Ghimire, Suvash: 2D+EM+QS-ThA-4, **26**  
Ghorbani-Asl, Mahdi: 2D+AP+EM+QS+SS+TF-TuM-5, 2  
Giorgieri, Claudia: 2D-ThP-14, 29  
Glaser, Timo: SS+2D+AMS-WeM-15, 14  
Gosztola, David J.: 2D-ThP-18, 30  
Graham, Ian: 2D+EM+MN+TF-FrM-5, 31  
Green, Robert: MI+2D+AC+TF-WeM-14, 12  
Groot, Irene: SS+2D+AMS-WeA-10, **19**  
Groven, Benjamin: 2D-ThM-15, 23  
Grubbs, Robert K.: 2D-ThM-15, **23**  
Gruenewald, Marco: 2D+AP+EM+QS+SS+TF-TuM-5, 2  
Grutter, Alexander: MI+2D+AC+TF-WeA-3, 17  
Grutter, Karen E.: 2D+EM+MI+QS-WeM-3, 9  
Guisinger, Nathan: SS+2D+AMS-WeA-14, **20**  
— **H** —  
Hachtel, Jordan: 2D+AP+EM+QS+SS+TF-TuM-4, 2; 2D-ThM-6, 22  
Hajzuz, Jenifer: 2D+AP+EM+QS+SS+TF-TuM-16, **4**; EM+2D+AP+QS+TF-ThM-2, 23; EM+2D+AP+QS+TF-ThM-3, 24  
Hall, Hannah: MI+2D+AC+TF-WeM-7, 11  
Hammer, Lutz: MI+2D+AC+TF-WeM-13, 12  
Hanbicki, Aubrey: 2D-WeA-5, 15; NS1+2D+QS-MoA-3, 1  
Hanbicki, Aubrey T.: 2D+EM+MI+QS-WeM-3, 9; 2D-WeA-6, 15  
Haraldsen, Jason: 2D-ThM-1, 21  
Haraldsen, Jason T.: 2D-ThM-2, 21  
Harris, Sumner B.: 2D+AP+EM+QS+SS+TF-TuM-8, 3  
Harrison, Ian: MI+2D+AC+TF-WeM-3, 10  
Hasani, Amirhossein: 2D+LS+NS+SS-TuA-5, 5  
He, Gaohang: 2D+EM+MI+QS-WeM-4, 9  
Hedhilij, Mohamed Nejjib: 2D-ThP-15, **29**  
Heiman, Don: MI+2D+AC+TF-WeA-3, 17  
Heldebrant, David: SS+2D+AMS-WeM-17, 14  
Hendricks, Nicholas: 2D-ThP-12, **29**  
Hersam, Mark: NS1+2D+QS-MoA-1, 1  
Hight Walker, Angela: NS1+2D+QS-MoA-3, 1  
Hilse, Maria: 2D+EM+MN+TF-FrM-5, 31; 2D-ThM-14, 22  
Hirushan, H. H.: SS+2D+AMS-WeM-8, 13  
Hoang, Lauren: 2D-ThM-7, 22  
Hofmann, Jonathan: 2D-WeA-12, 16  
Holcomb, Mikel: MI+2D+AC+TF-WeM-4, 11  
Hruza, Dominik: SS+2D+AMS-WeM-4, 13  
Hu, Bin: MI+2D+AC+TF-WeA-9, 17  
Hu, Jonathan: EM+2D+BI+QS+TF-TuA-5, 7  
Hu, Juejun: EM+2D+BI+QS+TF-TuA-11, 8; EM+2D+BI+QS+TF-TuA-9, 8  
Huang, Yu min: 2D+AP+EM+QS+SS+TF-TuM-3, 2  
Hug, Hans Josef: MI+2D+AC+TF-WeA-11, 18  
Hui, Haolei: 2D+AP+EM+QS+SS+TF-TuM-6, 3  
Hüttner, Johanna: SS+2D+AMS-WeA-5, **19**  
— **I** —  
Ilevlev, Anton: 2D+AP+EM+QS+SS+TF-TuM-4, 2  
Ingram, David C.: MI+2D+AC+TF-WeA-4, 17  
Irisawa, Toshifumi: 2D+AP+EM+QS+SS+TF-TuM-3, 2  
Ishigami, Masahiro: 2D+LS+NS+SS-TuA-10, 6; 2D-WeA-3, 15; 2D-WeA-4, 15  
Islam Mondal, Mazharul: 2D-ThP-9, 28  
Islam, Md. Roxy: 2D+EM+QS-ThA-4, 26  
— **J** —  
J. Koester, Steven: EM+2D+AP+QS+TF-ThM-6, 25  
J. Lockhart de la Rosa, Cesar: 2D+EM+MI+QS-WeM-4, 9  
Jaekel, Simon: SS+2D+AMS-WeA-15, 20  
Jakub, Zdenek: SS+2D+AMS-WeM-4, **13**  
Jalan, Bharat: EM+2D+AP+QS+TF-ThM-6, 25  
Jangid, Rahul: 2D+EM+MI+QS-WeM-7, 9  
Janotti, Anderson: 2D-ThM-3, 21  
Jarret, Damani: 2D-ThP-9, 28  
Jeff, Dylan: 2D-ThP-9, 28  
Jessup, Devin: SS+2D+AMS-WeA-11, 20  
Jin, Mengru: 2D-WeA-13, **16**  
Jin, Rongying: MI+2D+AC+TF-WeM-3, 10  
Johnson, Kedar: 2D+AP+EM+QS+SS+TF-TuM-7, 3; 2D-ThP-17, 29  
Johnson, Matthew: MI+2D+AC+TF-WeM-4, 11  
Jois, Sharadh: 2D-WeA-5, **15**  
Jonker, Berend T.: 2D+LS+NS+SS-TuA-3, 5  
Jozwiak, Chris: 2D+LS+NS+SS-TuA-3, 5; 2D-ThP-10, 28  
Jurca, Titel: 2D+AP+EM+QS+SS+TF-TuM-17, 4  
— **K** —  
Kaczorowski, Dariusz: 2D-ThP-9, 28  
Kaganovich, Igor: 2D-ThP-6, 27  
Kaisar, Tahmid: 2D+EM+MN+TF-FrM-7, 31  
Kanatzidis, Mercouri: 2D-WeA-13, 16  
Kanjolia, Ravi: 2D+EM+MI+QS-WeM-13, 10  
Kanne Nordqvist, Thomas: EM+2D+BI+QS+TF-TuA-3, 7  
Kao, I-Hsuan: 2D-ThP-10, 28  
Kar, Gouri: 2D-ThM-15, 23  
Karbasizadeh, Siavash: MI+2D+AC+TF-WeM-3, 10  
Katoch, Jyoti: 2D+LS+NS+SS-TuA-3, 5; 2D-ThP-10, 28  
Kayastha, Rohil: EM+2D+BI+QS+TF-TuA-5, **7**  
Keeney, Patrick: 2D-ThM-1, 21; 2D-ThM-2, **21**  
Kempa, Thomas J.: 2D-WeA-6, 15  
Khalid, Shoab: 2D-ThM-3, **21**; 2D-ThP-6, **27**  
Khatun, Salma: 2D+AP+EM+QS+SS+TF-TuM-14, **4**  
Khondaker, Saiful: 2D-ThP-9, 28  
Kilic, Ufuk: MI+2D+AC+TF-WeA-10, **18**  
Kim, Andrew: 2D+LS+NS+SS-TuA-11, 6  
Kim, Jihyun: 2D-ThM-4, 21; EM+2D+BI+QS+TF-TuA-12, 8  
Kim, Lauren: SS+2D+AMS-WeA-12, **20**  
Kim, Philip: 2D+EM+MI+QS-WeM-7, 9  
Kim, Soyoung: EM+2D+BI+QS+TF-TuA-4, 7  
Kim, Yoosuk: 2D-ThM-16, 23; 2D-ThP-18, **30**  
Kim, Yunjo: EM+2D+AP+QS+TF-ThM-5, 24  
King, Wilson: 2D-ThM-16, 23  
KIBlinger, Tilman: MI+2D+AC+TF-WeM-13, 12  
Kjellberg Jensen, Thomas: EM+2D+BI+QS+TF-TuA-3, **7**  
Koch, Roland: 2D+LS+NS+SS-TuA-3, 5  
Koert, Ulrich: SS+2D+AMS-WeM-15, 14  
Kong, Dejjia: MI+2D+AC+TF-WeM-3, **10**  
Kong, Jing: 2D-ThM-7, 22  
Koroluk, Skylar: MI+2D+AC+TF-WeM-14, 12  
Kovalchuk, Serhii: 2D-WeA-12, 16  
Krashennikov, Arkady: 2D+AP+EM+QS+SS+TF-TuM-5, 2  
Krayev, Andrey: 2D-ThM-7, **22**  
Kretschmer, Silvan: 2D+AP+EM+QS+SS+TF-TuM-5, 2  
Krüger, Peter: MI+2D+AC+TF-WeM-13, 12  
Kugler, David: SS+2D+AMS-WeA-5, 19  
Kühnle, Angelika: SS+2D+AMS-WeA-5, 19  
Kuljanishvili, Irma: 2D-ThM-16, **23**; 2D-ThP-18, 30  
Kumar, Dhananjay: EM+2D+BI+QS+TF-TuA-4, 7  
Kwak, Seungjae: 2D-ThM-4, 21  
— **L** —  
La Mendola, Diego: 2D-ThP-14, **29**  
Lang, Junyu: SS+2D+AMS-WeA-9, 19  
Lasek, Kinga: 2D-ThP-2, 27  
Lass, Steven: EM+2D+BI+QS+TF-TuA-10, 8  
Lauter, Valeria: MI+2D+AC+TF-WeA-3, 17; MI+2D+AC+TF-WeA-9, 17  
Law, Stephanie: 2D+AP+EM+QS+SS+TF-TuM-15, 4; 2D+EM+MN+TF-FrM-5, 31; 2D-ThM-14, 22; EM+2D+AP+QS+TF-ThM-4, **24**  
Le, Son: NS1+2D+QS-MoA-3, **1**  
Le, Son T.: 2D+EM+MI+QS-WeM-3, 9  
Lee, Donggyu: 2D-ThM-4, 21  
Lee, Erica: 2D-WeA-5, 15  
Lee, Jaesung: 2D+EM+MN+TF-FrM-7, 31  
Lee, Juwon: 2D-ThP-5, **27**  
Lee, Kyeong Yeon: 2D-WeA-13, 16  
Lee, Soobeen: EM+2D+BI+QS+TF-TuA-12, **8**  
Lee, Won Gyu: 2D-ThP-8, **28**  
Lee, Wonbo: 2D-ThM-4, **21**  
Lefler, Benjamin: MI+2D+AC+TF-WeM-14, 12  
Lei, Chi-Hou: 2D-ThP-18, 30  
Lespasio, Marcus: 2D-ThP-18, 30  
Li, Huamin: 2D+AP+EM+QS+SS+TF-TuM-6, 3; 2D-ThP-11, **28**  
Li, Jian: EM+2D+AP+QS+TF-ThM-5, 24  
Li, Nichole: EM+2D+BI+QS+TF-TuA-9, 8  
Li, Philip: 2D-WeA-5, 15  
Liang, Liangbo: 2D+EM+QS-ThA-5, 26  
Lidsky, David: MI+2D+AC+TF-WeA-3, 17  
Lilley, Carmen: SS+2D+AMS-WeA-14, 20  
Lina, Kirsten: 2D-WeA-3, 15  
Lindner, Morris: MI+2D+AC+TF-WeA-3, 17  
Liu, Derrick: 2D-ThM-14, 22  
Liu, Derrick Shao-Heng: 2D+EM+MN+TF-FrM-5, 31  
Liu, Yang: SS+2D+AMS-WeA-9, 19  
Lodge, Michael: 2D-WeA-3, 15; 2D-WeA-4, 15  
Löffström, Nathanael: EM+2D+BI+QS+TF-TuA-3, 7  
Longo, Filippo: MI+2D+AC+TF-WeA-11, **18**  
Lough, Stephanie: 2D+LS+NS+SS-TuA-10, **6**  
Lu, Tzu-Ming: MI+2D+AC+TF-WeA-3, 17  
Lucinec, Jake: EM+2D+BI+QS+TF-TuA-11, 8  
Luican-Mayer, Adina: NS1+2D+QS-MoA-6, **1**  
Luo, Bin: MI+2D+AC+TF-WeA-3, **17**  
Lüpke, Felix: 2D-WeA-12, 16  
— **M** —  
Mack, Shawn: 2D+AP+EM+QS+SS+TF-TuM-16, 4  
Maehara, Hiroki: 2D+AP+EM+QS+SS+TF-TuM-3, 2  
Magruder, Benjamin: EM+2D+BI+QS+TF-TuA-8, 7  
Mahadik, Nadeemullah: EM+2D+AP+QS+TF-ThM-3, 24  
Mahl, Johannes: EM+2D+BI+QS+TF-TuA-4, 7  
Mai, Thuc: NS1+2D+QS-MoA-3, 1  
Makkar, Priyanka: 2D+EM+QS-ThA-4, 26  
Mannix, Andrew: 2D-ThM-7, 22  
Mao, Nannan: 2D-ThM-7, 22  
Marini, Sebastian: 2D-ThM-14, 22  
Martin, Catalin: EM+2D+BI+QS+TF-TuA-4, 7  
Marzo, Tiziano: 2D-ThP-14, 29

## Author Index

- Matzelle, Matthew: MI+2D+AC+TF-WeA-3, 17
- May, Steven: MI+2D+AC+TF-WeM-14, 12
- Mazzoli, Claudio: 2D+EM+MI+QS-WeM-7, 9
- McCreary, Kathleen M.: 2D+LS+NS+SS-TuA-3, 5
- McDonnell, Stephen: 2D-ThM-6, 22
- McDowell, Matthew: 2D-ThM-14, 22
- McGuinness, Emily: EM+2D+BI+QS+TF-TuA-8, 7
- Medasani, Bharat: 2D-ThM-3, 21
- Meißner, Oliver: 2D+AP+EM+QS+SS+TF-TuM-5, 2
- Merkling, Clement: 2D+EM+MI+QS-WeM-4, 9
- Mikkelsen, Anders: EM+2D+BI+QS+TF-TuA-3, 7
- Miller, Michael: 2D+EM+MI+QS-WeM-13, 10
- Mills, Brian: EM+2D+BI+QS+TF-TuA-11, 8; EM+2D+BI+QS+TF-TuA-9, 8
- Missale, Elena: 2D-ThP-18, 30
- Miura, Hitoshi: 2D+AP+EM+QS+SS+TF-TuM-3, 2
- Miwa, Jill: 2D+LS+NS+SS-TuA-3, 5
- Mkhoyan, K. Andre: EM+2D+AP+QS+TF-ThM-6, 25
- Mock, Alyssa: MI+2D+AC+TF-WeA-10, 18
- Moffitt, Chris: 2D+LS+NS+SS-TuA-4, 5
- Moinpour, Mansour: 2D+EM+MI+QS-WeM-13, 10
- Monson, Todd C.: MI+2D+AC+TF-WeA-3, 17
- Moretti, Federico: EM+2D+BI+QS+TF-TuA-10, 8
- Morin, Pierre: 2D-ThM-15, 23
- Moselund, Kirsten E.: EM+2D+AP+QS+TF-ThM-1, 23
- Mou, Shin: EM+2D+AP+QS+TF-ThM-5, 24
- Mowbray, Duncan John: SS+2D+AMS-WeA-15, 20
- Mu, Sai: MI+2D+AC+TF-WeM-3, 10
- Mukherjee, Shagorika: EM+2D+AP+QS+TF-ThM-4, 24
- Mukhopadhyay, Kausik: 2D+EM+QS-ThA-4, 26
- Munoz, Maria: NS1+2D+QS-MoA-3, 1
- Murphy, Thomas E.: 2D-WeA-6, 15
- Myers-Ward, Rachael: 2D+AP+EM+QS+SS+TF-TuM-16, 4; EM+2D+AP+QS+TF-ThM-2, 23; EM+2D+AP+QS+TF-ThM-3, 24
- N —
- Narasimha, Ganesh: MI+2D+AC+TF-WeM-3, 10
- Naveed, Muhammad Ashar: 2D+EM+MN+TF-FrM-4, 31
- Nayir, Nadire: 2D+EM+MN+TF-FrM-5, 31
- Neal, Adam: EM+2D+AP+QS+TF-ThM-5, 24
- Nemeth, Stefan: 2D-ThM-15, 23
- Netzke, Sam: 2D+EM+MN+TF-FrM-3, 31
- Neumann, Christof: 2D+AP+EM+QS+SS+TF-TuM-5, 2
- Neupane, Madhab: 2D-ThP-9, 28
- Ngo, Thong: 2D+EM+MI+QS-WeM-13, 10
- Niu, Yuran: SS+2D+AMS-WeA-11, 20
- Noesges, Brenton: EM+2D+AP+QS+TF-ThM-5, 24
- Nygård, Jesper: EM+2D+BI+QS+TF-TuA-3, 7
- O —
- Ogaki, Takeshi: SS+2D+AMS-WeA-2, 18
- Ogunbiyi, Olugbenga: 2D+EM+QS-ThA-5, 26
- Ohta, Taisuke: 2D+LS+NS+SS-TuA-11, 6; 2D-ThM-6, 22
- Okada, Naoya: 2D+AP+EM+QS+SS+TF-TuM-3, 2
- ones, Alfred J: 2D+LS+NS+SS-TuA-3, 5
- Orson, Keithen: SS+2D+AMS-WeA-11, 20
- Otto, Felix: 2D+AP+EM+QS+SS+TF-TuM-5, 2
- P —
- Pandit, Sanchaya: 2D+EM+MN+TF-FrM-4, 31
- Pantano, Gina: MI+2D+AC+TF-WeM-15, 12
- Pantano, Maria F.: 2D-ThP-18, 30
- Papp, Christian: SS+2D+AMS-WeA-15, 20
- Park, Jinhong: 2D-ThP-5, 27
- Pathirage, Vimukthi: 2D+AP+EM+QS+SS+TF-TuM-14, 4
- Pearce, Charles J.: MI+2D+AC+TF-WeA-3, 17
- Pekarek, Thomas: 2D-ThM-1, 21
- Penland, Lindsey: SS+2D+AMS-WeM-8, 13
- Pennachio, Daniel: 2D+AP+EM+QS+SS+TF-TuM-16, 4; EM+2D+AP+QS+TF-ThM-2, 23; EM+2D+AP+QS+TF-ThM-3, 24
- Peremadathil Pradeep, Reshma: MI+2D+AC+TF-WeA-11, 18
- Peters, Jannick: SS+2D+AMS-WeM-15, 14
- Petralia, Salvatore: 2D+EM+QS-ThA-3, 26
- Pichugin, Kostyantyn: 2D+EM+MN+TF-FrM-3, 31
- Picker, Julian: 2D+AP+EM+QS+SS+TF-TuM-5, 2
- Planer, Jakob: SS+2D+AMS-WeM-4, 13
- Poccia, Nicola: 2D+EM+MI+QS-WeM-7, 9
- Pookpanratana, Sujitra: SS+2D+AMS-WeA-3, 18
- Pop, Eric: 2D-ThM-7, 22
- Pradhan Sakhya, Anup: 2D-ThP-9, 28
- Prem, Priscilla: 2D-WeA-1, 15
- Prochazka, Pavel: SS+2D+AMS-WeM-4, 13
- Ptok, Andrzej: 2D-ThP-9, 28
- Puggioni, Danilo: MI+2D+AC+TF-WeM-14, 12
- Puretzky, Alexander: 2D+AP+EM+QS+SS+TF-TuM-4, 2; 2D+AP+EM+QS+SS+TF-TuM-8, 3
- Q —
- Quinn, Edwin: 2D-WeA-5, 15
- Quintero-Torres, Rafael: EM+2D+BI+QS+TF-TuA-5, 7
- R —
- Rafique, Muhammad Shahbaz: 2D-ThM-8, 22
- Rajapakse, Nirosha: 2D-ThP-2, 27
- Ramisa, Martí: EM+2D+AP+QS+TF-ThM-6, 25
- Ravula, Sudhir: SS+2D+AMS-WeM-17, 14
- Regmi, Paras: MI+2D+AC+TF-WeM-3, 10
- Regmi, Sabin: 2D-ThP-9, 28
- Reimann, Timmy: MI+2D+AC+TF-WeA-3, 17
- Reinert, Friedrich: MI+2D+AC+TF-WeM-1, 10
- Reinke, Petra: 2D-ThM-5, 21; SS+2D+AMS-WeA-11, 20
- Richardson, Kathleen: EM+2D+BI+QS+TF-TuA-11, 8; EM+2D+BI+QS+TF-TuA-9, 8
- Richter, Curt: NS1+2D+QS-MoA-3, 1
- Robinson, Jeremy: 2D+LS+NS+SS-TuA-11, 6
- Robinson, Jeremy T.: 2D+LS+NS+SS-TuA-3, 5
- Roe, Abigail: 2D-ThM-16, 23
- Rogge, Paul: MI+2D+AC+TF-WeM-14, 12
- Romanova, Tetiana: 2D-ThP-9, 28
- Rondinelli, James: MI+2D+AC+TF-WeM-14, 12
- Roorda, Tycho: SS+2D+AMS-WeA-10, 19
- Rosner, Malte: 2D+LS+NS+SS-TuA-3, 5
- Rotenberg, Eli: 2D+LS+NS+SS-TuA-3, 5; 2D-ThP-10, 28
- Rouleau, Christopher: 2D+AP+EM+QS+SS+TF-TuM-4, 2
- Russell, Daniel: MI+2D+AC+TF-WeM-8, 11
- S —
- S. McLeod, Alexander: EM+2D+AP+QS+TF-ThM-6, 25
- Sabath, Franziska: SS+2D+AMS-WeA-5, 19
- Sadowski, Jurek: SS+2D+AMS-WeA-11, 20
- Sakaguchi, Isao: SS+2D+AMS-WeA-2, 18
- Sankar Kar, Gouri: 2D+EM+MI+QS-WeM-4, 9
- Sarawate, Dnyanesh: 2D-WeA-1, 15
- Sasmal, Souvik: 2D-ThP-10, 28
- Satriano, Cristina: 2D+EM+QS-ThA-3, 26; 2D-ThP-14, 29
- Schaal, Maximilian: 2D+AP+EM+QS+SS+TF-TuM-5, 2
- Scharf, Dominik: SS+2D+AMS-WeM-15, 14
- Scheiman, David: EM+2D+AP+QS+TF-ThM-3, 24
- Scherrer, Markus: EM+2D+AP+QS+TF-ThM-1, 23
- Schmid, Heinz: EM+2D+AP+QS+TF-ThM-1, 23
- Schmid, Michael: SS+2D+AMS-WeA-5, 19
- Schmidt, Heidemarie: MI+2D+AC+TF-WeA-10, 18
- Schneider, M. Alexander: MI+2D+AC+TF-WeM-13, 12
- Schöttke, Fabian: MI+2D+AC+TF-WeM-13, 12
- Schubert, Eva: MI+2D+AC+TF-WeA-10, 18
- Schubert, Mathias: MI+2D+AC+TF-WeA-10, 18
- Schwartz, Jeffrey J.: 2D+EM+MI+QS-WeM-3, 9
- Schwarz, Casey: EM+2D+BI+QS+TF-TuA-11, 8; EM+2D+BI+QS+TF-TuA-9, 8
- Sciacca, Stefania: 2D+EM+QS-ThA-3, 26
- Sciaini, German: 2D+EM+MN+TF-FrM-3, 31
- Scirè, Salvatore: 2D+EM+QS-ThA-3, 26
- Sekora, Derek: MI+2D+AC+TF-WeA-10, 18
- Senevirathna, M.K. Indika: 2D+AP+EM+QS+SS+TF-TuM-7, 3; 2D-ThP-17, 29
- Shah, Jay: EM+2D+AP+QS+TF-ThM-6, 25
- Shahsavari, Azin: SS+2D+AMS-WeM-4, 13
- Shallenberger, Jeffery: 2D+EM+MN+TF-FrM-5, 31
- Shallenberger, Jeffrey: 2D-ThM-14, 22
- Shang, Anyu: SS+2D+AMS-WeA-13, 20
- Shang, zhongxia: SS+2D+AMS-WeA-13, 20
- Sharma, Peter: MI+2D+AC+TF-WeA-3, 17
- Sharma, Prince: SS+2D+AMS-WeA-12, 20
- Sharma, Rashi: EM+2D+BI+QS+TF-TuA-11, 8; EM+2D+BI+QS+TF-TuA-9, 8
- Shaw, Steven: 2D+EM+MN+TF-FrM-7, 31
- Sheng, Xuanyu: SS+2D+AMS-WeA-13, 20
- Shin, Yun Kyung: 2D+EM+MN+TF-FrM-5, 31
- Shrestha, Ashok: MI+2D+AC+TF-WeA-4, 17; MI+2D+AC+TF-WeM-7, 11; MI+2D+AC+TF-WeM-8, 11
- Silva Quinones, Dhamelyz: 2D-ThP-13, 29
- Singh, Simranjeet: 2D+LS+NS+SS-TuA-3, 5; 2D-ThP-10, 28
- Sinova, Jairo: MI+2D+AC+TF-WeM-15, 12
- Sinsheimer, John: 2D+EM+MI+QS-WeM-7, 9
- Sitaram, Rahul: EM+2D+AP+QS+TF-ThM-4, 24
- Slaets, Robbe: 2D+EM+MI+QS-WeM-4, 9
- Šmejkal, Libor: MI+2D+AC+TF-WeM-15, 12; MI+2D+AC+TF-WeM-5, 11
- Smith, Arthur: MI+2D+AC+TF-WeM-7, 11
- Smith, Arthur R.: MI+2D+AC+TF-WeA-4, 17; MI+2D+AC+TF-WeM-8, 11
- Smyth, Christopher: 2D-ThM-6, 22
- Snapp, Peter: 2D-ThM-8, 22
- Soomary, Liam: 2D+LS+NS+SS-TuA-4, 5
- Spanopoulos, Ioannis: 2D-WeA-13, 16
- Spataru, Catalin: 2D+LS+NS+SS-TuA-11, 6
- Speranza, Giorgio: 2D-ThP-18, 30
- Sprague, Milo: 2D-ThP-9, 28
- Srikanth, Hari: MI+2D+AC+TF-WeA-5, 17
- Stacchiola, Dario: SS+2D+AMS-WeM-16, 14
- Stackawitz, Jasper: EM+2D+BI+QS+TF-TuA-11, 8
- Steinrück, Hans-Peter: SS+2D+AMS-WeA-15, 20

## Author Index

- Strange, Lyndi: SS+2D+AMS-WeM-17, 14  
Subedi, Arjun: SS+2D+AMS-WeA-6, **19**  
Sugar, Josh: 2D+LS+NS+SS-TuA-11, 6  
Sun, Nian Xiang: MI+2D+AC+TF-WeA-3, 17  
Sun, Y.-J. Leo: 2D-WeA-6, **15**  
Surman, David: 2D+LS+NS+SS-TuA-4, 5  
Sutter, Eli: 2D+EM+MI+QS-WeM-1, 9  
Sutter, Peter: 2D+EM+MI+QS-WeM-1, **9**  
Suzuki, Taku: SS+2D+AMS-WeA-2, **18**  
Swerts, Johan: 2D-ThM-15, 23  
Sykes, Charles: SS+2D+AMS-WeM-7, 13  
Sykes, Marie: EM+2D+BI+QS+TF-TuA-11, 8  
— **T** —  
Tan, Chao Dun: 2D-WeA-11, **16**  
Tanabe, Shinichi: 2D+AP+EM+QS+SS+TF-TuM-3, **2**  
Tao, Chenggang: MI+2D+AC+TF-WeM-3, 10  
Tautz, Stefan: 2D-WeA-12, 16  
Tavazohi, Pedram: MI+2D+AC+TF-WeM-4, 11  
Tenorio, Jacob: 2D-ThP-4, **27**  
Tetard, Laurene: 2D+AP+EM+QS+SS+TF-TuM-17, 4  
Thareja, Eklavya: MI+2D+AC+TF-WeM-15, 12  
Thompson, Liam: EM+2D+AP+QS+TF-ThM-6, 25  
Thuermer, Konrad: 2D+LS+NS+SS-TuA-11, 6  
Timmermans, Marina: 2D+EM+MI+QS-WeM-4, 9  
Tiwari, Aalok: 2D-ThP-10, **28**  
TORRES AVILA, ITZEL PAMELA: 2D-ThP-7, **28**  
Tranchida, Gabriella: 2D+EM+QS-ThA-3, 26  
Truhart, Elaina: 2D-ThM-5, 21; 2D-ThM-6, 22  
Tsuchikawa, Ryuichi: 2D-WeA-4, 15  
Tu, Qing: 2D-WeA-13, 16  
Turchanin, Andrey: 2D+AP+EM+QS+SS+TF-TuM-1, **2**; 2D+AP+EM+QS+SS+TF-TuM-5, 2  
Turkowski, Volodymyr: 2D+AP+EM+QS+SS+TF-TuM-4, 2  
— **U** —  
Ullah, Ahsan: MI+2D+AC+TF-WeA-10, 18  
Ulstrup, Soren: 2D+LS+NS+SS-TuA-3, 5  
Ünzelmann, Maximilian: MI+2D+AC+TF-WeM-1, **10**  
Upadhyay, Sneha: MI+2D+AC+TF-WeM-7, 11  
— **V** —  
V. Sokolov, Alexei: EM+2D+BI+QS+TF-TuA-5, 7  
Valadez, Nathan: 2D-ThP-9, **28**  
Valdez, Nichole R.: MI+2D+AC+TF-WeA-3, 17  
van Pelt, Thomas: 2D-ThM-15, 23  
VARGAS LÓPEZ, MISAEEL: 2D-ThP-7, 28  
Varshney, Shivasheesh: EM+2D+AP+QS+TF-ThM-6, **25**  
Vasileiadou, Eugenia: 2D-WeA-13, 16  
Vasudevan, Rama: MI+2D+AC+TF-WeM-3, 10  
Veld, Yannin 't: 2D+LS+NS+SS-TuA-3, 5  
Viernes, Christian: 2D+EM+MN+TF-FrM-3, 31  
Vlassioux, Ivan: 2D+AP+EM+QS+SS+TF-TuM-8, 3  
Voigtländer, Bert: 2D-WeA-12, **16**  
Vovk, Evgeny: SS+2D+AMS-WeA-9, 19  
Vu, Nguyen: 2D+EM+MI+QS-WeM-13, 10  
— **W** —  
Waleska-Wellenhofer, Natalie J.: SS+2D+AMS-WeA-15, 20  
Wang, Danyu: SS+2D+AMS-WeA-9, 19  
Wang, Haiyan: SS+2D+AMS-WeA-13, 20  
Wang, Haozhe: 2D-ThP-13, **29**  
Wang, Jiayi: MI+2D+AC+TF-WeM-14, 12  
Wang, Ke: 2D+EM+MN+TF-FrM-5, 31  
Wang, Mengyi: 2D+EM+MN+TF-FrM-5, 31  
Wang, Michael Cai: 2D-ThM-8, 22  
Wang, Qinjin: NS1+2D+QS-MoA-5, **1**  
Wang, Xi: EM+2D+AP+QS+TF-ThM-4, 24  
Wang, Yanan: 2D+EM+MN+TF-FrM-4, 31  
Wang, Yunong: 2D+EM+MN+TF-FrM-6, **31**  
Wang, Zhenxing: 2D+EM+MI+QS-WeM-4, 9  
Wang, Zhiwei: 2D-WeA-12, 16  
Wang, Zijun: 2D-ThM-16, 23  
Warashina, Hisashi: 2D+AP+EM+QS+SS+TF-TuM-3, 2  
Wasik, Patryk: 2D+EM+MI+QS-WeM-7, **9**  
Wei, Daiyue: 2D-ThM-8, 22  
Wen, Jiaxuan: EM+2D+AP+QS+TF-ThM-6, 25  
White, Samuel: EM+2D+AP+QS+TF-ThM-3, 24  
Wiedeman, Daniel: EM+2D+BI+QS+TF-TuA-11, **8**; EM+2D+BI+QS+TF-TuA-9, 8  
Willcole, Alexandria: MI+2D+AC+TF-WeA-3, 17  
Williams, Michael D.: 2D+AP+EM+QS+SS+TF-TuM-7, 3; 2D-ThP-17, 29  
Wolszczak, Weronika: EM+2D+BI+QS+TF-TuA-10, 8  
Wong, Keith: 2D+AP+EM+QS+SS+TF-TuM-6, 3  
Wright, Elycia: 2D+AP+EM+QS+SS+TF-TuM-7, **3**; 2D-ThP-17, **29**  
Wyndaele, Pieter-Jan: 2D+EM+MI+QS-WeM-4, 9  
— **X** —  
Xiao, Kai: 2D+AP+EM+QS+SS+TF-TuM-4, **2**; 2D+AP+EM+QS+SS+TF-TuM-8, 3  
Xu, Ke: 2D-WeA-1, 15  
Xu, Xiaoshan: SS+2D+AMS-WeA-6, 19  
— **Y** —  
Yadav, Ajay: 2D+AP+EM+QS+SS+TF-TuM-6, 3  
Yang, Detian: SS+2D+AMS-WeA-6, 19  
Yang, Fei: 2D-ThP-12, 29  
Yang, Fengyuan: MI+2D+AC+TF-WeM-8, 11  
Yang, Yingchao: 2D+EM+QS-ThA-5, 26  
Yang, Yong: SS+2D+AMS-WeA-9, **19**  
Yang, Zhifei: EM+2D+AP+QS+TF-ThM-6, 25  
Yano, Junko: EM+2D+BI+QS+TF-TuA-4, 7  
Yao, Fei: 2D+AP+EM+QS+SS+TF-TuM-6, 3  
Yao, Fei (Faye): 2D-ThP-11, 28  
Yao, Jennifer: SS+2D+AMS-WeM-17, **14**  
Yao, Yugui: 2D-WeA-12, 16  
Yimam, Daniel T.: 2D+AP+EM+QS+SS+TF-TuM-8, **3**  
Yin, Zhewen: 2D-ThM-8, 22  
Yousuf, S M Enamul Hoque: 2D+EM+MN+TF-FrM-7, **31**  
Yousuf, SM Enamul Hoque: 2D+EM+MN+TF-FrM-6, 31  
Yu, Liping: 2D+EM+QS-ThA-5, 26  
Yu, Mingyu: 2D+AP+EM+QS+SS+TF-TuM-15, **4**  
Yu, Yiling: 2D+AP+EM+QS+SS+TF-TuM-4, 2  
Yu, Young-Jun: 2D-WeA-9, **15**  
— **Z** —  
Zachman, Michael J: 2D+EM+QS-ThA-5, 26  
Zahra, Khadisha: 2D+LS+NS+SS-TuA-4, 5  
Zakharov, Alexei: SS+2D+AMS-WeA-11, 20  
Zamora Alviarez, Daniela: 2D-ThM-8, 22  
Zeng, Hao: 2D+AP+EM+QS+SS+TF-TuM-6, 3  
Zhang, Tianyi: 2D-ThM-7, 22  
Zhang, Wei: EM+2D+BI+QS+TF-TuA-5, 7  
Zhang, Xiao-Xiao: 2D+EM+MN+TF-FrM-6, 31  
Zhang, Xinghang: SS+2D+AMS-WeA-13, 20  
Zhang, Zhenrong: EM+2D+BI+QS+TF-TuA-5, 7  
Zhao, Shu Yang Frank: 2D+EM+MI+QS-WeM-7, 9  
Zheng, Ruofei: 2D+EM+MN+TF-FrM-3, 31  
Zhu, Tiancong: 2D+LS+NS+SS-TuA-8, **5**  
Zhu, Zihua: SS+2D+AMS-WeM-17, 14